Modelling and Analysis of Neural
Networks in the Visuomotor System
of Anuran Amphibian

Francisco Cervantes-Perez

COINS Technical Report 85-27

MODELLING AND ANALYSIS OF NEURAL NETWORKS IN THE VISUOMOTOR
SYSTEM OF ANURAN AMPHIBIAN

A Dissertation Presented

By

FRANCISCO CERVANTES-PEREZ

Submitted to the Graduate School of the
University of Massachusetts in partial fulfillment
of the requirements for the degree of

DOCTOR OF PHILOSOPHY

September 1985

Department of Computer and Information Science

ii

MODELLING AND ANALYSIS OF NEURAL NETWORKS IN THE VISUOMOTOR
SYSTEM OF ANURAN AMPHIBIAN

A Dissertation Presented
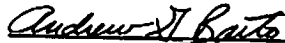
By

FRANCISCO CERVANTES-PEREZ

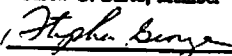Approved as to style and content by:

_____
Michael A. Arbib, Chairperson of Committee

_____
Andrew G. Barto, Member

_____
Stephen George, Outside Member

_____
Edward M. Riseman, Department Chair
Computer and Information Science

iii

iv

Tectum and Pretectum), each of which computes specific features of the external situation.

The models reproduce experimental observations adequately, and allow us to analyse qualitatively the neural mechanisms that might be subserving "worm-antiworm" discrimination, with direction invariance of this phenomenon being a consequence of the tectal architecture, and size selection and changes in response latency depending on the animal's motivational state.

We conduct a stability and parameter sensitivity analysis of the Facilitation Tectal Column model proposed by Lara et al [1982]. Here, we study how with different parametric combinations the neural model may present different qualitative behaviors. In addition, these analyses in combination with computer simulations were used to learn more about why the hypotheses embedded in the model yield the appropriate behaviors, and what are the critical conditions under which these behaviors are displayed.

Finally, the model is also used to address phenomena not considered during its design. We analyse in detail the controversy between the assertions of Ewert [1980, 1984] and of Roth [1979, 1980] about whether or not stimuli preference in the response of PY tectal cells is invariant to the stimulus velocity. Computer simulations suggested that PY cells' response might be velocity dependent if pretectal inhibition over tectal elements is delayed or reduced. Under these conditions, there will be a switch in PY cells' preference between "square" and "worm-like" stimuli.

I also benefited greatly from discussions with the other two members of my committee, Andrew Barto and Stephen George. The models design and theoretical analysis were improved after Andrew's suggestions; whereas the empirical considerations and predictions suggested by the models benefited from Stephen's comments.

ABSTRACT

MODELLING AND ANALYSIS OF NEURAL NETWORKS IN THE VISUOMOTOR
SYSTEM OF ANURAN AMPHIBIAN

September 1985

Francisco Cervantes-Pérez

B.E., Universidad Nacional Autónoma de México

M.E., Universidad Nacional Autónoma de México

Ph.D., University of Massachusetts

Directed by: Professor Michael A. Arbib

In the process of adapting adequately to the world, anuran amphibians present very stereotyped cognitive and motor behaviors, e.g., prey-catching and predator-avoidance behaviors. Neuroethological studies have shown that there are innate mechanisms in frogs and toads that recognize key-stimuli to elicit the proper motor response.

In this dissertation, we present and analyze a neural net "family-model", based on empirical grounds, that raises specific hypotheses of how different physiological events occurring during prey-catching and predator-avoidance behavior might be carried out by the interactions among different brain regions (i.e., Retina, Optic

LIST OF TABLES

LIST OF FIGURES

TABLE OF CONTENTS

CHAPTER

CHAPTER I

INTRODUCTION

Introduction

Survival is one of the most important concerns in any animal's, including a human's, life. Animals ensure survival by controlling their interactions with both their external and internal worlds. Interactions with the external world are represented by the coordination of sensory-motor processes, i.e., animals perceive their environment to modify it or to adapt to it in order to survive.

For many years scientists from different disciplines, such as philosophy, physiology, anatomy, ethology and brain theory, have studied sensory-motor phenomena involved in animal life. Sensory-motor processes are controlled by the Central Nervous System (CNS), henceforth referred to as "the Brain" or CNS without distinction. Thus the understanding of these phenomena can be reduced to the understanding of how the CNS, based on its internal representation of the world, carries out the coordination of motor behaviors.

Empirical and theoretical studies have pursued the understanding of the brain at different levels of analysis. At one extreme, there are analyses trying to explain behavior in terms of functional units representing perceptions and actions of the animal. At the other extreme we find analyses correlating behavior with neural mechanisms. In this dissertation we emphasize the importance of the interplay of empirical and theoretical efforts in seeking neural mechanisms underlying sensory-motor coordination.

In this Chapter we first discuss two similar approaches to the understanding of processes involved in sensory-motor coordination. One of them is empirical (Neuroethology), and the other is theoretical (Brain Theory). Then, our research goals are summarized by defining our approach, and methodology, to the understanding of visuomotor coordination in anuran amphibia. We also place our approach within the scope of Brain Theory. Finally, to guide the interested reader, the organization of this dissertation is described, pointing out the most important points presented in the following Chapters and Appendices.

Sensory-Motor Coordination : Neuroethology and Brain Theory

Neuroethology, whose concern is the experimental analysis of releasing and control mechanisms of behavior [Ewert, 1980, 1984; Ewert, Ingle & Capranica, 1983; Grüsser & Grüsser-Cornehls, 1976; Grüsser-Cornehls, 1984; Ingle, 1976b, 1983], and Brain Theory, whose concern is the study of the CNS's function via mathematical modelling and computer simulations [Arbib, 1972, 1981a, 1981b; Reichardt & Poggio, 1979], follow similar interdisciplinary approaches, at different levels of analysis, in studying the processes of perception and motor control.

Based on the fact that animals' actions are the outcome of the processing of information that takes place within neural networks in the CNS, Neuroethology and Brain Theory address similar issues in neuroscience and share a concern for developing new methodologies, both experimental and theoretical, to identify neural mechanisms subserving specific behaviors.

The animal's behavioral interactions with the environment require that ex-
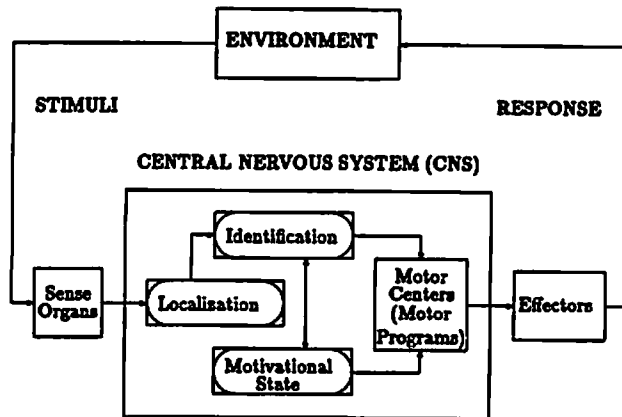
Figure 1: An organism interacting with its environment Information processing steps in the Central Nervous System (CNS) leading to a behavioral action in response to an external situation (adapted from Ewert [1980]).

ternal stimuli be sensed by organs (eye, ear, skin, etc.), and then incorporated into an internal representation of environmental situations through different levels of neural activity. Sense organs transmit this preprocessed information to Primary Sensor Centers (PSC), brain regions receiving direct input from sense organs, which participate in the processes of stimuli identification and localization. PSC's send, directly or indirectly, efferents to Motor Centers (MC), brain structures that decide the animal's next movement, whose function is to produce the most appropriate behavior to interact with the current situation. MC's activate particular groups of muscles that contract according to a Motor Program (MP) yielding spatio-temporal coordinated patterns of movement, that is, behavior. New stimuli update the internal state of the organism, modifying the animal's perception of its situation and its decision as to what to do next, forming in this way an Action-Perception cycle [Arbib, 1981a]. The efficacy of external stimuli to release a form of behavior, i.e., the activation of a MP, has been found to be dependent on the animal's "Motivational State". Thus, these animals' goals are defined by the CNS itself and can be influenced by the hormonal system or by environmental signals, i.e. seasonal changes, food smelling, threatening stimulus, etc. (see Fig. 1).

One approach to Brain Theory, Arbib's Schema Theory [Arbib, 1981a, 1981b], suggests that Sensory-motor Coordination is usefully decomposed into three different types of entity (see Fig. 2):

1. *Perceptual Schemas* (PS) are defined as the units of knowledge that represent, within the brain, a situation of the environment the animal may interact with.

2. *Motor Schemas* (MS) are defined as the units of motor control that use information generated by one or several PS's to direct an animal's action to adequately interact with the current situation. Thus, PS's generate parameters to be used by MS's, but need not activate such MS's. Furthermore, there may be different PS's active at the same time which may cooperate or

compete with each other in giving the necessary conditions to control the activation of MS's.

3. *Planning* is defined as a mechanism that selects information from activated PS's in order to activate the proper MS's in accord with the organism's current goals.

Neuroethologists have also tried to establish correlations between data generated by different empirical disciplines. Data found in some of them, such as neurophysiology and anatomy, should explain results obtained in others, such as ethology. In brain modelling, similar approaches are found and may be classified into three different groups:

1. The *Top-Down* approach is mainly concerned with explaining overall behavior in terms of interacting computations, without a great deal of concern for physiological or anatomical detail at the level of neural circuits [House, 1984; Arbib & House, 1983; Lara et al, 1985; Marr & Poggio, 1979].

2. The *Bottom-Up* approach is generally concerned with the analysis of models of neural networks [An der Heiden & Roth, 1983; Byrne, 1980, 1982; Hodgkin-Huxley model; Lara, Arbib & Cromarty, 1982].

3. The *Middle-Out* analysis proceeds via integrated cycles of top-down and bottom-up modelling, as initial top-down hypotheses are modified in the light of neural data [Didday, 1970, 1976; Ewert & Von Seelen, 1974; Arbib & Lara, 1982; Lara & Arbib, 1982]. All the levels that fall in between the first two extremes of neural modelling, fit in this category [Arbib, 1984].

In summary, that Neuroethology and Brain Theory share interests in the analysis of important issues in neuroscience that explore the following main questions :

1. In what way is sensory-motor coordination carried out by the CNS?

2. How do sense organs (and brain) differentiate behaviorally important stimuli from non-important ones?

3. What is the representation of external stimuli within the CNS?

4. How does the CNS identify different stimuli patterns?

5. How does the CNS localise stimuli in the environment?
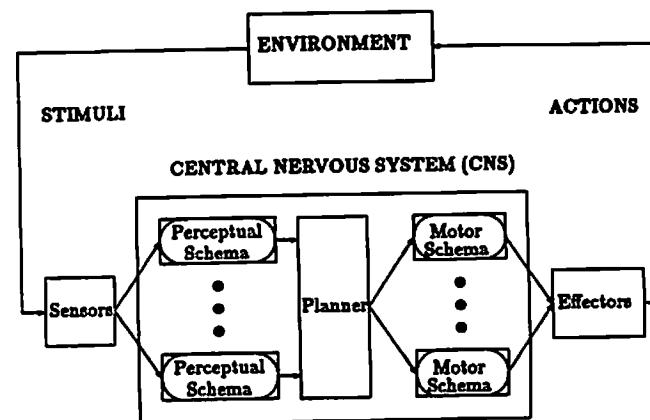
Figure 2: Sensory-motor coordination according to Schema Theory
The internal state of the organism is updated by new stimuli, whose internal representation (Perceptual Schema) is used by the organism (Planner) to decide what action (Motor Schema) should be produced next. This forms an Action-Perception cycle [Arbib, 1981a].

6. What are the means of perceiving, storing and retrieving information in the CNS?

7. How is the release of behavioral patterns modulated by the motivational state of the animal?

Research Objectives

Our goal in this research is to offer a conceptual analysis of some of the neural mechanisms used by the CNS during sensory-motor coordination. The available empirical evidence makes it very difficult to deal with the general question of how inputs from different sense organs are integrated by the CNS to control the animal's interactions with the environment. So, in this dissertation, we restrict our analysis to processes occurring during *Visuomotor Coordination*. To do so, data from studies on frogs and toads, i.e., *anuran amphibians*, were chosen to lay the empirical basis of a family of models of visually guided behaviors in vertebrates.

The visual systems of frogs and toads has been extensively studied from different points of view, such as anatomical, neurophysiological, ethological and theoretical. These animals present very stereotyped behaviors which are released by relatively simple visual key-stimuli. When they confront visual stimuli with a high probability of representing a prey or a predator, innate mechanisms recognise the key-stimulus and elicit the most adequate motor behavior, such as prey-catching or predator-avoidance. Additionally, anurans are vertebrates and their nervous systems share interesting parallels to the way in which higher vertebrates, including humans, coordinate their actions according to what they see.

In this dissertation, we develop and analyse a family of models of the parallel distributed interactions among retina, optic tectum and pretectum that subserve

anuran's visuomotor coordination. These models represent the latest stage of an evolving model, defined by Arbib [1982] as *Rana Computatrix*, of frog and toad's visuomotor system. The features of the modelling *style* embodied in *Rana Computatrix* at each stage are:

1. New phenomena are addressed by refining and expanding the models created in previous stages. That is, new models, subsuming previous models as subunits, are used to explain a wider range of behaviors in a manner consistent with current neurophysiological and anatomical data.

2. To produce a new "model" in the sequence, we design, based on empirical grounds, and analyse a "family of models". Computer simulations are conducted to choose the set of parameters (connectivities, synaptic weights, and time and membrane constants) that yield the neural dynamics compatible with available data.

3. These choices are constrained by experimental results when available. When empirical information is not available, we make choices posing explicit hypotheses which may serve to stimulate new experiments. Results from those experiments, in turn, are to be used to refine and develop the models accordingly.

The first stage of *Rana Computatrix* was a neural model of a single "Tectal Column" [Lara, Arbib & Cromarty, 1982], abstracted from anatomical studies in frogs [Székely & Lázár, 1976], which analyses physiological data [Ingle, 1975] for prey-catching facilitation. The second model [Lara & Arbib, 1982] was a unidimensional array of only 8 tectal columns. It explains the increase in the response of pyramidal cells when a "worm-like" stimulus is elongated, and the facilitation to double stimuli moved along the direction of motion with the animal preferring to orient to the leading of the two objects. In the third stage [Arbib & Lara, 1982], some notions of Didday [1970, 1976] and Amari and Arbib [1977] were incorporated to develop a model of retino-tectal-pretectal interactions underlying prey-selection [Ingle, 1968].

In this work, three of the main advantages of brain modelling are exploited.

First, our models, built upon those just described, are based on realistic spatial and temporal neuronal interactions. These models are used to analyse neuro-physiological and ethological data [Ewert, 1976, 1980, 1984; Grüsser & Grüsser-Cornehls, 1976; Grüsser-Cornehls, 1984; Roth & Jordan, 1982] in a way that postulates explicit hypotheses about neuronal connectivity within the tectum and about the spatio-temporal tectal outflow. Here, the objective is to explain a wider range of phenomena not addressed by previous models, such as:

1. How the spatio-temporal characteristics of visual stimuli are used by the animal's brain to release patterns of movement.

2. How the tectal architecture subserves physiological responses, in the presence and in the absence of pretectal inhibition, of different tectal units, i.e., Ewert's tectal cells of type T5(2) and T5(3).

3. How the levels of activity in those units contribute to the elicitation of a wider range of behaviors in pattern recognition in frogs and toads, such as "worm-antiworm" discrimination, size-preference, prey-catching orienting and predator-avoidance behaviors.

4. Mechanisms by which tectal pyramidal cell response might be velocity de-pendent.

Second, computer simulations are used to test different hypotheses that may clarify the suitability of specific interpretations of experimental data, and to ex-plain data beyond those which specifically entered into the models' design, pre-dicting in this way new results that may be tested experimentally. We design our models to be flexible enough so that the results of those experiments can be used to refine and develop the models accordingly.

And third, using Non-linear Systems Theory techniques, a stability analysis is developed to study the sensitivity of the Tectal Column model of Lara et al [1982] to changes in different parameters. This analysis is conducted in combination with computer simulations to learn more about why the hypotheses embedded in the models yield the appropriate behaviors, and what are the critical situations under

which these behaviors are displayed. Results obtained from this analysis should stimulate new experiments that may be tested empirically.

Organisation of the Dissertation

This dissertation is organised into three main parts (Chapters 3, 4 and 5). Each one of these parts has enough material to be read independently from the others without affecting its understanding. Empirical and theoretical studies, which are background material for all three parts, are described in Chapter 2. Additionally, all three parts are complemented by material contained in Appen-dices A, B and C. In Chapter 2, we review anatomical, neurophysiological and ethological studies of the anuran's visual system which are relevant to the un-derstanding of how visuomotor coordination is carried out by the animal's brain. These studies lay the basis of our models of neural substrates subserving visually guided behaviors in vertebrates. Special attention is paid to studies of the retina, optic tectum and pretectum and their interactions, which have been suggested to play a prominent role during "worm-antiworm" discrimination, prey-selection, prey-catching orienting and predator-avoidance behaviors. We also review previ-ous [Didday, 1970; Ewert & Von Seelen, 1974] and alternative [an der Heiden & Roth, 1983] models of the retino-tectal-pretectal interactions. In later Chapters, these models are compared and contrasted with our models.

In Part I (Chapter 3), we present the development and analysis of a family of neural models of the retino-tectal-pretectal interactions. Perception of visual in-formation in the CNS starts when the light pattern representing external stimuli hits photoreceptors of the retina. Thus, a model of neural substrates subserving visuomotor coordination requires a model of the retinal preprocessing of informa-

tion. In this Chapter we describe a *Black Box*, curve fitting, retina model that, according to the specification of external stimuli, produces the corresponding levels of activity of ganglion cells R2, R3 and R4 in response to different configurations of "dummy" stimuli, such as horizontal and vertical rectangles, and squares of different sizes. This model reproduces physiological data (curves) reported by Ewert [1976, 1980]. It also considers the effects of varying the stimulus velocity and contrast according to the exponential formulas obtained by Grüsser and Grüsser-Cornehls [1976], Finkelstein and Grüsser [1965], and Ewert [1976, 1980].

The models presented in this Part embody hypotheses about tectal architecture and its role in the processing of visual information. Here, using a refined version of the Tectal Column model of Lara et al [1982] as a subunit, we present a two-dimensional model of the retino-tectal-pretectal interactions subserving physiological responses, in the presence and in the absence of pretectal inhibition, during the behaviors of "worm-antiworm" discrimination, size-preference and prey-catching orienting. The only efferent element of the Tectal Column model, the pyramidal (PY) cell, is suggested to be equivalent to the tectal cell T5(2) defined physiologically by Ewert [1976]. In this model we postulate that direction invariance of "worm-antiworm" discrimination is a consequence of the tectal architecture, and that size-preference and response latency depend on the motivational state of the animal.

Finally, in the discussion of this Chapter we describe our hypotheses of how "worm-like" and "antiworm-like" stimuli are represented (Perceptual Schemas) by the anuran's brain through levels of neural activity of different units within the retina, the optic tectum and the pretectum, as well as how this representation is used by Motor Centers, such as the spinal cord, medulla oblongata, and probably

reticular formation and cerebellum, to activate the proper motor behavior (Motor Schemas).

Given that in Part I a model that reproduces satisfactorily empirical observations has been developed, now, we want to explore the model-family to determine what range of models, different parametric combinations, is acceptable. Therefore in Part II (Chapter 4), we analyse a refined version of the model of a single tectal column proposed by Lara et al [1982]. Based on the model characteristics and the introduction of new tectal units [Cervantes-Pérez, Lara and Arbib, 1985], we redefine it as the Facilitation Tectal Column (FTC) model. We point out the main hypotheses embodied in the model of how the tectal architecture and interactions among tectal elements account for prey-catching facilitation. Then, stability and parameter-sensitivity analyses of the model are conducted to establish the ranges of parameter values within which the FTC still behaves in a manner that is consistent with the available physiological results.

In Part III (Chapter 5) computer simulations of the the models developed in Part I are used to design new physiological and behavioral experiments that raise new hypotheses about neural mechanisms subserving visuomotor coordination in frogs and toads. These experiments are posed to be tested empirically, so we outline possible experimental paradigms to test them. We analyse in detail the controversial issue (e.g. the controversy between the assertions of Ewert [1980, 1984] and of Roth and collaborators [Luthardt & Roth, 1979; Himstedt & Roth, 1980; Roth & Jordan, 1982; Roth, 1976, 1982]) about whether or not stimuli preference in PY cell's response is invariant to the stimulus velocity.

Finally, in Chapter 6, we present a summary of our models' contributions to the understanding of how processes related to visuomotor coordination in frogs and toads are carried out by the CNS. Our models are compared and contrasted

with a previous model developed by Ewert and Von Seelen [1974] and an alternative model proposed by An der Heiden and Roth [1983] pointing out the scope of the hypotheses that each model can explain. Additionally, possible future extensions of this research are outlined in detail.

The information presented in the Appendices, about the mathematical representation of our models and its computer implementation, is intended to show how the results reported in this dissertation can be reproduced. In Appendix A we describe the mathematical representation of the models and provide tables with the final choices of values of thresholds, time constants, membrane constants and synaptic weight coupling factors. Finally, in Appendix B we analyze different numerical methods for solving systems of first order differential equations. Here we define what numerical methods are well suited to solve the system of first order differential equations that represents the dynamics of the neural net model. These methods are compared according to the criteria established by Hull *et al* [1972], where the cost of a particular method applied to a particular problem is measured by both the number of function calls and the overhead cost.

TABLE OF CONTENTS

CHAPTER II

VISUOMOTOR COORDINATION IN FROG AND TOAD

Introduction

In this Chapter we provide an overview of data generated by empirical and theoretical studies related to processes of visuomotor coordination in frogs and toads. Here, our aim is threefold: first, to present the theoretical and experimental findings that were considered in the development of the family-models described in this dissertation (see Chapters 3, 4 and 5); second, to provide enough background material to facilitate the understanding of the models and of the type of information processing carried out by the anuran's brain to control the animal's behavior; and third, to introduce material required to outline further research in our efforts to elucidate the neural mechanisms underlying visuomotor coordination in frog and toad.

So far, our models have been used to explain phenomena related with prey-catching and predator-avoidance behaviors. Therefore, in this Chapter we restrict our review to data from studies related to events occurring during the elicitation of these behaviors. Thus, our review begins with the discussion of ethological studies which describe the sequence of events that take place during prey-catching and avoidance behaviors, as well as the key-stimuli that release them. Then, proceeding from the outside to the inside, we discuss results from studies of different brain regions along the visual system of frogs and toads. Our review starts

with the eye and the retina, followed by data from studies of the optic tectum, henceforth referred to as "tectum" for short, and the thalamic pretectal pc/pl region, henceforth referred to as "pretectum" for short. Brain lesion and brain point stimulation experiments, whose goal is to identify those brain structures that seem most likely to be responsible for the activation of particular behavioral events, have pointed to the two latter regions and their interactions as playing a prominent role in the elicitation of prey-catching orienting and predator-avoidance behaviors. Thus, we review current anatomical and physiological studies that analyze the intrinsic organization of the tectum and pretectum, and the nature of the interactions among their elements. In addition we also include data on the effects of retinal axon terminals impinging upon tectal and pretectal elements. Finally, our review ends with a survey of previous and alternative theoretical models of the anuran visual system. In later Chapters, some of these models will be compared and contrasted with our models, which seek to explain how different physiological events occurring during prey-catching and predator-avoidance behaviors might be released by the conjoint activity of different brain regions, each one computing specific features of the world.

Neuroethology of the Anuran's Visual System

One of the advantages of working with amphibians, such as frogs and toads, is that they have a limited repertoire of behaviors. These animals present fixed action patterns, which can be repetitively elicited, when a key-stimulus appears in the visual field. Grüsser and Grüsser-Cornehls [1976] classified the visually guided behaviors in anurans into seven categories:

1. general visual orientation in the habitat,
2. prey-catching behavior,

3. avoidance and hiding responses,

4. responses of the eye (accommodation, dilation or constriction of the pupil, and eye movements),

5. short-latency vegetative responses to visual stimuli, such as respiration and heart beat,

6. long-latency vegetative responses to visual stimuli, such as annual rhythms and hormonal variations associated with these rythms, and

7. changes in skin color of animals under different illumination or on different backgrounds.

The behavioral patterns of each category depend on visual stimulation, on information coming from other senses and on the motivational state of the animal [Ewert, 1980, 1984; Grüsser and Grüsser-Cornehls 1976; Comer and Grobstein, 1981a, 1981b, 1981c; Ingle, 1976a, 1981]. The models developed in this dissertation relate only to two of those categories, prey-catching and predator-avoidance. That is, our approach to visuomotor coordination starts with two basic behaviors of the animal — it will attack "prey-like" objects, and it will avoid "predator-like" objects.

Prey-Catching Behavior

Prey-catching behavior is elicited by different types of natural prey objects in frogs and toads. Toads catch earthworms, slugs, beetles and other small insects; while frogs catch mainly flies [Ewert, 1984]. In both animals prey-catching involves the execution of a fixed sequence of motor actions [Grüsser-Cornehls, 1984; Ewert, 1984]. This behavior is very similar in both species, differing only in few parts of the sequence. Before a stimulus appears in the animal's visual field, frogs wait motionless in their hunting habitat; while toads search for prey behaving as "hunters". Fig. 3 shows the stimulus-response chain presented by toads when a prey-like object appears somewhere in its visual field [Ewert, 1980]:
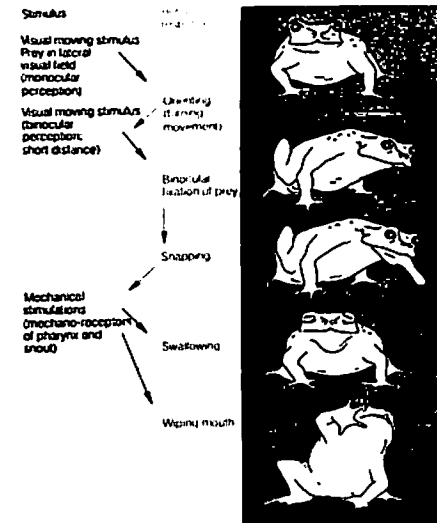
Figure 3: Behavioral patterns of the prey-catching sequence.
See text for explanation [from Ewert, 1980].

1. Toads (and frogs) exhibit an "orienting" response toward the prey.

2. When the orienting response brings the prey candidate into the binocular visual field, the animal "approaches" the prey by stalking (frogs do it by jumping).

3. When the prey is in the binocular part of the visual field and within a certain distance, then "binocular fixation" occurs.

4. Once the prey is at a reaching distance, the animal "snaps" at it.

5. Then, there comes the "swallowing".

6. Finally, the animal wipes its mouth and readjusts to a new hunting position.

In this chain, each response generates a new situation whose perception triggers the next proper response in the chain. It is clear, that in performing the entire sequence of prey-catching behavior an action-perception cycle [Arbib, 1981a, 1981b] takes place.

Behavioral studies have shown that prey-catching behavior in frogs and toads is released by relatively simple key-stimuli. The first characteristics these stimuli must have are movement and contrast [Ewert, 1976, 1980, 1984; Grüsser & Grüsser-Cornehls, 1976; Grüsser-Cornehls, 1984; Ingle, 1976b]. Ewert and collaborators [Ewert, 1976, 1980, 1984; Schürg-Pfeiffer & Ewert, 1981] have studied in detail one of the action patterns in prey-catching, the "orienting" behavior. They showed that both the size of a moving stimulus and its geometry in relation to the direction of motion play a prominent role in the prey-catching behavior of the animal: rectangular objects whose longest axis moves in the direction of motion ("worm-like") are treated as prey; while if the same objects are moved with their longitudinal axis perpendicular to the direction of movement ("antiworm-like"), the animal does not exhibit prey-catching orienting behavior, or may assume a freezing posture, or may even exhibit avoidance behavior (see Fig. 4Ba).
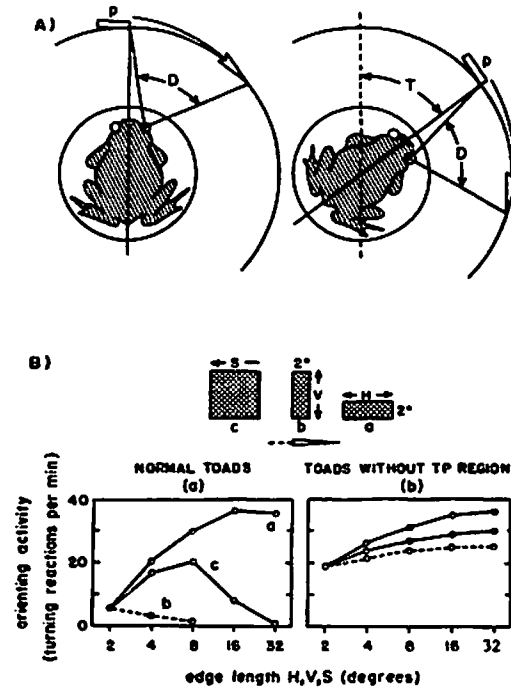
Figure 4: Turning behavior to different configurational stimuli.
A) Turning reaction to the stimulus presentation. D: effective angular displacement of the stimulus (p); T: angle of turning movements. B) Orienting activity to three stimulus configurations, horizontal ("worm": type a) and perpendicular ("anti-worm": type b) rectangles, and squares (type c). B.a) Normal toad's response; B.b) Response of toads with pretectal lesion [from Ewert, 1976].

Ewert *et al.* [1979] showed that in toads this "worm-antiworm" discrimination is invariant to both the direction of motion and to the velocity function of the stimulus. When the shape, size and background contrast of a prey-like stimulus were kept constant, the orienting rate activity R varied depending on the velocity function v as follows:

$$R = k_v \cdot v^\delta$$

where k_v and δ are constants. In the same way, when the contrast c is varied while all other parameters are held constant, the orienting activity changes as follows:

$$R = k_c \cdot c^\sigma$$

where k_c and σ are constants.

It is interesting to note that the search for these invariant behavioral operations has created some controversies between different laboratories. In *urodeles*, Luthardt and Roth [1979] reported that in Salamandra Salamandra worm-antiworm discrimination varies with the velocity, the animal preferring "worm-like" to "antiworm-like" stimuli at low velocities, while at high velocities the "antiworm-like" stimulus is more effective. However, Himstedt [1982] argues that this phenomenon is not observed in all salamanders, and that it probably depends on the animal's experience with certain types of prey; while Ewert (personal communication) has not found such change of preference.

Ingle and coworkers [Ingle, 1973a, 1976a, 1982a; Ingle & Cook, 1977] in frogs and Ewert and collaborators [Ewert, 1980; Ewert & Burghagen, 1979a] in toads have shown that the releasing value of prey stimuli can change depending on the motivational state of the animal. They showed that animals highly motivated (i.e. with hunger or by smelling worms) had low response thresholds and increase the response rate to prey stimuli, even to those normally ineffective. Ingle showed

that under these conditions, when a pair of "worm-like" stimuli (i.e., cylindrical objects attached to wire holders moving with their longitudinal axis parallel to the direction of motion) are present in the monocular receptive field, frogs prefer stimuli subtending a visual angle of 16 degrees to the normally preferred stimulus subtending a visual angle of 6 degrees, and present a lower latency in the response. That is, animals under an increased motivational state present an enhanced *response readiness* and a reduced response latency. Ewert and Burghagen [1979a] showed that although the prey-catching activity is greatly increased in motivated animals, the size selection phenomenon (i.e., determination of the *optimal prey-size* to be preferred) remains almost the same for, within certain limits, changes in the motivational state of the animal.

Predator-Avoidance Response

Although frogs and toads act as predators, they are preyed upon by other animals in their environment, such as snakes and birds [Brodie, 1977; Ewert, 1980, 1984; Ewert and Traud, 1979]. Frogs and Toads may show a variety of responses in the presence of a large dark (i.e., "predator-like") moving object. Depending on the stimulus parameters (e.g., shape and size) and its location in the visual field, the animal could present any of the following responses [Ewert, 1976, 1980, 1984; Ewert and Rehn, 1969; Ewert and Traud, 1979; Ingle, 1976a, 1976b; Grüsser and Grüsser-Cornehls, 1976]:

1. When confronted with a "threatening object", such as a rectangle moving as an antiworm, the animal sits without moving any part of the body.

2. If attacked by a "ground enemy" then the animal may turn away and jump or it may run from the stimulus. A toad may also stand up and inflate its lymphatic sacks making its body look bigger than normal.

3. Enemies flying over evoke ducking or jumping. When ducking the animal assumes a defensive posture, and before jumping it turns away from the
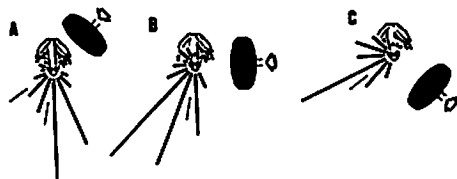
Figure 5: Directed avoidance behaviors in R. *Pipiens*.

See text for explanation [from Ingle, 1976a].

flying object.

4. Toads confronting a snake display a particular type of avoidance behavior: stiff-legged posture with inflated limphatic sacks, presenting the dorsal surface or flank of the body towards the head of the predator.

Grüsser and Grüsser-Cornehls [1976] observed that the avoidance response is not necessarily directed away from the threatening stimulus. Frogs confronting a bird regularly turn towards a refuge (i.e., water ditch) even if they have to jump towards the flying enemy.

Ingle [1976a, 1976b] proposed that, within the laboratory, the direction of the avoidance jump, when the animal is confronted with a looming black disc, depends on a compromise between the forward direction and the direction opposite to the direction of the threatening object. As can be observed in Fig. 5A, when the disc approached the frogs at 135 deg from their frontal midline, they jumped straight forward. If the disc was presented at 90 deg from the frontal midline then they jumped with a direction at 45 deg from the frontal midline into the

opposite visual field (Fig. 5B). Finally, frogs avoid a disc coming at 45 deg from the frontal midline by jumping further into the opposite visual field (Fig. 5C).

In toads, Ewert and Rehn [1969] determined an optimal size for a prey-like stimulus. These authors showed that when black discs of different sizes were rotated within a horizontal plane 10 cm above the toad's head, those of 47 deg diameter released maximal escape response (see Fig. 6A). Then they tested the effects of reducing the surface area of the disc (see Fig. 6B) and different disc-based patterns. They found that circular rings of 10 deg width and 50 deg diameter and a pattern of four discs of 10 deg diameter arranged in a square pattern with 30 deg between adjacent discs were equally effective as the disc of optimal size.

Grüsser and Grüsser-Cornehls [1976] and Ewert [1971, 1976] determined that avoidance behavior also depends on the stimulus velocity. In toads, Ewert found an approximately linear relationship between the avoidance activity and the stimulus velocity v for $1\,deg/sec < v < 50\,deg/sec$. In frogs, Grüsser and Grüsser-Cornehls found that, in a range of $1\,deg/sec < v < 60\,deg/sec$, the probability of eliciting an avoidance response increases as the stimulus velocity increases. In toads, enemy objects with a velocity function of $100\,deg/sec$ or more do not elicit an avoidance response [Ewert, 1976]; whereas in frogs in their natural habitat, avoidance responses to stimuli moving at $300\,deg/sec$ can be observed [Grüsser & Grüsser-Cornehls, 1976].

Neural Mechanisms for Prey-Catching and Avoidance behavior

The ultimate goal of neuroethology is to explain behavior in terms of levels of activity within neural networks. Thus, once the behaviors to be studied have been indicated and classified, the next step is to go inside the animal's brain and try to identify the neural mechanisms underlying such behaviors. This goal is
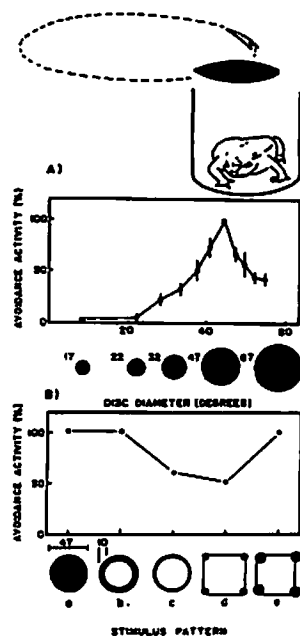
Figure 6: Key-stimuli for releasing Avoidance behavior.
A) Discs of different sizes, B) different stimulus patterns. See text for explanation
[from Ewert, 1976].

pursued by brain lesion and brain point stimulation experiments in combination with anatomical and physiological studies.

The Eye. In anurans, the size of the eyes is considerable and their periscopic position provides the animal with a large visual field. Using optical methods, Schneider [1954] and Fite and coworkers [Fite, 1973; Fite and Scalia, 1976] showed that in some species of frog the visual field subtends approximately 360 deg. Additionally, an extensive part of this field is binocular, it may extend some 40–55 deg below the horizontal meridian and some 160–170 deg over the head. Electrophysiologically, Gaze and collaborators [1959, 1962] measured the optic tectum monocular visual field. Their findings correspond rather well with results obtained by the optical methods.

The Retina. The Central Nervous System (CNS) starts processing visual information when light patterns hit the photoreceptors in the retina. The cell perikarya of the retina are organized into three layers [Dowling, 1976; Grüsser and Grüsser-Cornehls, 1976]: the "outer nuclear layer" (ONL), which is composed by the perikarya of the receptor cells; the "inner nuclear layer" (INL), which contains the perikarya of bipolar, horizontal and amacrine cells; and a third layer consisting of the ganglion cells. The synapses among retinal elements are mainly confined in two layers: the "outer plexiform" layer (OPL) containing synapses among receptors, and horizontal and bipolar cells; and the "inner plexiform" layer (IPL) involving synapses among bipolar, amacrine and ganglion cells.

The synaptic organisation of the frog retina is shown in Fig. 7. Processes from bipolar and horizontal cells make synaptic contacts with the receptors. The OPL also contains synapses between processes of the horizontal cells with dendrites of the bipolar cells, as well as with other horizontal cells processes (not shown in the figure) [Dowling, 1976]. The IPL contains synapses between bipolar
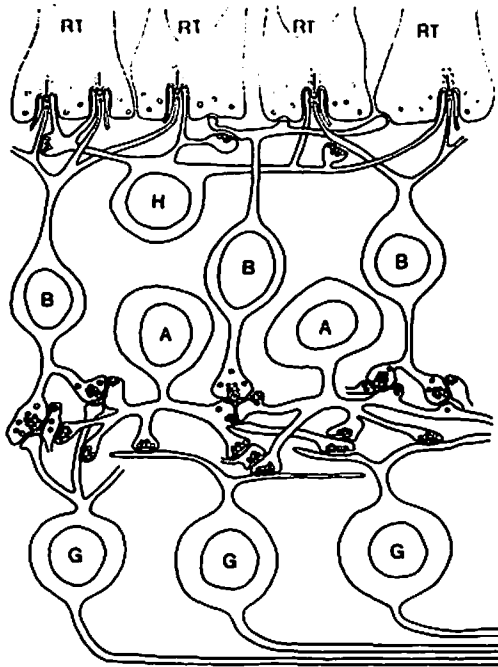
Figure 7: Synaptic contacts in the frog retina.
RT-receptor terminals; H-horizontal cell; B-bipolar cell; A-amacrine cell; G-ganglion cell [from Dowling, 1976].

terminals and amacrine cell processes, bipolar cell terminals and ganglion cell dendrites, amacrine processes and ganglion cells dendrites, and serial synapses between processes of morphologically identical amacrine cells.

In the present work we are interested only in the physiological properties of the ganglion cells, so the interested reader is referred to Shepherd [1979], Werblin and Dowling [1969] and Dowling [1976] for a detailed anatomical and physiological study. Additionally, an extensive review of the literature is found in Lee [1985].

Electrophysiological studies in frogs have classified different types of retinal ganglion cells according to their receptive fields or their responses to either simple flashes or complex stimulus patterns. Hartline [1940], recording from the retina, defined three types of ganglion cells: "on" neurons, "on-off" neurons and "off" neurons; whereas, Maturana et al [1960] recording from the optic tectum, defined four types: "sustained edge" detectors, "convex edge" detectors, "changing contrast" detectors and "dimming" detectors. Grüsser and Grüsser-Cornehls [1976], using the classification of Maturana et al [1960] with some modifications, defined six types of ganglion cells:

1. CLASS 0 neurons ("on" neuron). These cells respond to the onset of the stimulus, presenting a strong transient response to red light and a sustained response, which might last up to one minute, to blue light. It has an excitatory receptive field (ERF) of 4-15 deg of visual angle, and the simultaneous stimulation of the ERF and the inhibitory receptive field (IRF) yields a weak depolarisation. It responds to stimulus with velocities above 1 deg/sec, and it shows no directional sensitivity.

2. CLASS 1 neurons. This type of cells corresponds to the "edge" detector of Maturana et al [1960]. It shows no response to changes in diffuse illumination, and a sustained "on-activity" to a small spot projected onto its ERF. The ERF extends from 1.5 to 4 deg, and is surrounded by an IRF of 5 to 6 deg minimum.

3. CLASS 2 neurons. These cells are the "convex" detectors of Maturana et al [1960]. They have an ERF of 2.5 to 4 deg surrounded by an IRF which extends, depending on the type of stimulus, from 20 to 45 deg. The maximal

sensitivity of these cells lies in the center of the ERF. These units show no response to off stimulation of the whole receptive field, and, unlike class 1 neurons, they do not resume firing when the illumination is restored. The response of these units, for stimuli large enough to cover both the ERF and the IRF, is more strongly inhibited by the stimulus expansion perpendicular to the direction of motion. In addition, black stimuli on a white background are more effective than white stimuli on a black background.

4. CLASS 3 neurons. These cells are Hartline's [1940] "on-off" neurons, which are also Maturana's [1960] "changing contrast" detectors. The ERF is of 6-10 deg and it has in most cases an oval shape. The IRF extends from 12 to 20 deg in diameter. As long as the stimulus is smaller than the ERF, the response of these cells depends on the size rather than on the shape of moving stimuli. These units respond to both the onset and the termination of the stimulus. These neurons have their maximal sensitivity in the center of the ERF, and white stimuli on a black background are equally effective as black stimuli on a white background.

5. CLASS 4 neurons. These cells correspond to the "off" neurons of Hartline [1940], which are also called "dimming" detectors by Lettvin et al [1959]. These units respond with an increase in impulse rate to a reduction in illumination. The ERF of these cells is of 10 to 15 deg. Any stimulus that dims the ERF evokes a response regardless of the size.

6. CLASS 5 neurons. Maturana et al [1960] classified these cells as "dark" detectors, they respond continuously and their activity increases as the illumination decreases. They respond slowly to changes in background illumination and show no response to dark moving stimuli. These units are rarely observed in the retina or in the tectum.

Ewert has shown that in toads [Ewert, 1976, 1980, 1984] the response of retinal ganglion cells of type R2, R3 and R4 depends on the size, shape and geometry with respect to the direction of motion (see Fig. 8). The notation used by Ewert is equivalent to the one proposed by Grüsser and Grüsser-Cornehls [1976], differing only in an R before the cell's class number. The three types of ganglion cells respond almost with the same intensity to "worm-like" stimuli, rectangles moving along their longitudinal axis (type a in Fig. 8), of different sizes. To "antiworm-like", rectangles moving perpendicular to their longest axis (type b), or "square"
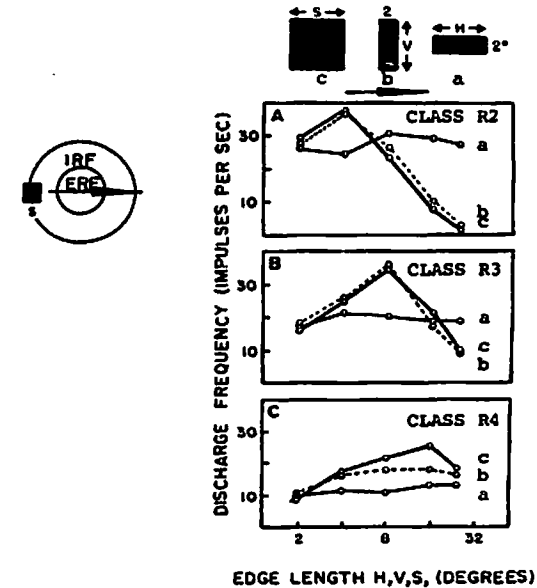
Figure 8: Response of toads retinal ganglion cells
Response of ganglion cells class R2, R3 and R4 to different configurations (type a, b and c) of moving stimuli with a visual angular velocity of 7.6 deg/sec [From Ewert, 1976].

stimuli (type c), ganglion cells class R2 and R3 increase their rate of response up to their respective receptive field sizes and then progressively decrease for larger objects; whereas cells class R4 increase their rate of response as the stimulus size increases, giving the strongest response to square stimuli.

Retinal ganglion cell response is also sensitive to the velocity function [Ewert, 1976; Finkelstein & Grüsser, 1965; Grüsser et al, 1967; Grüsser & Grüsser-Cornehls, 1976], contrast [Grüsser & Grüsser-Cornehls, 1976; Ewert, 1976, 1980], and chromatic composition of the moving stimulus [Grüsser-Cornehls & Saunders, 1981a,b]. The quantitative relationship between average impulse rate R of ganglion cells of all classes and the stimulus angular velocity can be expressed as follows:

$$R = kv^{\epsilon}$$

where k and ϵ are constants, k depending on other stimulus parameters, such as size, shape and contrast with respect to the background. Similarly, the relationship between the firing rate R and the stimulus contrast with respect to the background can be expressed by

$$R = kc^{\theta}$$

where k and θ are constants, and, again, k depends on the other parameters of the stimulus. Some ganglion cells class R2 and R3 also exhibit stronger response for a particular movement direction [Ewert & Hock, 1972; Ewert, Krug and Schönits, 1979]. From now on, when referring to ganglion cells, we wil follow Ewert's notation.

Retinotopical Projections. In the frog, the retina projects to five different regions in the brain. Three of them, the nucleus of Bellonci, the lateral geniculate nucleus and the pretectal neuropil area are located in the diencephalon; whereas

the other two, the optic tectum and the basal optic root, are in the mesencephalon [Székely & Lázár, 1976; Scalia & Fite, 1974; Scalia, 1976; Fite & Scalia, 1976]. This can be observed in Fig. 9. Ganglion cells of different classes project *retinotopically* to both the tectum and the thalamic pretectal region [Grüsser & Grüsser-Cornehls, 1976; Ewert, 1976, 1980; Fite & Scalia, 1976]. The retinotectal projection is contralateral; while the retino-pretectal is both contralateral and ipsilateral, though the contralateral projection is stronger. Neuroanatomical and neurophysiological studies in frogs [Potter, 1969, 1972; Lázár & Székely, 1969; Székely & Lázár, 1976; Witpaard & Keurs, 1975; Maturana et al, 1960] and in toads [Ewert & Hock, 1972; Ewert, 1976, 1980; Grüsser & Grüsser-Cornehls, 1976] have shown that the optic tectum receives axon terminals from retinal ganglion cells R2, R3 and R4, while the pretectum is activated by classes R3 and R4.

The Optic Tectum. A great deal of research has been aimed at trying to find the neuronal mechanisms responsible for visually guided behaviors. Thus, the next step is to study the Primary Visual Centers (PVC), those brain regions that receive topographical maps from the retina. In this section we explore the work done in the optic tectum, while in the next section studies of the thalamic pretectal region are reviewed.

In toads, lesion experiments [Ewert, 1976, 1980; Comer & Grobstein, 1981a, 1981b] have been used to show that prey-catching orienting and avoidance behaviors are disrupted when the tectum is destroyed. Furthermore, as might be expected, since the tectum receives information from the retina in a retinotopic way, electrical brain point stimulation experiments [Ewert, 1976, 1980] have shown that the stimulation of a specific tectal region, via an implanted microelectrode, elicits the prey-catching orienting response to the corresponding retinal projec-
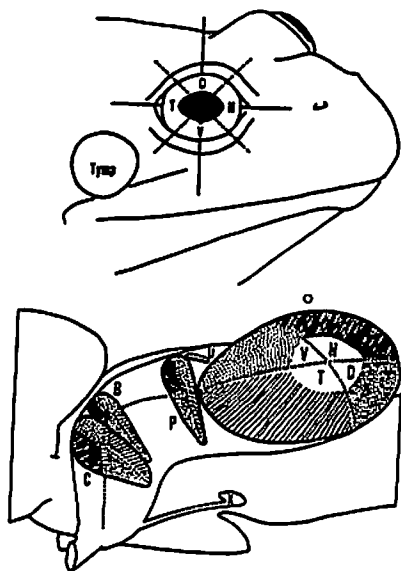
Figure 9: Retinal projections in the anuran brain
A) Labeling convention of the four quadrants of the eye: T—temporal, D—dorsal,
N—nasal and V—ventral. B) The retina projects to the optic tectum (O), nucleus
of Bellonci (B), lateral geniculate nucleus (C), thalamic pretectal neuropil (P) and
basal optic root (X) [from Scalia and Fite, 1974].

tion. This points to the tectum as playing a prominent role in eliciting visually guided behavior. Comer and Grobstein's [1981a, 1981b] experiments showed that in atectal animals the orienting behavior could be elicited by touch stimulation. This suggests that the activation of motor programs does not takes place in the tectum, but in a subsequent stage in the visual chain.

The optic tectum is the main visual center in the anuran's brain. Its main input consists of afferents fibres from the contralateral retina. Depending on the class, these fibres project to different depths of the most superficial tectal layers. Axon terminals from retinal ganglion cells class R2 reach the tectum at the most superficial part of layer 9 (see below), from class R3 deeper and class R4 even deeper into the same layer [Maturana et al, 1960; Gaze & Keating, 1968; Potter, 1969, 1972; Grüsser & Grüsser-Cornehls, 1976; Grüsser-Cornehls, 1984; Székely & Lázár, 1976; Lázár, 1984; Witpaard & Keurs, 1975].

In addition to the fibres from the contralateral retina, the tectum receives afferent fibres from other non-visual and visual centers. This can be observed in Fig. 10. Its ipsilateral input is comprised by fibres from the rostral thalamus, the nucleus posterolateralis thalami, the dorsal posterior nucleus thalami, the nucleus geniculate lateralis, the large-celled pretectal nucleus, and the anterodorsal, posterodorsal and posteroventral tegmental fields. Its contraletral input consists of fibres from the nucleus posterolateralis thalami, the dorsal posterior nucleus thalami and the optic tectum. Additionally, the tectum receives afferent fibres bilaterally from the nucleus isthmi, the ventral preoptic hypothalamus and the suprapeduncular nucleus[Rubinson, 1968; Lázár, 1969, 1984; Scalia & Fite, 1974; Trachtenberg & Ingle, 1974; Grüsser & Grüsser-Cornehls, 1976; Grüsser-Cornehls, 1984; Wicsynski & Northcutt, 1977; Grobstein et al, 1978, 1982; Székely & Lázár, 1976; Fite & Scalia, 1976; Gruberg & Udin, 1978; Mont-
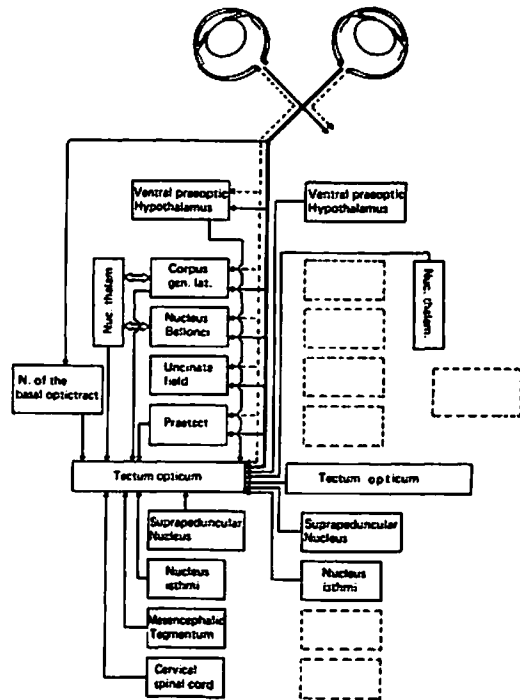
Figure 10: Projections from other brain regions to the tectum
Block diagram of the projections from the retina and other brain regions to the optic tectum [from Grüsser-Cornehls, 1984].

gomery, Fite & Grigonis, 1985].

The intrinsic architecture of the tectum has been the center of attention of many neuroanatomical studies since the time of Ramon y Cajal. Lázár and collaborators [Ssékely & Lázár, 1976; Lázár, 1983; Lázár, 1984] have conducted detailed Golgi and HRP studies of the frog optic tectum (see Fig. 11). The optic tectum of anuran amphibians is composed of nine different layers, which are numbered with arabic numerals in the left part of Fig. 11. Layer 9 is divided into seven sublayers, identified with capital letters in the same figure. The number of cells inside each tectum is of approximately 450,000 in *Rana Esculenta*. It is interesting to note that this number corresponds rather well with the number of retinal ganglion cells found by Maturana [1960].

Ssékely and Lázár, [1976] identified as many as seven different types of cells, which were classified according to their shape:

1. **Large Pear-Shaped cells.** These cells are located in layers 2, 4 and 6, and form two subgroups on the basis of the dendritic arborisation fields. Group type (a): with narrow dendritic tree, a single ascending dendrite that reaches layer 9, tiny basal dendrites, and an axon that originates from the main dendrite and ascends to layer 9 (marked with number 1 in Fig. 11). Group type (b): with a larger cell body and larger basal dendrites than type (a), they present an ascending single apical dendrite that rarely breaks up into two main branches, and do not have axons (marked with number 2 in Fig. 11).

2. **Small Perar-Shaped cells.** These cells constitute most of the cellular population in layer 8. The soma and the dendritic arborisation of these cells is very similar to those of large pear-shaped cells, but smaller and rarely present basal dendrites. The axon may originate from the perikarion opposite to the apical dendrite (marked with number 5 in Fig. 11), descend for a while and then turn back and terminate in the lower part of layer 9; or from the thicker dendrite and arborise within the dendritic tree (marked with number 6 in Fig. 11).

3. **Bipolar cells.** These cells are located in layers 8 and 9, and can be oriented vertically or horizontally. They obtain the form from the two main dendrites
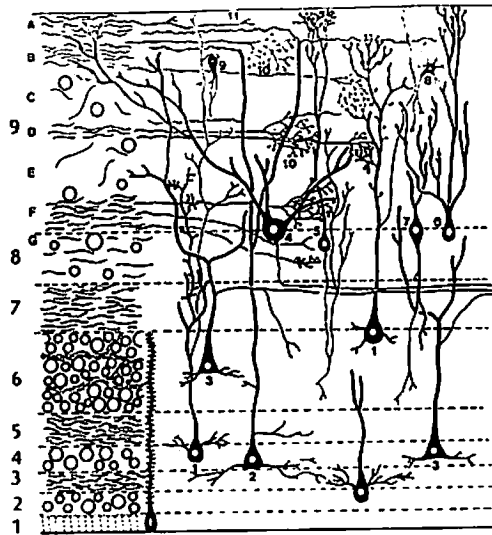
Figure 11: Intrinsic organisation of the Frog Optic Tectum.
Numbers on the left indicate the different tectal layers, while the letters indicate the sublayers of the most superficial layer 9. Tectal neurons are classified according to their shape, and labeled with numbers. (1) Large Pear-shaped cell with dendritic appendages and ascending axon. (2) Large Pear-shaped cell with dendritic collaterals. (3) Large Pyramidal neuron with axon projecting outside the tectum. (4) Large tectal Ganglionic neuron with efferent axon. (5-6) Small Pear-shaped cells with descending and ascending axons respectively. (7) Bipolar neuron. (8) Stellate neuron. (9) Amacrine cell. (10) Axon terminals from retinal ganglion cells. (11) Assumed evidence of Diencephalic fibres [from Székely & Lázár, 1976].

that originate in the opposite poles of the soma. In the vertical bipolar cells the axon originates from a dendrite and descends to layer 6 (marked with number 7 in Fig. 11); whereas in the horizontal bipolar cells it originates from the perikarion or from a dendrite and courses into layer 9.

4. Stellate neurons. These cells constitute the biggest part of the cellular population in layer 9. They have a few short dendrites, and thin axon-like processes that originate from such dendrites (marked with number 8 in Fig. 11).

5. Amacrine cells. These cells are also located in layer 9. They have small oval perikarya with their long axis perpendicular to the surface. These cells have only a single short process which splits into two or three branches, and are axonless (marked with number 9 in Fig. 11).

6. Pyramidal cells. They are found abundantly in layer 6. The perikarion is pyramidal or ovoid. These cells present a thick apical dendrite, which sends branches to the deeper sublayers of layer 9, and dendrites arising from the base of the cell body giving it a pyramidal form. The axon originates from the main or secondary dendrite, and at layer 7 it turns laterally, or medially if the neuron is close to the midline, and leaves the tectum. Therefore, this type of cell is regarded as an efferent element of the tectum (marked with number 3 in Fig. 11).

7. Large Ganglionic cells. These are the largest cells of the tectum. The diameter of their dendritic arborisation can reach up to 1mm. Large ganglionic cells can be found in the boundary of layer 8 and layer 9. Their axon originates from the cell body and descends to layer 7 where it leaves the tectum. Thus they are also regarded as efferent elements of the tectum (marked with number 4 in Fig. 11).

Other anatomical studies have suggested that more tectal cells project outside the tectum. Using the technique of retrograde filling with HRP, Gruberg and Lettvin [1980] reported that almost all types of tectal neurons became stained after an HRP injection in the nucleus isthmi; while Lázár et al [1983], using the technique of cobalt filling, identified two types of small pear-shaped cells in layer 8 as projecting to the nucleus isthmi.

As seen above, the tectum receives afferents fibres from the retina and from other brain regions. Diencephalic (marked with number 11 in Fig. 11) and retinal

inputs (marked with number 10 in Fig. 11) arrive at the superficial layer 9 of the optic tectum. Thalamic axon terminals can be seen in the most superficial sublayers, though they may ramify into deeper layers [Székely & Lázár, 1976].

Other classifications of tectal cells are the result of electrophysiological recordings [Lettvin et al, 1961; Ewert, 1976, 1980, 1984; Grüsser & Grüsser-Cornehls, 1976; Grüsser-Cornehls, 1984; Ingle, 1973b, 1975; Roth & Jordan, 1982]. Lettvin et al [1961] were the first in giving a classification of tectal cells on the basis of their physiological responses. They identified two types of cells:

1. "Newness" neurons. These cells have receptive fields of about 30 deg in diameter, with great overlap with those of other newness cells. They produce small responses to sharp changes in illumination, and their rate frequency increased when the stimulus presented a "jerky" movement. They habituate rapidily, and habituation is erased with a step of darkness.

2. "Sameness" neurons. The receptive field of these cells includes the whole visual field of one eye, but a "blind" spot. They do not respond to changes in illumination. They respond to the presence of an object in their receptive field by generating a pulse train of low frequency. They present the maximal response to stimuli of 3 deg in diameter. When presented with several stimuli simultaneously, they focus their attention on the one with the most irregular movement.

Ingle [1973b, 1975] studied behavioral and physiological correlates involved in prey-catching facilitation in frogs. He observed, and classified as "attention" units, two tectal neurons whose firing response accounted rather well for such a facilitation phenomenon:

1. Neurons giving a first burst of activity when the stimulus was presented, then a period of silence followed by a second burst of activity after the stimulus was removed, i.e., these cells presented rebound excitation.

2. Cells presenting a slow steady discharge for 3 to 6 seconds with a delay of 1 or 2 seconds after the stimulus was removed from the visual field.

Ingle [1973b] also observed that these cells were found more easily in animals with thalamic/pretectal lesions than in normal ones.
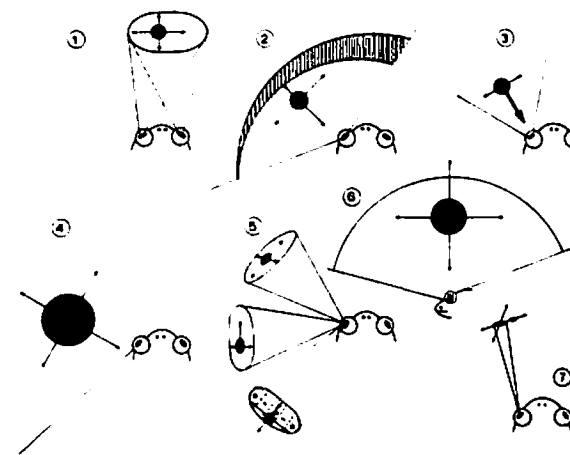
Figure 12: Schematic diagram of different tectal cells.
Classes (1 to 7) of tectal neurons found in *Rana Esculenta* [from Grüsser-Cornehls, 1984].

Grüsser and Grüsser-Cornehls [1976] provided a wider classification of tectal cells on the basis of their electrophysiological work on *Rana Pipiens*, *Rana Esculenta*, *Bufo Bufo* and *Hyla septentrionalis*. They found evidence for at least seven main classes of tectal cells in the anuran optic tectum (see Fig. 12):

1. Class T1. These cells have an oval ERF that extends from 15 to 30 deg over the binocular part of the visual field. They are located in the anterior and lateral part of the deeper tectal layers. Despite the location of their ERF, a subgroup of these cells is activated only by stimulation of the contralateral eye, another subgroup responds to monocular stimulation of the ipsilateral or contralateral eye, and a third subclass to the simultaneous stimulation of both eyes. Class T1 neurons respond to black or white stimuli moving on a contrast background, and become inactive when the stimulus is stopped

inside the ERF. The firing response of these cells depends on the velocity function of the stimulus, it increases as the stimulus velocity increases.

2. Class T2. The ERF of these cells extends more than 90 deg, including the binocular part. Despite including the binocular visual field, the response of T2 cells is driven monocularly by the contralateral eye when small objects subtending 2–15deg of visual angle are presented. A subclass of these neurons exhibits directional selectivity whereby the preferred direction points from the temporal to the nasal part of the visual field. Frequently, these cells display spontaneous activity. If the stimulus is stopped within the ERF then the neuronal response decreases to the spontaneous level within 1 to 2 sec. Likewise class T1 neurons, the response of T2 cells depends on the velocity of the stimulus.

3. Class T3. The ERF of these neurons is located predominantly in the nasal part of the visual field. Class T3 cells are found in the deeper regions of the anterior and lateral tectum. They present a short weak on–off or off response or none at all to changes in illumination. A strong neuronal response is produced by stimuli bigger than 3 deg moving along the s-axis towards the contralateral eye; whereas stimuli moving along the s-axis away from the animal yield no response.

4. Class T4. These cells are located in the deeper layers of the tectum, especially in the medial and caudal parts. Their ERF extends throughout the entire visual field, or a major part of it. Class T4 neurons are activated by small (less than 5 deg) or large (up to 30 deg) moving objects. These neurons display strong neuronal adaptation, which is limited to the part of the visual field stimulated during the last 30–50 sec.

5. Class T5. These cells have an oval ERF of 8 to 30 deg. They are probably the "newness" cells of Letttvin et al [1961]. A subclass of T5 neurons exhibits directional selectivity to an extent that varies from cell to cell; this subclass may correspond to the T5(1) neurons of Ewert [1976] (see below). A second subclass of T5 cells have a "striated" receptive field with excitatory zones interrupted by "silent" zones (perhaps equivalent to the blind spots of the newness cells of Lettvin et al [1959]). Class T5 neurons have been extensively studied from the physiological point of view, and later we discuss some of those studies in detail.

6. Class T6. The ERF of these neurons is located above the animal, and covers large monocular regions for both eyes. Therefore, a response of these cells is elicited by the left or right eye depending on the location of the stimulus within the visual field. A stronger neuronal response is obtained

if the stimulus is larger than 8 deg in diameter and its velocity is above 5deg/sec. The ERF of these cells extends frontocaudally at least 120 deg and left to right 90 deg. Neurons of this class are located in the medial and deeper layers of the tectum.

7. Class T7. These neurons have a very small receptive field of about 2 to 5 deg in diameter. These cells have been recorded within the superficial layer of the optic tectum. Therefore, it is assumed that the recorded impulses are "dendritic spikes". Class T7 cells do not respond to diffuse light on or off. They respond best to small moving objects with a side length of 1–2 deg. The response of these neurons increases as the stimulus velocity and contrast with the background increase.

Tectal cells of type T5 have been extensively studied. It has been reported that in toads [Ewert, 1976, 1980; Roth & Jordan, 1982] and in frogs [Schürg-Pfeiffer & Ewert, 1981] a subgroup of these cells, classified as T5(2) by Ewert following Grüsser and Grüsser-Cornehls' notation, responded to different configurations of moving stimuli with an overall firing level that resembled the probability that the stimulus under investigation fitted the prey category (see Fig. 13C). Moreover, when pretectal ablation occurs, the overall response of this tectal cell (T5(2)) also resembled the behavioral response of the animal to the different stimuli. That is, it responded indiscriminately to any moving object crossing its receptive field. (see Fig. 13D and compare it with Fig. 4Bb).

Ewert and collaborators [Ewert, 1980,1984; Ewert et al, 1979] found that the response preference of T5(2) cells was invariant to the stimulus direction of motion and velocity; whereas the response of T5(1) were directionally sensitive.

Other authors have reported a larger number of response type neurons with respect to the stimulus geometry and velocity. They found five different types of cells in the tectum of toads [Roth & Jordan, 1982] and of salamanders [Himstedt & Roth, 1980], some of which showed changes in their stimulus preference as the stimulus velocity was varied. The stimuli used during this study were moved hor-
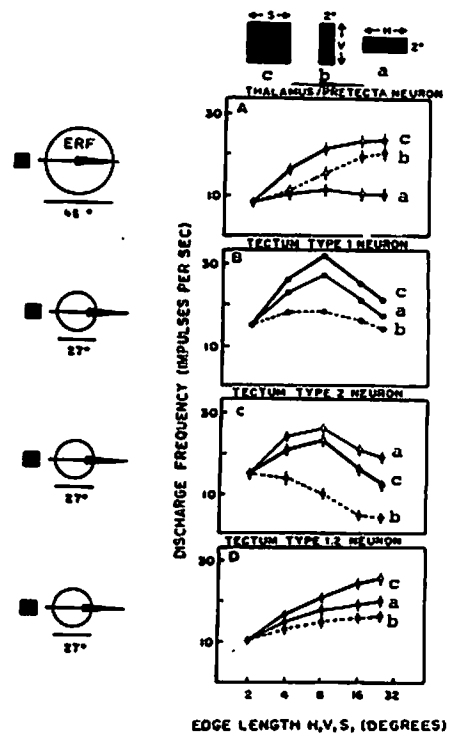
Figure 13: Response of Tectal and Pretectal cells to dummy stimuli. Tectal and pretectal cells response, in common toads, to different configurations of moving stimuli. A) Response of a pretectal neuron TH3. B) Response of a tectal cell T5(1). C) Response of tectal neuron T5(2). D) Response of both tectal cells (T5(1) and T5(2)) after thalamic pretectal lesions [From Ewert, 1976].

isontally, and were "squares" (S), and horizontal (H) and vertical (V) rectangles . That is, the latter were rectangles moved as "worm-like" or "antiworm-like" stimuli, respectively. They classified these cells as follows (see Fig. 14):

1. Neurons with preference $S > H > V$ (Fig. 14A). At low velocities, these cells preferred the square to the horizontal rectangle, and this stimulus to the vertical rectangle.

2. Neurons with preference $S > V > H$ (Fig. 14B). This group of cells also preferred best the square to the other stimuli, but now the vertical rectangle was preferred to the horizontal one. These cells are equivalent to the T5(1) of Ewert.

3. Neurons with preference $H > S > V$ (Fig. 14C). The best stimulus for these cells at all velocities was the horizontal rectangle, then the square and the weakest response was given to the vertical rectangle. This cells correspond to the T5(2) of Ewert.

4. Neurons with preference inversion $H \times S > V$ (Fig. 14D). At low velocities, these cells preferred the horizontal rectangle to the square, but at higher velocities this preference switched. At all velocities the vertical rectangle was the least effective.

5. Neurons with preference inversion $S > V \times H$. These authors claimed that at low velocities the horizontal rectangle was the least effective stimulus, while at high velocities the response to this stimulus increased such that it became as effective as the square, which was the best preferred by these cells. However, this inversion is not very easy to observe in Fig. 14E.

Axons from efferent tectal cells leave the tectum through layer 7 [Székely & Lázár, 1976; Lázár et al, 1983; Lázár, 1984]. Grüsser-Cornehls [1984] has summarised the anatomical work that has shown the ipsilateral and contralateral projections of the optic tectum. These projections occur through two main pathways (see Fig. 15): one ascending and one descending. The ascending path reaches, ipsilaterally, the nucleus of Bellonci and the corpus geniculatus lateralis, ipsilaterally and contralaterally, the pretectum and the nucleus medial thalami, and contralaterally, the nucleus isthmi. Through the descending path, the tec-

tum projects ipsilaterally to the tegmentum, the nucleus isthmi and the caudal brainstem [Ingle, 1982b; Grobstein, 1982; Lázár, 1984].

The Pretectum. The interactions among tectum and pretectum, both receiving retinal input, have been hypothesized to be the neural substrata for prey-predator discrimination [Ewert, 1980, 1984; Ingle, 1973b, 1980]. In addition, the pretectum has also been postulated to be involved in horizontal optokinetic nystagmus [Montgomery et al, 1981]. Ewert [1970, 1976] has shown that in toads lesions of the dorsal pc/pl region within the thalamic-pretectal region (i.e., "pretectum") disrupt the ability of the animal to discriminate different configurations of the stimulus (see Fig. 4Bb). He also observed that animals with pretectal ablation snap indiscriminately any moving object regardless of the size and shape, they switched their preference from white to black moving visual stimuli, and they lost size selectivity. He postulated an inhibitory effect from pretectum upon tectum as crucial the mechanism used by the animal to discriminate between different configurational stimuli. The hypothesis of Ewert that pretectal neurons modulate tectal activity through an inhibitory effect has been confirmed in frogs by Ingle and collaborators [Ingle, 1973b,1982b; Trachtenberg & Ingle, 1974]. These authors also found that there was some recovery of the avoidance behavior within a few weeks of the lesion. Although the animal never completely recovers its normal discriminatory ability, this suggests that, in addition to the pretectal inhibitory mechanism, there must be other mechanisms that in the absence of the pretectum inhibit tectal activity when large objects appear in the visual field.

Anatomically, using HRP and Golgi techniques, Montgomery et al [1985] conducted a detailed analysis of the morphology of pretectal neurons in *Rana Pipiens*. They established that, in addition to the retinal input, the pretectum receives afferents from other primary visual centers, e.g., tectum and the nucleus of the

basal optic root. They found four types of neurons within the pretectal region (see Fig. 16):

1. "Large" neurons with elongated soma 25 μm in diameter. These cells have long apical dendrites with second and third order branches occurring at an average of 30 μm and 150 μm from the soma. They also present basal dendrites emerging from the soma.

2. "Fusiform" neurons also with elongated somata 12 μm in diameter. These cells have a single apical dendrite and two basilar dendrites.

3. "Stellate" neurons with round somata 10 μm in diameter and two or three spineless dendrites which terminate in an end-bulb from which fine processes emerge.

4. A smaller class of cells 7.5 μm in diameter, which may be glial cells.

The pretectum projects to the optic tectum, the ventral brainstem, the opposite pretectum and the nucleus of the basal optic root [Fite and Scalia, 1976; Ewert, 1980; Ingle, 1980, 1982; Grüsser and Grüsser-Cornehls, 1976; Grobstein, 1982; Montgomery et al, 1985]. The large and fusiform cells project to the ipsilateral optic tectum, terminating in layers 7, 8 and 9 [Székely & Lázár, 1976; Montgomery et al, 1985].

Neurophysiologically, ten different types of cells that respond to visual stimulation have been described [Ewert, 1971, 1984]. Here, we only describe one of them, TH3, which has been postulated by Ewert [1976, 1980] to exert an inhibitory effect upon tectal cells during the process of prey-predator discrimination. The interested reader is referred to the original paper of Ewert [1971] or to the reviews done by Ewert [1984] and by Grüsser and Grüsser-Cornehls, [1976]. The pretectal cells TH3, defined physiologically by Ewert [1971], are movement sensitive cells with relatively small visual receptive fields. These cells have an ERF of 15 to 30 deg and respond to diffuse light only with a brief off burst. They were activated mainly by stimuli of at least 10 deg of visual angle moving
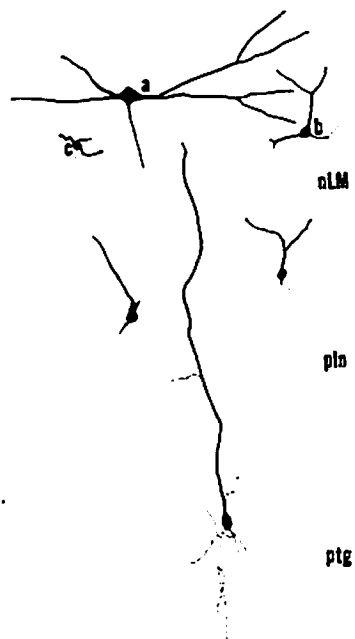
Figure 16: Pretectal Neurons.
Types of cells within the pretectal nucleus lentiformis mesencephali of *Rana Pipiens* as determined from HRP staining. a—large cells; b—elongated cells; c—stellate neurons [from Montgomery *et al*, 1985].

through their ERF. Their maximal response was to stimuli that covered the entire 30 deg of the ERF. When presenting different configurational ("dummy") stimuli, Ewert [1976, 1980] found that these cells responded mostly to non-prey stimuli (Fig. 13A). They preferred squares to antiworm-like stimuli, and the weakest response was to worm-like stimuli. Ewert suggested that this type of cell may exert an inhibitory effect upon tectal cell activity when the animal is confronted with large objects, allowing the animal, in this way, to orient towards the proper prey stimulus.

The pretectal effect upon the tectum is modulated by other brain structures. Ewert [1976] has shown that after an ablation of the forebrain, prey-catching behavior failed to occur, while predator-avoidance behavior was facilitated. If, in addition to ablation of the forebrain, the pretectal region was also lesioned then the animals recovered the capability of presenting prey-catching behavior, while predator avoidance was completely eliminated. Ewert suggested that the level of the pretectal inhibitory effect over the tectum is being modulated by the forebrain, which receives information from other senses, and so might be a result of the motivational state of the animal.

Theoretical Models of Visuomotor Coordination in Anurans

Models of processes related to visuomotor coordination in frogs and toads have been developed to conduct analyses at different levels. In this section we discuss two models [House, 1984; Ewert & Von Seelen, 1974] that follow a *Top-Down* approach, seeking to explain behavior in terms of interacting computation units, which may be classified as "schemas" [Arbib, 1981a], and two models [Didday, 1970, 1976; An der heiden & Roth, 1983] that exemplify the *Middle-Out* analysis,

seeking to relate functions described at the behavioral level to mechanisms defined at the neural level. Our models build upon a series of models of the anuran optic tectum and its interactions with the retina and pretectum developed by Lara and collaborators [Lara, 1982; Lara, Arbib & Cromarty, 1982; Lara & Arbib, 1982; Arbib & Lara, 1982]. These models will be discussed in detail in Chapter 3 and Chapter 4.

Didday's Model

Didday [1970, 1976] developed a theoretical model of the frog's optic tectum that accounts for the phenomenon of prey-selection. His motivation came from Ingle's [1968] study of the frog's snapping response when confronted with two "fly-like" stimuli. Ingle observed that if two fly-like objects, either of which is attractive enough that it alone could produce a snapping response, were presented in the animal's visual field then the frog could either snap at one of the stimuli, not snap at all, or snap in between the two objects at the "average fly". Didday's model suggested that different regions, arranged in layers, of the tectum compete in such a way that only the loci receiving the strongest stimulation from the retina sends an above-threshold signal to the motor output. He considered two layer of cells, the "foodness" layer receiving a retinotopic mapping from the retina and the "masked" layer that is in topographical correspondence with the foodness layer, and that produces the input to the motor centers (see Fig. 17). The masked layer interacts in a retinotopic correspondence with a population of "sameness" cells. Each "sameness" cell receives information from all the cells in the masked layer but the ones corresponding to its projection. That is, it contains a blind spot. At the same time, the sameness cell inhibits the activity of those cells in its region proportionally to the level of activity outside its region. This guaranties that a
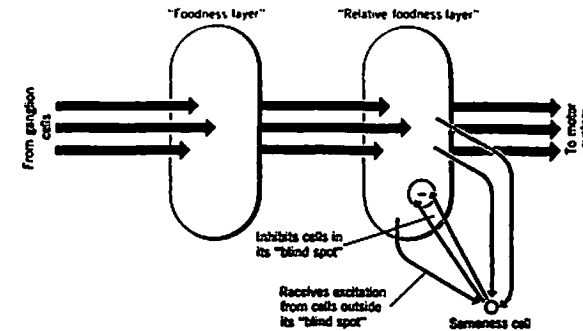
Figure 17: Didday's model of prey-selection

See text for explanation [from Arbib, 1972].

locus of activity reaches the motor centers only if its neighboring areas do not contain sufficiently high activity to counteract it.

With this network, Didday was able to explain the three possible behaviors observed by Ingle. That is, if the activity in one regions is much stronger than the the activity of any other region, then this region eventually overwhelms all other regions and a message to produce a snapping response at the corresponding space in the visual field is sent to the motor centers. If two regions are very active then two thing may occur: they may both, provided that they are very close, overwhelm all the other regions and a peak of activity would be produced in the overlapping region, which will yield a snapping response at the space corresponding to the region between the two original regions; or, if they are far apart, they may simply counteract each other's activity, as well as the activity of all other regions, in which case there will be no response at all.

Each element, "neuron-like", in Didday's model is represented by a lumped model, and so did not address the issue of of how the intrinsic tectal architecture might produce the prey-recognition required prior to the process of prey-selection. In the light of new empirical evidence, Lara and Arbib [Lara, 1982; Lara & Arbib, 1982] (see Chapters 3 and 5) redefine Didday's model so that the samness cells, instead of being inside the tectum, were located in the pretectum. That is, they postulated that prey-selection is the outcome of a closed loop interaction between tectum and pretectum. Additionally, these authors considered the anatomical architecture of the optic tectum and the interactions between tectal and pretectal elements. Thus, they postulated a neural network that explained how the internal architecture of the tectum might subserve prey-recognition and prey-selection.

House's Model

House [1984] developed a model of depth perception in toads and frogs. This model is composed by four different layers (see Fig. 18):

1. Layer A. An accommodative depth inference system, whose concern is to provide the model with monocular depth cues from lens accommodation.

2. Layer D. A disparity depth inference system which job is to provide the model with binocular depth cues from disparity matching.

3. Layer M. This layer represents a spatially organised field (Monocular Accomodative driven field) over which a depth mapping process based on monocular cues operates. This field sends to and receives from layer S excitatory connections, mapping in this way each local region in one layer onto the corresponding local region of the other layer. There is also competition among depth estimates within this field, in a manner similar to that used by Didday's model (see above).

4. Layer S. This layer represents a spatially organised field (Stereoscopic Disparity driven field) over which a depth mapping process based on binocular cues operates. As seen above, this layer has reciprocal excitatory connections with layer M, cooperating in this way to enhance the level of activity
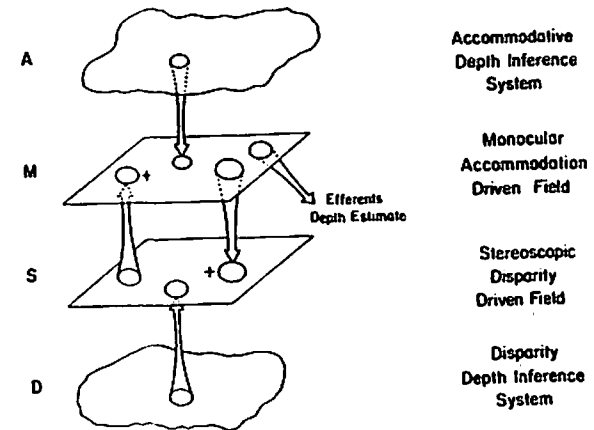
Figure 18: House's model of depth perception

See text for explanation [from House, 1984].

of the regions where both fields agree in their depth estimates. Similarly, there is competition among local regions inside this field.

In this model, the two depth mapping processes cooperate to create a single depth map, whose accuracy is governed by binocular cues and the lens accommodation cues are used to disambiguate the correspondence problem of stereopsis. Based on computer simulations, House suggested that frogs and toads use the mechanisms embodied in his depth perception model to navigate through the environment. This author [House, 1984] presented a second model, within the *Top-Down* approach, that explores how the processes of prey-selection and lens-accommodation might interact to correct incorrect binocular matches. Both models are high-level models, which seek to explain behavior in terms of the spatial distribution of response, but they do not present the details of temporal processing.

Ewert and von Seelen's Model

Ewert and von Seelen [1974] developed a theoretical model to analyse how the interactions among retina, optic tectum and pretectum would suffice for the physiological responses exhibited by tectal cells T5(2) to rectangular moving objects. As described earlier in this Chapter, Ewert [1976] found that this cell responds better to "worm-like" stimuli than to "square" or "antiworm-like" stimuli. Additionally, brain lesion experiments have shown that toads [Ewert, 1976, 1980] and frogs [Ingle, 1973b] with pretectal lesions will attack large moving stimuli which a normal animal will avoid. These observations suggested that prey-predator discrimination may be the result of an inhibitory effect from pretectum upon tectum. In Ewert and von Seelen's model, retinal output was passed to a tectal "worm filter", and to a "pretectal filter", with the output of the latter inhibiting tectal

(T5(2)) activity which was excited by the former. Their model can be observed in Fig. 19A. Fig. 19B shows how a worm-like stimulus would tend to produce a strong excitation of the worm filter and little inhibition of the the pretectal antiworm filter, thus yielding a vigorous T5(2) response; while in Fig. 19C we can observe that an antiworm-like object would have the opposite effect on the filters yielding a very weak activity in T5(2). The square would produce an intermediate behavior, as can be observed in Fig. 19D. Ewert and von Seelen were able to adjust the model parameters to fit the empirical data over a linear subrange of the results. However their model was "lumped" in both space and time. Thus, while the level of activity of the output properly reproduces the average level of activity of T5(2), which correlates well with the average turning rate of the toad, their model cannot explain the spatio-temporal of the animal's behavior.

An der Heiden and Roth's Model

An der Heiden and Roth [1983] have proposed a lateral inhibition model of tectum which can reproduce important properties of "worm-antiworm" discrimination. This model unlumps Ewert and von Seelen's model a step further, though it still does not address the issue of of intrinsic tectal architecture, nor does it consider the tectal-pretectal interactions defined by Ewert [1976] and Ingle [1973b]. The essential feature of their model (see Fig. 20) is that it postulates that the response of the tectum is the outcome of the spatio-temporal summation of the activity of retinal ganglion cells type R2 and R3, and of lateral recurrent inhibition among tectal elements. With this model, they were able to adjust the level of lateral inhibition required to reproduce the response of tectal cells T5(2), obtained by Ewert [1976,1980], to squares or antiworm-like objects. Because of the tectal architecture proposed in their model, the response of T5(2) cells increases as the

Figure 20: An der Heiden and Roth's model.
Tectal elements (TC) receive axon terminals from retinal ganglion cells (RGC), as well as from other tectal elements [from An der Heiden and Roth, 1983].

stimulus size increases, so T5(2) response to large prey objects is not reproduced. The authors suggested that an influence, from thalamic or pretectal cells, upon the tectum could be assumed in the presence of non-prey objects. Additionally, for the same reason, their model could not explain the disinhibitory effect in the tectum, after pretectal lesion, observed by Ewert [1976, 1980] in toads and by Ingle [1973b] in frogs.

Figure 19: Ewert and von Seelen's model of prey-predator discrimination.

A) The retina, tectum and pretectum act as filters. One tectal cell is a "worm filter" and a pretectal neuron (TH-3) is an "antiworm filter"; whereas another tectal neuron (T5(2)) receives excitation from the tectal filter and inhibition from the pretectal filter. B) When a "worm-like" object is presented, the tectal filter response is strong and there is almost no pretectal activity, so the level of activity of T5(2) is high. C) The response of tectal and pretectal filters is strong when a "square" stimulus is presented, so that T5(2) response becomes weaker. D) When an "antiworm-like" object is presented, the pretectal filter activity is strong and the tectal filter response is almost null, thus T5(2) presents almost no response [from Ewert, 1974].

CHAPTER III

A NEURAL NET MODEL OF THE OPTIC TECTUM

Introduction

The study presented in this chapter builds on a family of models developed by Lara and Arbib [Arbib & Lara, 1982; Lara & Arbib, 1982; Lara et al, 1982]. First, in Lara et al [1982], they simulated a single tectal column to reproduce behavioral and physiological results obtained during prey-catching facilitation. Then, in Arbib and Lara [1982], they analyzed an array of these tectal columns to provide a one-dimensional model of the tectum which reproduced the facilitation of tectal response when the stimulus is elongated along the direction of motion as well as facilitation to double stimuli moved along the direction of motion, with the preference of the animal being to orient to the leading of the two objects. Finally, in Lara and Arbib [1982],these authors incorporated some notions of Didday [1970, 1976] and Amari and Arbib [1977] to form a one-dimensional model of interactions among retina, optic tectum and pretectum for prey selection. With the expansion to two dimensions, in the present project, we have been able to reproduce prey-predator recognition and changes in response latency depending on the motivational state of the animal, all this being independent of the direction of motion of the stimulus. This work, then, offers the latest stage in the *evolutionary development* of a computational model of increased hierarchical complexity showing how different regions of the anuran brain may interact with each other

to control the animal's behavior [refer to Arbib, 1982].

Ethological studies [Ewert, 1976, 1980; Grüsser & Grüsser-Cornehls, 1976; Ingle, 1976; Schürg-Pfeiffer & Ewert, 1981] have shown that there are fixed action patterns in frogs and toads released by relatively simple key-stimuli. Both the size of a moving stimulus and its geometry in relation to the direction of motion play a prominent role in the prey-catching behavior of the animal: rectangular objects whose longest axis moves in the direction of motion ("worm-like") are treated as prey; while if the same objects are moved with their longitudinal axis perpendicular to the direction of movement ("antiworm-like"), the animal does not exhibit prey-catching orienting behavior, or may assume a freezing posture, or may even exhibit avoidance behavior [Ewert, 1976] (see Fig. 21Ba). In toads this "worm-antiworm" discrimination is invariant to both the direction of motion [Ewert et al, 1979] and to the velocity function of the stimulus [Ewert, 1976, 1980]. Luthardt and Roth [1979] reported that in Salamandra Salamandra worm-antiworm discrimination varies with the velocity, the animal preferring "worm-like" to "antiworm-like" stimuli at low velocities, while at high velocities the "antiworm-like" stimulus is more effective. However, Himstedt [1982] argues that this phenomenon is not observed in all salamanders, and that it probably depends on the animal's experience with certain types of prey, and Ewert (personal communication) has not found such change of preference. In Chapter 5 we analyze this controversy in detail.

Ingle and coworkers [Ingle, 1973, 1976, 1981; Ingle & Cook, 1977] in frogs and Ewert and collaborators [Ewert, 1980; Ewert & Burghagen, 1979] in toads have shown that the releasing value of prey stimuli can change depending on the motivational state of the animal. They showed that animals highly motivated (i.e. with hunger or by smelling worms) had low response thresholds and in-

crease the response rate to prey stimuli, even to those normally ineffective. Ingle showed that under these conditions, when a pair of "worm-like" stimuli (cylindrical objects attached to wire holders moving with their longitudinal axis parallel to the direction of motion) are present in the monocular receptive field, frogs prefer stimuli subtending a visual angle of 16 degrees to the normally preferred stimulus subtending a visual angle of 6 degrees, and present a lower latency in the response. Following Ewert's hypothesis of pretectal inhibition upon tectal activity, Ingle suggested that changes in size preference and in response latency could also be modulated by the pretectum. He postulated that for small objects tectal cells are mostly guided by retinal ganglion cells of type R2, and the effects of ganglion cells type R3 and R4 upon the optic tectum (henceforth referred to as "tectum" for short) are normally counteracted by a pretectal inhibitory effect. He suggested that R2 cells overcome pretectal inhibition through a facilitatory effect, which is a consequence of recurrent excitatory activity, though this response has a longer latency. In this way, he explained why animals normally prefer small stimuli. Whenever pretectal inhibition is decreased, either by an increased motivational state or by a lesion, tectal response is now controlled by ganglion cells that respond to larger objects (class R3 and R4), i.e., cells with bigger receptive fields, thus increasing the *response readiness* and reducing the response latency.

Ewert [1980] showed that prey-catching activity is greatly increased in motivated animals. He and Burghagen [1979] argue that the size selection phenomenon (determination of the *optimal prey-size* to be preferred) remains almost the same for, within certain limits, changes in the motivational state of the animal (see Fig. 33A).

A great deal of research has been aimed at trying to find the neuronal mechanisms responsible for these processes. In toads, lesion experiments [Ewert,

1976,1980; Comer & Grobstein, 1981] have been used to show that prey-catching orienting behavior is disrupted when the tectum is destroyed. Furthermore, as might be expected, since the tectum receives information from the retina in a retinotopic way, electrical brain point stimulation experiments [Ewert, 1976, 1980] have shown that the stimulation of a specific tectal region, via an implanted micro-electrode, elicits the prey-catching orienting response to the corresponding retinal projection. This points to the tectum as being involved, playing a prominent role, in this sort of behavior.

Ewert [1970, 1976] has also shown that in toads lesions of the dorsal pc/pl region within the thalamic-pretectal region (henceforth referred to as "pretectum" for short) disrupts the ability of the animal to discriminate different configurations of the stimulus (see Fig. 21Bb). He also observed that animals with pretectal ablation snap indiscriminately to any moving object, they switched their preference from white to black moving visual stimuli, and they lost size selectivity. This suggested that interactions among retina, tectum and pretectum may be the neural substrata for processes like prey-predator discrimination, response latency, size selection, and size constancy. The hypothesis of Ewert that pretectal neurons modulate tectal activity through an inhibitory effect has been confirmed in frogs by Ingle and collaborators [Ingle, 1973b,1982b; Trachtenberg & Ingle, 1974]. They found that there was some recovery of the behavior within a few weeks of the lesion, although the animal never completely recovers its normal discriminatory ability. This suggests that there must be other mechanisms, probably inside the tectum itself, which in addition to the pretectum exert an inhibitory effect upon the tectum, giving the animal the ability to discriminate between worm and antiworm stimuli. These mechanisms somehow must increase their participation in the absence of pretectal activity, and so might in this way be responsible for
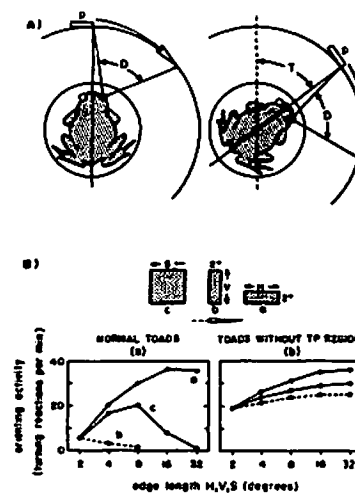
Figure 21: Prey-catching orienting behavior
Prey-catching orienting behavior to different configurations of the stimulus. A) Turning reaction to the stimulus presentation. D: effective angular displacement of the stimulus (p); T: angle of turning movements. B) Orienting activity to three stimulus configurations, horizontal ("worm": type a) and perpendicular ("anti-worm": type b) rectangles, and squares (type c). B.a) Normal animal's response becomes more frequent if dimension (H) of a stimulus type a is larger, whereas response frequency rapidly drops to zero if dimension (V) of a type b stimulus is larger, and a sort of summation of these two responses is obtained when both dimensions of stimulus type c are incremented. B.b) This discrimination is lost in toads with pretectal lesions [From Ewert, 1976].

the recovery. Ewert [1976, 1980] reported a cell in the optic tectum (T5(3)) that was most sensitive to large stimuli which, through interactions with other tectal cells, is a good candidate for being such a mechanism. This cell has also been postulated to be involved in avoidance behavior and will be fully discussed in a future report [Cervantes-Péres et al, 1985].

Trying to establish the role that each one of these brain regions may play in the control of these behaviors, physiological studies [Ewert, 1971, 1976, 1980; Ewert & Hock, 1972; Ewert, Krug & Schönits, 1971; Grüsser & Grüsser-Cornehls, 1976; Grüsser-Cornehls & Saunders, 1981a,b; Grüsser-Cornehls, 1984; Roth & Jordan, 1982] have been conducted at the retinal, tectal and pretectal levels to analyse neural responses to changes in different parameters of visual stimuli. It has been shown that in toad and frog, retinal ganglion cells of type R2, R3 and R4 respond with almost the same intensity to a "worm-like" stimulus (type a in Fig. 22). To an "antiworm-like" or a square stimulus (same figure, types b and c respectively) the response rate of ganglion cells type R2 and R3 initially increased up to the size of their respective excitatory receptive fields (ERF) and then progressively decreased for larger objects [Butenandt & Grüsser, 1968; Ewert, 1976, 1980; Schürg-Pfeiffer & Ewert, 1981]; while R4 ganglion cells increase their response when the size of stimuli of type b or c is extended (see Fig. 22C), giving the strongest response to a stimulus of type c. Ganglion cells R2, R3 and R4 also increase their rate of response depending on the angular velocity of the object [Ewert, 1976; Grüsser & Grüsser-Cornehls, 1976]. There are class R2 and R3 ganglion cells exhibiting stronger response for a particular movement direction [Ewert & Hock, 1972; Ewert et al, 1979b]. However, almost no cells have been recorded showing null-directions. Thus, directional sensitivity at this level may not significantly contribute to the processing of visual signals.
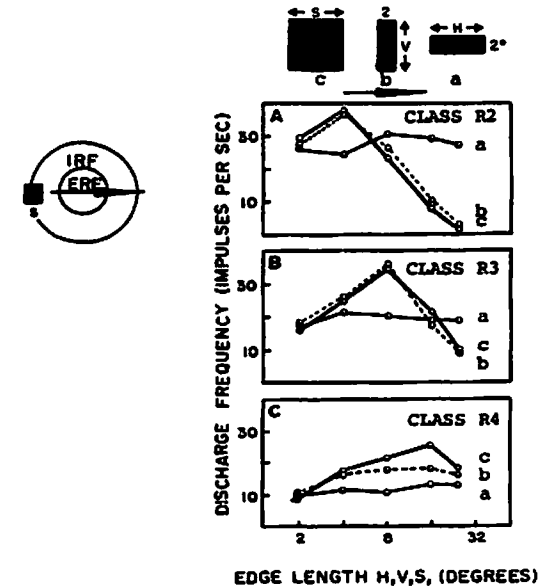
Figure 22: Retinal ganglion cells response
R2, R3, and R4 ganglion cells response to different configurations (type a, b and c) of moving stimuli with a visual angular velocity of 7.6 deg/sec. Left, they present a receptive field formed by a central excitatory (ERF) and a peripheral inhibitory (IRF) area. The three ganglion neurons respond almost with the same intensity to stimulus type a of different sizes. For stimulus type b and c, ganglion cells R2 and R3 increase their rate of response up to their respective receptive field sizes and then drop it down, whereas R4 cells increase their rate of response as the stimulus size increases, giving the strongest response to stimuli of type c [From Ewert, 1976].

At the tectal level, it has been reported that in toads [Ewert, 1976, 1980; Roth & Jordan, 1982] and in frogs [Grüsser & Grüsser-Cornehls, 1976; Grüsser-Cornehls, 1984; Schürg-Pfeiffer & Ewert, 1981] some cells, classified as T5(2) by Ewert following Grüsser and Grüsser-Cornehls' notation, responded to moving configurational visual stimuli with an overall firing level that resembled the probability that the stimulus under investigation fitted the prey category (see Fig. 23C). Moreover, when pretectal ablation occurs, the overall response of this tectal cell (T5(2)) also resembled the behavioral response of the animal to the different stimuli. That is, it responded indiscriminately to any moving object crossing its receptive field. (see Fig. 23D and compare it with Fig. 21Bb).

Ewert et al [1979a] also showed that T5(2) cells could discriminate between prey and non-prey stimuli independently of the direction of motion while other tectal neurons, classified as T5(1), were directionally sensitive. Based on these results, following Ewert's original hypothesis, it is suggested that tectal neuron type T5(2) must play an important role in the discrimination between prey and non-prey stimuli and in indicating the position to which the animal should orient next. T5(2) neurons perform this behavior through combined activity with pretectal cells, possibly through an inhibitory effect [Ewert & von Seelen, 1974], both regions receiving retinal input. One of the pretectal cells, classified as TH3 by Ewert [1971], responded mostly to non-prey stimuli (Fig. 23A), and so it has been postulated to exert an inhibitory effect upon tectal cell activity when large objects are presented, thus allowing the animal to orient to the proper prey stimulus.

Other authors [Luthardt & Roth, 1979; Himstedt & Roth, 1980; Roth & Jordan, 1982] claim to have found different types of neurons in the tectum whose stimulus preference varies with changes in stimulus velocity. These authors suggest that the properties of prey-orienting and prey-catching behavior are the out-
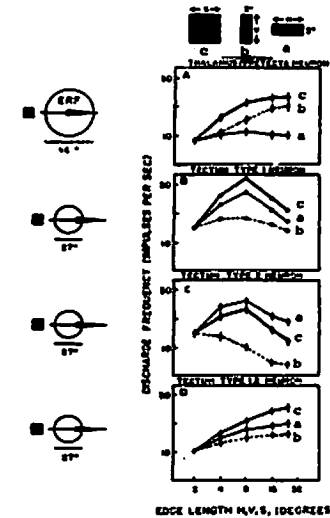
Figure 23: Tectal and Pretectal cells response
Tectal and pretectal cells response, in common toads, to different configurations of moving stimuli (see Fig. 21 legend). A) Response of a pretectal neuron TH3 which is mostly sensitive to large (type c) and perpendicular (type b) stimuli. B) Response of a tectal cell T5(1) which is most sensitive to stimuli type c than to type a or type b. C) Response of tectal neuron T5(2) that prefers mostly stimuli type a to type c, and gives a very weak response to type b. This neuron's response resembles the animal's behavior (see Fig. 21B). D) Response of both tectal cells (T5(1) and T5(2)) after thalamic pretectal lesions. It shows how the discriminative abilities of these cells are lost (From Ewert [1976]).

come of the joint activity of several neurons, rather than the response of a single neuron. Ewert and coworkers [Ewert, 1980; Schürg-Pfeiffer & Ewert, 1981] also postulate a theory of coordination of motor schemas, where there are recognition units for prey stimuli but they need the activity of other neurons or neural units, such as binocularity or depth perception neurons, to control prey-catching orienting behavior. Our model has been focussed on the behavioral correlates of activity in single cells, but in the Discussion of this chapter we propose a preliminary hypothesis of how the activity of several neurons, including the prey-recognition units, could control prey-catching orienting behavior. However, further studies, both theoretical and empirical, should clarify the real nature of these processes.

Modelling Procedures

The description of the model is divided into four parts; a brief explanation of the proposed architecture for the two-dimensional model of the tectum, a description of the *black box* model of the retina that supplies the retinal input corresponding to different visual stimuli, the description of pretectal cell TH3, and the proposed interactions among retina, tectum and pretectum subserving prey-predator recognition, size preference and response latency.

Two-dimensional Model of the Optic Tectum

Previously, Lara, Arbib and Cromarty [1982] analysed anatomical data from Székely and Lázár [1976], which emphasised the vertical organisation of the tectum, with a local *vertical sample* of the tectum being referred to as a *tectal column* — though with no suggestion of the sharp transitions between properties of adjacent columns suggested by some studies of mammalian cortex. These authors

offered a family of mathematical models of the tectal column (Fig. 24). Each column of the model comprises one glomerulus (GL), one large (LP) and one small (SP) pear shaped cell, one stellate neuron (SN) and one pyramidal (PY) cell, the only efferent cell of the column (see Chapter 4). In their model they hypothesise that PY corresponds to the neuron classified as T5(2) by Ewert. The present two-dimensional model of the optic tectum (see Fig. 25), is composed of an array of 8 by 8 tectal columns receiving retinal input from ganglion cells classes R2, R3 and R4. For this model the number of cells and their interactions has greatly increased. Here, the most important considerations are briefly described.

The main retinal input to the tectum is represented by ganglion cells R2 with excitatory receptive field (ERF) sizes of 2-4 deg [Grüsser et al [1976]; Ewert, 1980], so it is proposed that every column has a *focal* receptive field equal to the maximum ERF of ganglion cells R2 (4 deg) and a *non-focal* (8 deg) overlap with its neighbors' receptive fields. The receptive field of each element of the column is calculated according to their lateral interaction with neurons of other columns (see below). The interconnections among cells of a column are shown in Fig. 24, while lateral connections among cells of neighboring columns are all indicated in Table 1:

Table 1: Lateral interactions among tectal columns

Cells of column (i,j) receive afferents from cells of neighbor columns.			
	Cells of neighboring columns to (i,j) that impinge upon its neurons		
Cells of column (i,j)	GL	LP	SP	SN
GL		+	+	
LP			+	−
SP	+			
SN		+		
PY		+		

9 ___

8 ___

7 ___

6 ___

LAYERS
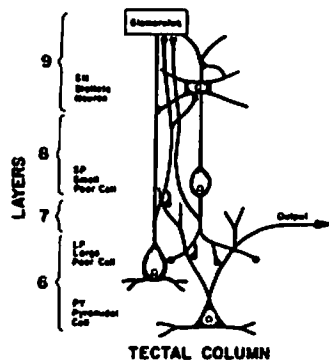
TECTAL COLUMN

Figure 24: Interconnections among cells of a tectal column
The pyramidal cell (PY) is activated by large (LP) and small (SP) pear shaped cells. The stellate neuron (SN) is excited only by the LP cell. The SP cell receives excitatory afferents from the glomerulus (GL), and it is inhibited by the SN neuron. The LP cell is excited by both the SP cell and the GL, and it is also inhibited by the SN neuron. GL receives afferents from recurrent axons of LP and SP cells. GL, LP and SP also receive afferents from retinal ganglion cells R2, whereas PY receives from R2, R3 and R4 [from Lara and Arbib, 1982] (see Fig. 25 and Fig. 26B).

a) The glomerulus (GL) is a synaptic complex comprising specific connections among axonal terminals from retinal ganglion cells, diencephalic regions, and recurrent axons (from LP and SP cells) and dendritic arborisations from tectal neurons, both from its own column as well as from neighboring ones. Each glomerulus has a receptive field of 12 deg, 4 focal deg plus 8 deg of overlap. This assumption is based on the fact that retinotectal axons project to a receptive field no larger than 15 deg [Ingle, 1973a].

b) Each small pear-shaped cell (SP) is activated by retinal ganglion cells of type R2 through the glomerulus and interglomerular dendrites both from its own and from neighboring columns. This cell is also inhibited by the stellate neuron (SN) from its own column. Thus, each SP cell has a receptive field of 16 deg, which is in accordance with physiological evidence that showed that the receptive field of superficial tectal cells range between 16 and 20 deg [Ingle, 1973b, 1982]. The role of the SP cell is the integration of the general state of activity in the tectal column to determine the proper time(s) for vertical recruitment of excitation to facilitate a response in the efferent (PY) neuron.

c) Each large pear-shaped cell (LP) receives afferents from retinal ganglion cells of type R2, both through the glomerulus and through its dendrites along the length between glomerulus and cell body, from the SP cells of its own column as well as of neighboring columns, and it is inhibited by the SN of its own and of neighboring columns. Lateral connections make its receptive field approximately 24 deg, which is in agreement with the observed receptive field for some cells in layer 6 of the tectum. Such a cell maintains both the activity level of its own column (glomerulus) and the state of excitation of neighboring glomeruli through collateral axons, thus spreading the excitation across the tectum when a "prey-like" stimulus is present.

d) The stellate neuron (SN) receives afferents from the LP cell, both from its own column and from neighboring columns. This cell is a candidate to produce inhibition [Székely & Lázár, 1976], so it is proposed as the only inhibitory cell in the model. Its function is to control the level of tectal activity.

e) The pyramidal cell (PY) is the only efferent of the tectal column model. It receives afferents from ganglion cells of type R2, R3 and R4, from the SP and LP cells of its own column and from the LP cell of neighboring columns, expanding its receptive field to approximately 28 deg, which agrees with physiological findings of Ewert [1976, 1980] for T5(2) cells.

For further details about empirical basis for elements of the tectal column and their roles in the processing of information refer to Lara et al [1982].

Black Box Model of the Retina

Visuomotor coordination in frogs and toads involves interactions among brain structures receiving a direct (Primary Visual Centers (PVC)) or indirect (some of the Modulatory Regions (MR)) topographic projection from the retina. Optic tectum and Pretectum are among those PVC's, while Nucleus Isthmi is an example of a MR and it is activated by visual information through its retinotopic mapping with the tectum. Thus, any model of PVC's and their interactions with other PVC's or MR's requires a model of the retinal processing of visual information.

Our models of the retino-tectal-pretectal interactions subserving prey-predator discrimination consider anatomical and neurophysiological experiments in frogs [Potter, 1969, 1972; Lázár & Székely, 1969; Székely & Lázár, 1976; Wit-paard & Keurs, 1975; Maturana et al, 1960] and in toads [Ewert & Hock, 1972; Ewert, 1976, 1980; Grüsser & Grüsser-Cornehls, 1976] which showed that the

optic tectum receives axon terminals from retinal ganglion cells R2, R3 and R4, while the pretectum is activated by classes R3 and R4. Additionally, our study is concentrated on specific configurations of moving "dummy" stimuli. Therefore, a retina model that generates the proper response of ganglion cells R2, R3 and R4 to such stimuli is required.

In this Chapter, a Black Box (curve fitting) retina model is described. This model generates the overall firing rates of R2, R3 and R4 in response to different configurational moving stimuli. It includes the fact that retinal ganglion cells are sensitive to several stimulus characteristics, such as size, geometry in relation to the direction of motion, angular velocity function, contrast [Grüsser & Grüsser-Cornehls, 1976; Ewert, 1976, 1980], and chromatic composition of the moving stimulus [Grüsser-Cornehls & Saunders, 1981a,b]. So far, we have only considered black stimuli on a white background, so the last two were treated as constants during the simulations.

Our Black Box model of different ganglion cells (types R2, R3, and R4) is based on the curves obtained by Ewert for their responses to different configurational stimuli (see Fig. 22), and the angular velocity function obtained by Grüsser and collaborators [Finkeltein & Grüsser, 1965; Grüsser & Grüsser-Cornehls, 1976] and Ewert [1976, 1980]. That is, the model simply defines the average response rate (as distinct from the course of firing) of ganglion cells R2, R3 and R4 depending on the stimulus size, geometry and velocity; the first with Ewert's graphs and the second with the equation

$$R = kv^\delta$$

where k and δ are constants and v is the angular velocity function of the object; k depending on other stimulus parameters, such as size, shape and contrast with respect to the background. R is the frequency response of the retinal cell.

Ganglion cells project *retinotopically* to each tectal and pretectal column [Grüsser & Grüsser-Cornehls, 1976; Ewert, 1976; Székely & Lázár, 1976]. In the present model we have not considered the spatial representation of the different retinal receptive fields; we have only assumed that the axon of each type of retinal cell projects to a specific column, and excites the surrounding neighbors with less intensity, either in the tectum or in the pretectum (see Fig. 25).

Stimulus parameters (i.e., stimulus horizontal and vertical dimension, initial location in the visual field, and velocity and direction of motion) are specified by the modeler at the beginning of the simulation. The unit to specify them is the "column", for example, the velocity has to be specified in columns per second. The values of the exponent δ were taken from Grüsser and Grüsser-Cornehls [1976], being

$$\delta_{R2} = 0.7 \; ; \; \delta_{R3} = 1.2 \; ; \; and \; \delta_{R4} = 1.1$$

Constant k was determined, for each of the types of ganglion cells (R2, R3 and R4), based on the curves obtained by Ewert [1976] (see Fig. 22) for black dummy stimuli moving in a white background. Thus, with the stimulus size and velocity three different levels of activity (overall firing rates) can be determined, one for each type of ganglion cell. Whereas with the initial location of the stimulus, its velocity function and its direction of motion, we can determine the changing pattern of saptio-temporal activity during the simulation time. That is, these parameters are used to determine what tectal columns in the two-dimensional model are beign activated by the active ganglion cells at a given time. The level of excitation also depends on the assumed retino-tectal projection (see Fig. 25). The stimulus motion through the model's receptive field is simulated by a stepwise movement. The effect of ganglion cells R2, R3 and R4 upon a specific tectal column is kept constant for the period of time the stimulus remains in the column's
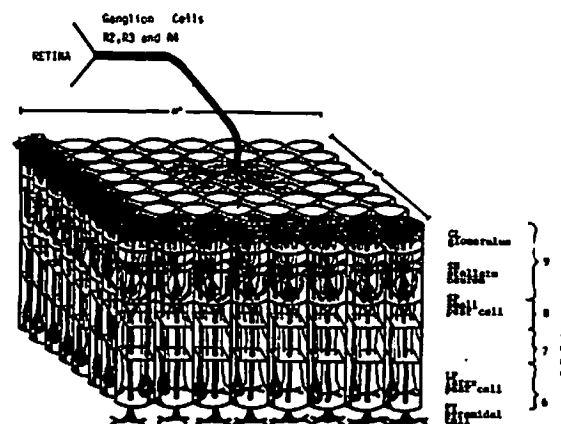
Figure 25: Retino-tectal projection.
Representation of the two-dimensional model of the optic tectum, constituted of an array of 8 by 8 columns, which cover a receptive field of approximately 32 by 32 deg (see text for explanation), and receive *focal* as well as overlapping information from retinal ganglion cells of classes R2, R3 and R4. For simplicity we only show the retinotopic projection to one tectal column and its neighbors.

receptive field. Additionally, the stimulus "jumps" from the receptive field of a group of columns to the next according to its size, shape, velocity function and direction of motion. A more detailed model of the spatio-temporal pattern of retinal activity, rather than the overall firing rates, is a target of current research in our group [Lee & Arbib, 1983; Lee, 1985] (see also an der Heiden and Roth [1983] for an "intermediate" model of retinal activity).

Two-dimensional Model of the Pretectum

Because of the limited data about the anatomy of the pretectal region, the pretectum is simply modelled as a two-dimensional array of models of Ewert's [1976, 1980] TH3 cell. This neuron integrates information received from ganglion cells type R3 and R4 [Grüsser & Grüsser-Cornehls, 1976; Ewert, 1976; Székely & Lázár, 1976], in such a way that it gives a stronger response to square stimuli and to "antiworm-like" stimuli than to "worm-like" stimuli (see Fig. 23A). This neuron is also postulated to be responsible, and here we hypothesize, for modulating changes in the latency of response of PY cells through a mechanism which is the outcome of a tonic inhibitory effect that is a function of the motivational state of the animal. That is, the behavior of these cells depends on two different mechanisms; one, which remains constant during normal conditions and varies with the animal's motivational state, is responsible for controlling the response latency; the other , which depends only on retinal input, gives tectal cells the capability for prey-predator recognition.

Interactions among Retina, Tectum and Pretectum

Fig. 26A shows the two-dimensional neural model of the interactions among retina, optic tectum and pretectum. For a better understanding of these connec-
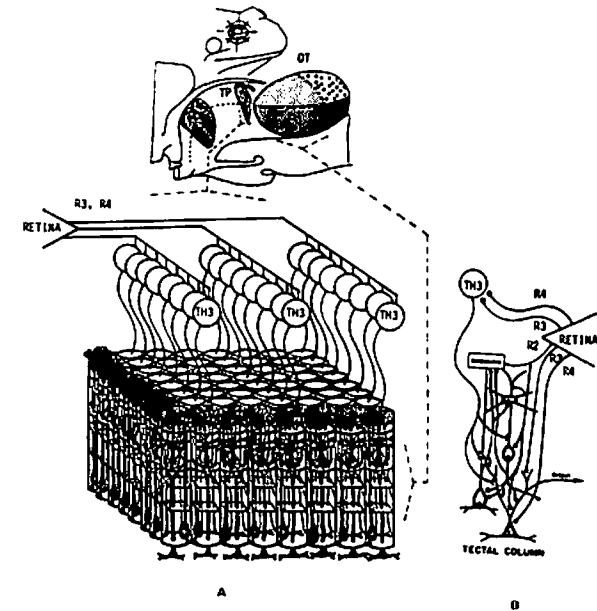
Figure 26: Interactions among Retina, Tectum and Pretectum.
The retina sends fibres in a retinotopical fashion to both optic tectum (class R2,R3 and R4), and pretectum (class R3 and R4)(see Fig. 25). A) TH3 neurons also project retinotopicaly to the optic tectum. For simplicity we only show the projection of three rows of TH3 cells projecting upon the tectal columns. B) A closer look of the interactions among retinal, tectal and pretectal cells. Pretectal cell TH3 inhibits LP, SP and PY cells of the tectal column corresponding to its retinotopic projection.

tions, in this figure, only three rows of pretectal cells projecting upon the tectal columns are shown. Fig. 26B presents a closer look at the projections from pre-tectal cells (arranged also in columnar fashion) to the cells of their corresponding tectal column. This figure shows that the retina projects retinotopically to both tectum (ganglion cells of class R2, R3 and R4) and pretectum (class R3 and R4) [Grüsser & Grüsser-Cornehls, 1976; Ewert, 1976; Székely & Lázár, 1976]. Every TH3 pretectal cell inhibits the activity of LP, SP and PY neurons of the tectal column corresponding to its projection. Finally, each PY cell's activity is posed to define the stimulus spatial location, the direction of the prey-catching orient-ing response and the prey-predator discriminative abilities of the tectum. When several PY cells are active, the target location of a response is determined by the average of their target loci as weighted by their activity.

The mathematical description of each of the neurons considered in this model of the retino-tectal-pretectal interactions is given in the Appendix A.

It is important to point out that the neural architecture proposed for the in-teractions among these brain regions takes into account the anatomical data now available with the purpose of obtaining the one that best reproduced empirical results. This model is the fourth stage of *Rana computatrix* [Arbib, 1982], an evolving model of neural circuitry subserving, through interactions of neural ac-tivity distributed over several brain regions, visually guided behavior in anurans. At each stage, a family of models is developed that becomes a subunit in the family of models analysed in the next stage which is developed to explain a wider range of phenomena.

Arbib and Lara [1982] studied how lateral excitation and inhibition among neighboring tectal columns in a unidimensional array may account for the spatio-temporal facilitation of tectal activity to a small moving object. Lara and Arbib

[1982] showed in the unidimensional model that the best configuration for the inhibitory projection from pretectum upon tectum, in terms of hysteresis effects and latency of response, was that pretectal fibers project to LP, SP, and PY cells. Now with the expansion of the model to two dimensions and by including the effect of ganglion cells of class R3 and R4 in the interactions among retina, tectum and pretectum, the goal is to explain how the spatio-temporal response of tectal units may give the animal the ability to discriminate among "worm-like", "antiworm-like" and square stimuli, with a pattern of response independent of the stimulus direction of motion, and with changes in pretectal inhibition, due to changes in the motivational state of the animal, modulating the latency and the response rate.

A symmetric architecture has been proposed for the lateral interactions among tectal columns. In an earlier study [Lara, Cervantes & Arbib, 1982b], a model of asymmetric connections among tectal units was analysed. In both cases sim-ilar results were observed, but the use of symmetric connections simplified the model's structure, and made the response invariance to the direction of motion of the stimulus an immediate consequence of the form of the tectal architec-ture. This avoids the postulate of the more complex innate wiring process in the amphibian brain presupposed by asymmetric connections. It seems to be more plausible that asymmetric connections among tectal columns are used by other types of tectal units that process other kinds of information, perhaps by T5(1) to process directional sensitivity [Ewert et al, 1979a]. Finally, in order to simulate changes in response latency and in the number of pulses discharged by PY cells, we postulated that the PY neuron is excited, directly and through LP and SP cells, by ganglion cells R2, R3, and R4 and inhibited by the pretectum (TH3). A family of models, represented by different values of the weights from these

various neurons upon the PY cell, has been analyzed. The goal was to ensure that without pretectum the response of the PY cell should be controlled by the activity of ganglion cells with larger receptive fields (classes R3 and R4) in such a way that it emulates the preference for stimulus type c over those of type a or type b (see Fig. 23D); whereas in the presence of pretectal inhibition the PY cell's sensitivity to a "worm-like" stimulus was the outcome of a facilitation of tectal column response through recurrent activity which responds best to objects representing potential preys. In this case, the choice had also to include the weight value selection for the inhibitory effect of TH3 upon tectal activity to reproduce the overall behavior presented by PY cells, that is, a preference for "worm-like" stimuli (type a) over those of type c, and a poor response to "antiworm-like" stimuli (type b) (see Fig. 23B).

Results

Results of computer simulation are presented in two ways. First, in four-dimensional graphs, showing the response of PY cells of all 64 columns in the model during a specific computer experiment, combined with two-dimensional graphs that offer a closer look of the PY cell response of the (ith,jth) tectal column to better appreciate the response rate and latency. Second, graphs with the same coordinates as those used to express experimental data, that is, graphs that may be directly compared with physiological and behavioral results. In the first case, the two-dimensional plane formed by the x and y axes represents the spatial location of the columns. This plane is divided into 64 sections, each one representing in the horizontal dimension the scale for the simulation time, while the s axis of the graph represents PY cell activity. This activity is shown

through the PY membrane potential, and whenever this potential reaches the threshold value it is indicated with spikes. The generation of action potentials is not simulated in our neurons but we simply used a *threshold rule* to provide results that could easily be compared with experimental data. These figures also show the experiment description (stimulus type, direction of motion with respect to the stimulus geometry, angular velocity, etc.). Both ways of showing the actual behavior of the model allow us to make analogies and comparisons with experimental observations.

For different simulations three types of stimuli were used: rectangles whose longest axis moves in the direction of motion, rectangles whose longest axis moves perpendicular to the direction of motion, and squares of different sizes, designated as type a, b and c respectively in the figures. The speed of the stimulus is defined as the time required to go from one column to the next, and the velocity value in most of the experiments was 2 columns per unit of time of simulation (uts), which is equivalent to 8 deg per unit of time (from above, each column receives 4 *focal* deg).

Behavior of Pretectal Cell TH3

The purpose in simulating the response of TH3 to different stimuli was to show how the combined interaction of ganglion cells R3 and R4 could generate their properties. Trying different weights (see Table 9 in the Appendix A for the final values) the response of this cell to different types of stimuli is shown in Fig. 27A. Once the membrane potential of this neuron reaches the threshold, its response is modeled to be proportional to its input (see Appendix A), otherwise it is equal to a tonic activity. The units of the vertical axis in this figure (Amplitude of Response) represent the overall effect that this cell exerts upon tectal activity.

As can be seen in this figure, the response of this cell to different types of stimuli is very similar to that of the pretectal cell that was suggested to be related to prey-predator recognition (see Fig. 23A for comparison). The response of this neuron increases with size, most strongly for square stimuli (type c) than to "antiworm-like" (type b), while the response to "worm-like" stimuli (type a) does not change much.

Behavior of PY Tectal Cells without Pretectal Inhibition

The response of the PY cell to the different types of stimuli when we simulated only the tectum is shown in Fig. 27D. It can be seen that it responds better to stimuli of type c than to those of type a or those of type b. This behavior reproduces in general the observed behavior of tectal cells (T5(2)) in animals without pretectum (see Fig. 23D for comparison). Fig. 28 presents the activity of the 64 tectal columns, while Fig. 29 shows the response of the PY cell of one tectal column. In these figures, the same stimulus preference, just described, is observed. That is, there is a better response to a square of 8x8 deg (Fig. 28C and 29C) than to a rectangle of 8x2 deg moved as a "worm-like" stimulus (Fig. 28A and 29A), and the weakest response is to the same rectangle moved as an "antiworm-like" stimulus (Fig. 28B and 29B). Here, we must point out that the overall tectal response is also stronger to type c stimulus (Fig. 28C) because it covers a larger area in the animal's receptive field, while in the case of a "worm-like" stimulus the tectal response is lower and concentrated in a narrower area. In these figures the maximal tectal cell response shifts in time as the stimulus moves across the retina, and it coincides with the time in which the stimulus is on its receptive field.
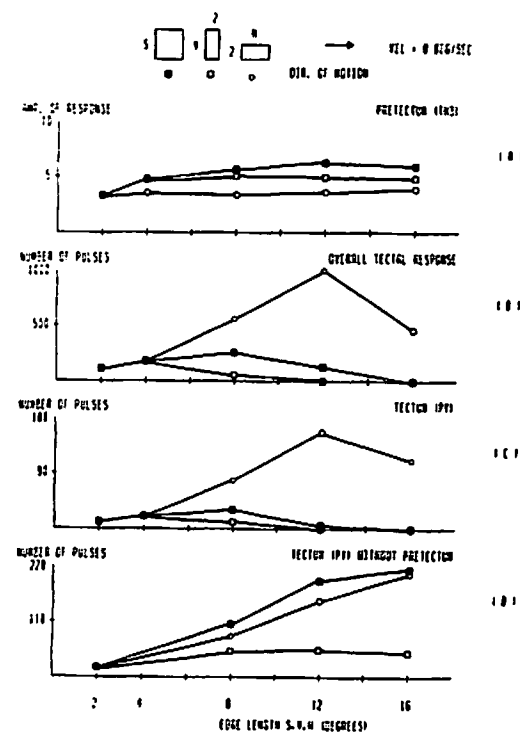
Figure 27: Simulation of tectal and pretectal cells response. Computer simulation of the tectal and pretectal cells' response to different configurations of moving stimuli (visual angular velocity of 8 deg/sec). A) Pretectal TH3 cell response: it is mostly sensitive to stimuli type c and b. B) Overall response of the tectum to the three types of stimulus (a, b and c): tectum response is mostly sensitive to stimulus type a and it is weaker to stimulus type b. C) PY cell response to the three different stimuli: it respond better to stimulus type a than to type c, and it gives a very weak response to a stimulus of type b. This curve is equivalent to B. D) PY response when pretectum ablation occurs: these cells are mostly sensitive to stimuli of type c or a, and less to those of type b.
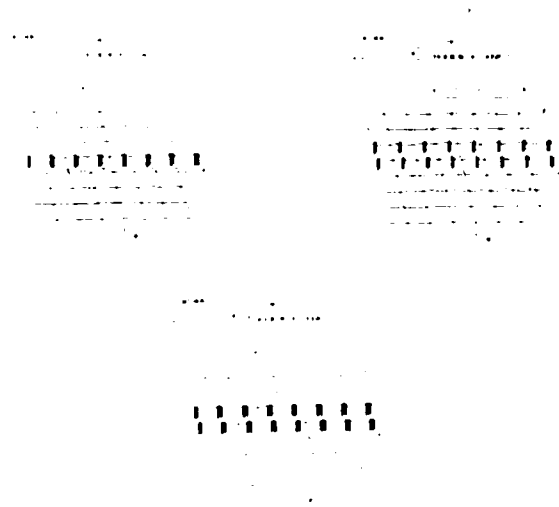
Figure 28: PY cells response when pretectal ablation is simulated.
Figures (28) and (29) present a computer simulation of the PY cell response to
different configurations of moving stimuli when pretectal ablation occurs: All
stimuli are moved from left to right with a visual angular velocity of 8 deg/sec.
Fig. 28 shows four-dimensional graphs, where the x and y axes are used to rep-
resent the spatial localisation of the (ith,jth) column. The y axis of this plane
is also used to show the time scale for the response of every column's PY cell,
while the vertical axis (z axis) represents its local membrane potential. In the
graph when the PY local potential is above the threshold, this is indicated by
spikes. Fig. 29 offers a closer look at the response of PY cell of column (4,5) for
different configurations of stimuli. In both graphs: A) response to a "worm-like"
stimulus (type a) of 8x2 deg; B) to the same stimulus moved as "antiworm-like"
(type b); and C) to a square stimulus (type c) of 8x8 deg. At the level of one PY
cell, tectal response is stronger for stimulus type c than to type a, or to those of
type b. The overall response of the tectum is also stronger to type c stimulus. It
is also wider spread, while the response to "worm-like" stimulus, although it is
strong too, is concentrated in a narrower area.
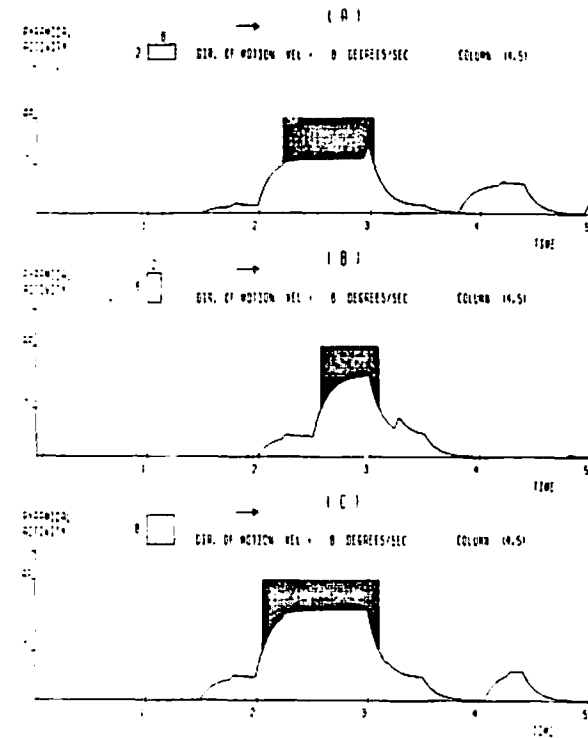
Figure 29: A single PY cell response without pretectal inhibition.

See legend for Fig. 28.

PY Tectal Cell Behavior with Pretectal Inhibition

Fig. 27B and 27C show tectal activity in the presence of pretectal inhibition through the response of PY cells to the three types of stimuli. Stimuli of different sizes were used, starting with 2x2 deg and expanding it in three different ways: expanding the dimension in the axis along the direction of motion (type a), expanding the dimension in the axis perpendicular to the direction of motion (type b), and expanding both dimensions (type c). They were moved with a speed of 2 columns/uts which is equivalent to 8 deg per unit of time. To build these graphs we counted the number of pulses of a given column (Fig. 27C) and the total activity in the tectum (Fig. 27B) to the presentation of the stimuli. PY cells respond better to stimulus type a than to type c. In both curves there is an initial increase in the response, as the stimulus size is incremented, followed by a decrease for larger stimuli; whereas they present a very weak response to stimuli of type b. These results reproduce in a general way the empirical observations (see Fig. 23C and 21Ba for comparison). Fig. 27B shows a graph of the number of times the tectum is activated when a stimulus is present, and is thus a better measure of the possible control of the orienting response exerted by the tectum. This figure is equivalent to Fig. 27C.

Fig. 30 shows the response of the 64 columns of the tectum to the three types of stimuli and Fig. 31 presents the response of the PY cell of the (4th,5th) tectal column. The abscissa time scale represents five units of time, while the vertical axis corresponds to the membrane potential of the 64 PY neurons. The stimulus moves from left to right with a speed of 8 deg/uts, so column (4,1) is active at the begining while column (4,8) responds at the end of the time scale. The stimuli used in these simulations were a stimulus of 8x2 deg moved as a "worm-like" (type a) and as an "antiworm-like" (type b) stimulus, and

a square of 8x8 deg (type c). From Fig. 30, it is clear that even though the response to a type c stimulus (Fig. 30C) is wider spread, it is weaker than that to a "worm-like" stimulus (Fig. 30A), whereas the weakest response is to an "antiworm-like" stimulus (Fig. 30B), though is also wider spread than that to a "worm-like" stimulus. At a one cell level, tectal activity is stronger for stimulus type a (Fig. 31A) than for type c (Fig. 31C), and the lowest activity is for stimulus type b (Fig. 31B).

Directional Invariance for Prey-predator Discrimination

It has been shown both behaviorally and physiologically that prey-predator recognition and discrimination are independent of the direction of motion of the stimulus [Ewert, 1976; Ewert et al, 1979b]. As a result, we used a symmetric connection scheme in our model. Thus direction invariance is to be expected. A simple test of this invariance was directed monitoring the model during the processes of discrimination and recognition of stimuli moved in eight different directions. A rectangle of 8 x 2 deg was used as stimulus. It is known that this stimulus produces a very weak response (almost no response in most tectal cells) when moved as "antiworm-like" (type b) and a strong response when moved as "worm-like" (type a) stimulus. Fig. 32 presents the overall tectal response of the 64 columns to "worm-like" (Fig. 32Left column) and to "antiworm-like" stimuli (Fig. 32Right column) in three directions (the results are the same for the other five). It is clear that the pattern of response to these stimuli is invariant to the their direction of motion.
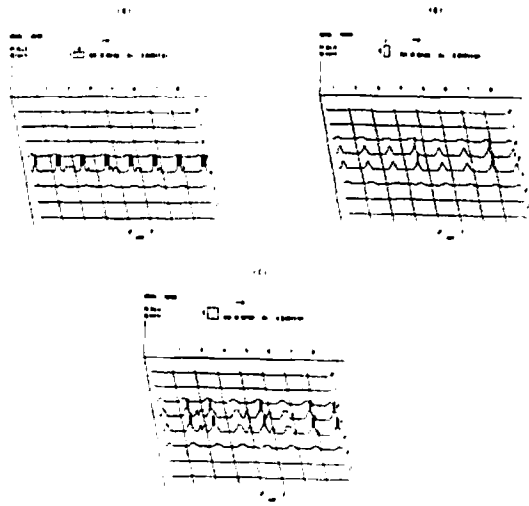
Figure 30: PY cells response when Pretectal inhibition is present.
Figures (30) and (31) present a computer simulation of the response of the PY cells of the retino-tectal-pretectal interactions model. All stimuli are moved from left to right with a speed of 8 deg/sec. (See Fig. 28 legend for an explanation of the graph characteristics). In both figures: A) Response to a "worm-like" stimulus of 8x2 deg (type a); B) Response to an "antiworm-like" stimulus of 2x8 deg (type b); and C) Response to a square stimulus of 8x8 deg (type c). In Fig. 30 it can be seen that the response to type c stimulus, although wider spread, is weaker than that to type a, whereas the weakest response is again to stimulus type b. In Fig. 31 it is clear that PY cells are most sensitive to "worm-like" stimuli, rather than to squares or to "antworm-like" stimuli.
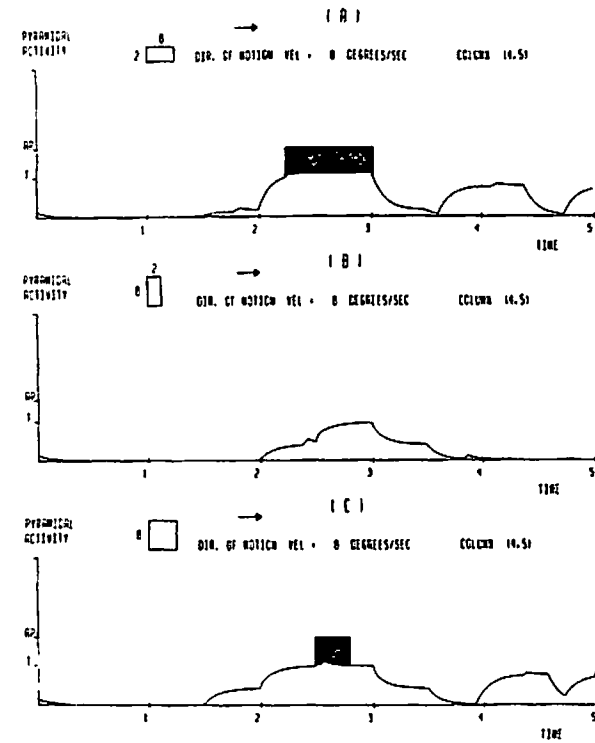
Figure 31: A single PY cell response with Pretectal inhibition.

See legend for Fig. 30.
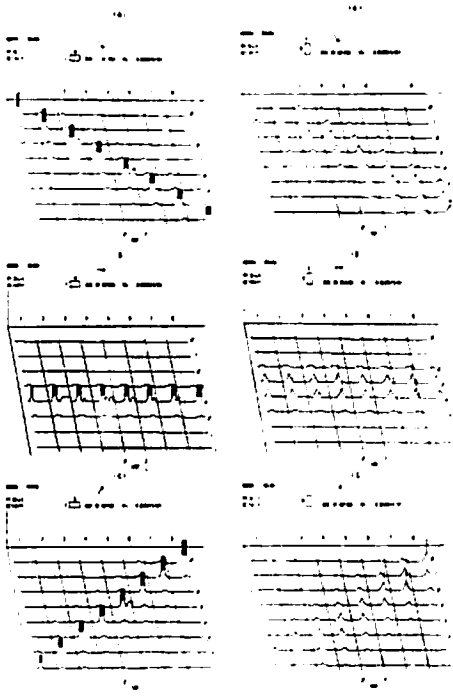
Figure 32: Simulation of Direction Invariance of PY response.
Computer simulation of the PY cell response of the 64 columns to a rectangle
stimulus, of 8x2 deg with a speed of 8 deg/sec. (see Fig. 30 legend). Left column:
The stimulus is moved as a "worm-like" stimulus in three different directions.
Right column: The stimulus is moved as an "antiworm-like" stimulus in the same
directions as in the left column. In both columns: A) moving from the upper
left corner of the figure to the lower right; B) from left to right in the middle of
the receptive field; and C) from the lower left to the upper right corner of the
figure. The response is direction invariant, so the recognition of both stimuli is
independent of the direction of motion.

Size Preference and Response Latency

The behavior of PY cells, which are postulated to control the prey-catching
orienting behavior of the animal, was simulated under normal conditions as well
as under motivated states. These experiments have not been reported in the
experimental literature, but it would not be too hard to design an experimental
paradigm in which the PY cell (T5(2) of Ewert) response to "worm-like" stimuli
of different sizes would be recorded during different motivational states of the
animal, that is, in animals highly motivated (with hunger, smelling worms, etc.),
or with low motivation (after presenting a threatening stimulus). "Worm-like"
stimuli of different sizes were presented. They moved from left to right with a
visual angular velocity of 8 deg/sec. The curve, to type a stimuli, obtained in
Fig. 27 was considered to be the behavior of PY cells under normal conditions.
Thus, the same stimuli were used to study how the response rate and latency
behave when the level of motivation is changed (through modifying the tonic in-
hibitory effect exerted by TH3 cells upon the tectal activity). Fig. 33B shows that
in normal conditions PY cell response presents a lower response rate (number of
spikes) than when it is motivated. This correlates with the empirical observa-
tions of Ewert [1976, 1980] (see Fig. 33A for comparison). To analyse changes in
response latency a "worm-like" stimulus of 8x2 deg was chosen. Fig. 34 displays
the response of the PY cell of the (4,5) column for different levels of motivation,
low (Fig. 34A), normal (Fig. 34B) and high (Fig. 34C). These results clearly show
that the latency of response is reduced and the number of spikes increases in mo-
tivated states. These results are in accordance with behavioral results reported
by Ingle [1973, 1982a].

In the case of size preference, if we present one stimulus at a time, the optimal
size preferred by the animal remains the same. In Ingle's case, the experiment he
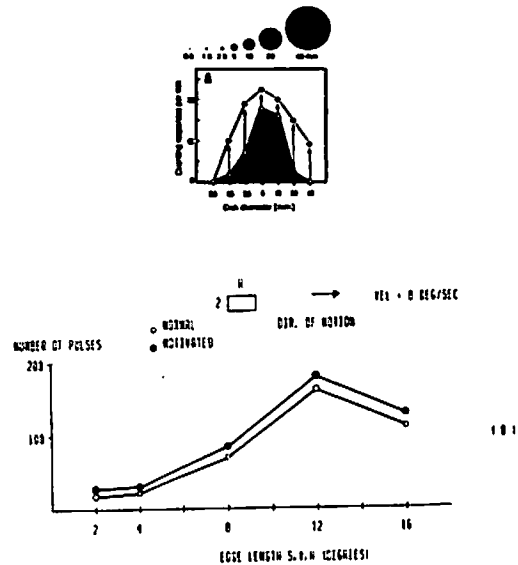
Figure 33: Computer simulation of different Motivational States.
Behavior of tectal cells to changes in the motivational state of the animal. A) Behavioral response of common toads to prey dummies (disks) of different sizes with a visual angular velocity of 20 deg/sec. In the presence of prey odor (motivated animal) the stimulus efficacy is greatly enhanced (see arrows) [from Ewert, 1980]. B) Computer simulation of the PY cells response to changes in the motivational state level. The curves correspond to normal (same as Fig. 27C) and motivated states when a "worm-like" stimuli of different sizes is presented (angular velocity of 8 deg/sec from left to right). o = normal, • = motivated. The response (number of spikes) increases if the motivated state is increased, although the size selection (selection of the *optimally* preferred prey size) remains the same.
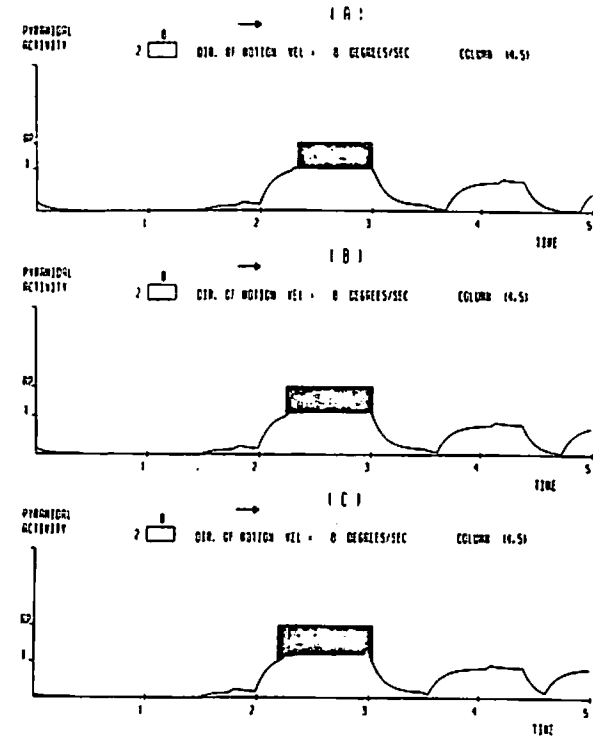
Figure 34: PY response latency for different Motivational States.
Computer simulation of the PY cells latency of response to different motivational levels. We used a "worm-like" stimulus of 8x2 deg moved with a visual angular velocity of 8 deg/sec. The curves show the response of the PY cell of the (4th,5th) tectal column with: A) low; B) normal; and C) high motivation level. It is clear that the latency of response reduces and the number of spikes increases when the motivational level increases.

describes is related to the phenomenon of prey-selection and will be completely discussed in another report. It has been shown that when two prey stimuli are presented simultaneously in the animal's receptive field, it prefers the one that represents the better prey [Amari & Arbib, 1977; Didday, 1976; Ingle, 1973a; Lara & Arbib, 1982]. What might be happening in this case is that, in normal animals, a stimulus subtending 6 deg of visual angle induces a response in the tectal columns it excites which is stronger than the combined response of the tectal columns excited by a stimulus subtending a visual angle of 16 deg. In this way the smaller stimulus represents a better prey and so it is selected. In motivated animals, on the other hand, tectal response is enhanced. The enhancement produced during the presentation of a 6 deg stimulus is lower than the overall enhancement produced for a 16 deg stimulus (it covers more tectal columns at a time). Furthermore, this difference in the response increment might be big enough to make the larger stimulus become the better prey, and thus be preferred.

Discussion

Our modelling studies present only a qualitative analysis of the functionality of the interactions among several brain regions in prey-predator recognition. However, these studies allow us to suggest that some brain regions of the visual system of anuran amphibians are organised in functional units (columns) with specific retinotopic configurations, where the interactions among cells of these regions yield stimulus recognition and consequently the proper motor response. The input at each of these units is distributed among all of its elements (neurons). Each unit extracts specific features of the stimulus and its level of activity is then combined with those from other functional units to produce motor behavior.

Previously, Lara and Arbib [Lara et al, 1982, Lara & Arbib, 1982; Arbib & Lara, 1982] adopted the hypothesis that the activity of PY cells controls prey-catching orienting behavior. However, it is important to stress that motor behavior in the animal is really the coordination of several, possibly linked, motor schemas which are activated by groups of neurons whose levels of activity define a specific situation in the world. Ewert and coworkers [Ewert & Burghagen, 1979; Schürg-pfeiffer & Ewert, 1981] have specifically postulated that motor schemas are activated by a group of cells and the action yields the activation of other neurons which in their turn activate other motor schemas and so on until the most adequate motor pattern is produced. Grüsser and Grüsser-Cornehls [1976] and Roth and coworkers [Lthardt & Roth, 1979; Hlmstedt & Roth, 1980; Roth & Jordan, 1982] argue that because some cells in the tectum are activated in the same way by different stimuli, prey-catching orienting behavior must be controlled by the joint activity of several neurons. Furthermore, Grüsser and Grüsser-Cornehls established that in order to prove correlation between physiological responses and the animal behavior, they must meet the following criteria:

1. The all-or-nothing character of the different components of prey-catching behavior.

2. The cells should respond to the real size of the stimulus and not to its angular size.

3. They should have a long latency of response.

4. They should change their response according to experience.

5. They should monitor the presence of the stimulus and the stationary world in detour behavior.

6. They should respond to a specific location of space in avoidance behavior.

These hypotheses, however, do not take into consideration how the firing of neurons could control the animals' behavior nor how planning as a result of linked

schemas or competition between schemas may occur. Arbib [1981] has outlined how cooperation and competition between schemas may occur, while Lara *et al* [1985] have specifically postulated how different brain regions could coordinate the activation of motor schemas in a primitive three-dimensional world.

In our model, the recognition unit response is only considered to indicate that a prey or a predator stimulus is present and possibly its location in the visual field, so that the activation of a specific motor schema is the outcome of its joint activity with that of other neurons [Lara *et al*, 1983]. Some of these problems can be dealt with as properties of integration of the motor schemas. It may be thought that motor centers receive information from several neurons, some sensitive to specific configurations of the stimulus and others measuring distance to prey objects and their relation to the stationary world. Thus, motor responses could then be elicited when the firing levels of such neurons reach a certain value as an all-or-none-response (argument 1), with a latency depending on the frequency of response (argument 3). At the same time, this information could be used in such a way as to give the size constancy effect (argument 2). Similarly, plasticity in behavior could be related to the motor center rather than to units in the tectum, although plastic changes have been observed in these neurons (argument 4) (see Lara & Arbib [1985]). Finally, detour behavior is not explained by Ewert's hypothesis nor by Grüsser and Grüsser-Cornehls'. In Ewert's case, his hypothesis does not show how schemas simultaneously activated could yield the proper sequential response, while Grüsser and Grüsser-Cornehls postulate a continuous feedback for the control of the behavior, which seems not to occur in these animals. To deal with these problems it is postulated that there should be a group of motor schemas linked together, acting as a single schema, which are activated by a given situation to produce the proper sequential motor

response. According with our hypothesis, the recognition unit reported in this Chapter is only an element of a complex interaction among groups of neurons that gives the animal the ability to select the next best motor behavior for a specific situation. Thus further modelling should integrate our tectal column modelling with our studies of other functional systems including depth perception [House, 1985], detour behavior [Arbib & House, 1983], and global interactions of motor schemas [Lara *et al*, 1983], so that we may have a clearer idea of how these functional units interact with each other to yield the proper motor response.

The specific hypotheses that have been tested with the present model can be listed as follows:

1. Tectal columns controlling prey-catching orienting behavior receive afferents from retinal ganglion cells of type R2, R3 and R4. The tectal column facilitates the response to retinal type R2 afferents; while retinal ganglion cells of type R3 and R4 also influence prey orienting behavior when large or "antiworm-like" stimuli are presented. In this chapter we also studied how the response of tectal neurons to retinal input could be changed by pretectal modulation when the animal is in a motivated state or for the regulation of the size constancy in the animal.

2. The inhibitory effect of pretectal cells gives tectal neurons the capability to discriminate between prey and predator. This inhibition is mainly directed to the PY cell although a smaller effect can also be seen on LP and SP cells, with which the overall activity of the tectum is inhibited when a predator-like stimulus is present.

3. Directional invariance of T5(2) (prey-predator recognition unit) response is the outcome of tectal architecture through symmetric interconnections among neighboring columns.

4. Changes in response latency are the result of a reduction in the tonic inhibitory effect of pretectal cells TH3 upon the tectal LP, SP and PY cells. This effect may be controlled by other brain regions (possibly by the telencephalon [Ewert, 1980]).

Our model can be considered as a way of *unlumping* the ideas of Ewert and von Seelen [1974] for the relations among retina, tectum and pretectum for prey-

predator recognition. They proposed a model of prey-predator recognition in which the retina, tectum and pretectum acted as filters for specific configurations of the stimulus. The inhibitory effect of the pretectum to the tectum enabled the latter to discriminate between "worm-like" and "antiworm-like" stimuli. As such, their model set forth the basic structure of regional interactions used in our model. However, their model had a number of limitations:

1. They did not show how the architecture of the different brain regions would give rise to the properties of their postulated filters.

2. They simulated only prey-predator recognition with neither the possibility to reproduce other phenomena nor the capacity for expansion.

3. Because of the linear nature of the model, it was restricted to a given range of values.

4. Because the model was lumped both in space and time, it could not be tested against the time course of response of specific cell types with specific retinotopic coordinates.

An der Heiden and Roth [1983] have proposed a lateral inhibition model of tectum which can reproduce important properties of worm-antiworm discrimination, but does not address the issues of tectal-pretectal interactions or of intrinsic tectal geometry. They postulate that the response of tectal cells is only the outcome of the spatio-temporal summation of retinal input (ganglion cells R2 and R3) combined with inhibitory interactions among the tectal neurons. Because of the tectal architecture proposed in their model, the response of T5(2) cells increases as the stimulus size increases, so T5(2) response to large prey objects is not reproduced. The authors mentioned that an influence, from thalamic or pretectal cells, upon the tectum could be assumed in the presence of non-prey objects. Finally, their model could not explain the disinhibitory effect in the tectum, observed by Ewert [1976, 1980] in toads and by Ingle [1973b] in frogs, after pretectal lesion.

TABLE OF CONTENTS

CHAPTER IV

ANALYSIS OF A FACILITATION TECTAL COLUMN (FTC)

Introduction

Physiological [Ingle, 1975] and anatomical evidence [Székely & Lázár, 1976] in frogs suggests that facilitation of prey-catching behavior involves self-exciting neural loops rather than synaptic strengthening. Lara, Arbib and Cromarty [1982] analysed a family of models of a single tectal column, defined as a functional unit of neural circuitry within the anuran's optic tectum. The model they proposed is composed of five elements, one glomerulus (GL), one large (LP) and one small (SP) pear-shaped cell, one stellate neuron (SN), and one pyramidal (PY) cell. The basic neural circuit for the tectal column model was abstracted from the detailed anatomical (Golgi) study of the frog's optic tectum done by Székely and Lázár [1976]. It includes only one efferent element in the column, which is the PY cell. Each element in the network was modelled by a differential equation, representing the dynamics of the membrane potential, and a threshold function that computes spike generation.

The model assumes that the retina projects *retinotopically* to the optic tectum and to other brain structures, such as the thalamic/pretectal region. Lara *et al.* only considered the effects upon tectal neurons of projecting axon terminals from ganglion cells of class R2, assuming, in this way, that the level of neural activity within the tectal column is controlled by retinal cells that respond best to small ("prey-like") objects. These authors, through the analysis of computer simulation results, traced prey-catching facilitation to the accumulation of excitation in the glomerulus and in SP cells, and argued for direct input from retinal fibres to the efferent (PY) cell.

In this chapter we present and analyse a refined version of the Tectal Column (TC) model proposed by Lara, Arbib and Cromarty [1982]. Because of the network characteristics and the introduction of new units to the circuit [Cervantes, Lara & Arbib, 1985], we refer to their model as the "Facilitation Tectal Column" (FTC) model. It has been shown experimentally that ganglion cells of types R3 and R4 also project to the optic tectum [Maturana *et al*, 1959; Grüsser & Grüsser-Cornehls, 1976; Székely & Lázár 1976; Witpaard & Ter Keurs, 1975]. Therefore, we now argue for direct input from ganglion cells R3 and R4 to the PY cell, modulating in this way the overt activity of this cell when presenting different configurational stimuli. This allows us (see also Chapter 3) to test the postulate that PY cell is equivalent to the tectal unit T5(2) defined physiologically by Ewert [1976]. Additionally, results from brain lesion experiments in frog [Ingle, 1973b, 1975] and in toad [Ewert, 1976] suggested an inhibitory effect from pretectum upon the tectum. A topographic mapping between tectum and pretectum is assumed in the FTC model. Specifically, the pretectal neuron TH3 defined physiologically by Ewert [1971] is considered as an integral part of the column model.

We first present the empirical results from anatomical, behavioral and neurophysiological studies considered during the FTC model development. These studies indicate that the anuran's brain processes visual information locally, with respect to the visual field, through an internal organisation of its optic tectum that shows mainly a vertical (columnar) orientation. That is, we try to establish

the empirical observations that constrained the development of the neural circuit machinery that best reproduced the proper physiological behavior. Here, we also analyse in some detail anatomical and physiological correlates hypothesised by the FTC model.

Then, we develop stability and parameter sensitivity analyses of the mathematical representation of the FTC model, which is given by a set of first order differential equations with small non-linearities (threshold functions). The aim here is to show how techniques from Non-linear Systems Theory can be used to analyse the stability of neural net models and their sensitivity to different parametric combinations. During our analysis we used a linearisation principle that explores the system behavior around the system equilibrium states. We studied how by choosing different sets of parameters a neural model may present different qualitative behaviors. Additionally, these analyses, in combination with computer simulations, are used to learn more about why the concepts (hypotheses) embedded in such neural models yield the appropriate behaviors, and what are the critical situations under which these behaviors are displayed. Results from these analyses should stimulate new experiments that may be tested via empirical paradigms.

Empirical Basis

The FTC model of Lara et al. [1982] is constrained by physiological, anatomical and behavioral studies in frogs and toads [Ingle, 1973b, 1975; Ewert, 1976, 1980; Grüsser & Grüsser-Cornehls, 1976; Székely & Lázár, 1976]. It also includes hypotheses based on properties shared by the optic tectum with other brain structures. Empirical data considered during the development of the FTC

model about characteristics shared by the tectum with other brain regions may be listed as follows:

1. In different brain regions, extrinsic input is first processed by a complex synaptic arrangement, a *glomerulus*, of interconnected axonal and dendritic terminals [Shepherd, 1970; Ssentágothai, 1970; Székely & Lázár, 1976]. A *glomerulus* may be considered to behave, to some extent, as a functional unit.

2. Within the brain, information may be processed in a lateral or vertical (columnar) fashion. It has been shown that in the olfactory bulb, in different parts of the cortex (visual, auditory and somatosensory) and in the amphibian optic tectum information is mainly processed vertically [Shepherd, 1979; Ssentágothai & Arbib, 1974; Hubel & Wiesel, 1963; Mountcastle, 1957; Székely & Lázár, 1976; Ingle, 1975]. The basic unit of vertical organisation is held to be a "column", which has been defined [Mountcastle, 1978; Ssentágothai & Arbib, 1974] as a unit of neural tissue of minimal size that, on the basis of internal connectivity, may be considered the basic organisational structure for elementary tasks of information processing. Elements in the column's neural circuitry must be activated by the same class of peripheral receptors and have similar receptive fields.

3. Neural networks showing an initial excitation followed by a long lasting inhibition have been described in brain regions involved in sensory-motor coordination, some of which also exhibit rebound excitation. Two different mechanisms have been proposed to account for the rebound excitation: first, recurrent axons that produce long lasting depolarisation in their respective cells, as was suggested to occur in the olfactory bulb [Shepherd, 1970] and in the amphibian optic tectum [Székely & Lázár, 1976]; second, reverberatory circuits as those in the cerebellum and reticular formation [Eccles, 1973], the hippocampus and septum [Raisman et al., 1965], and the thalamus and cortex [Singer, 1977]. These processes involve a combined effect of excitation, inhibition and re-excitation.

The Golgi studies of frog optic tectum by Székely and Lázár [1976] (see Fig. 35) laid the basis for the FTC model of Lara et al (see Fig. 37). The cells considered in the model may be classified into two main groups: "internal" neurons, whose axons project only to other cells within the tectum, and "efferent" neurons, whose axons form efferent pathways from the tectum to other brain regions (e.g.

pretectum, medulla oblongata, tegmentum, etc.). The "internal" neurons in the model are :

1. Large pear-shaped (LP) cells. These cells have dendritic appendages and ascending axons (marked 1 in Fig. 35). They correspond to the large pear-shaped cell type (a) of Székely and Lázár, and are located mainly in layer 6. These cells have a long apical dendrite that project towards the superficial layers in a most variable manner, and few basal dendrites. The dendritic arborisations receive mainly retinal input. The axons of cells of this type originate from the main dendrite, following an upward course close to the dendritic arbor of the same neuron until they reach layer 9 where they send out some branches.

2. Small pear-shaped (SP) cells. These cells are located in layer 8, and resemble the large pear-shaped neurons but without the basal dendrites. They correspond to the small-pear shaped cells type (b) of Székely and Lázár (marked 5 in Fig. 35). The axon of this type of cell descends until layer 6, few collaterals reach cells in this layer, then with a sharp loop it turns back and ends up in the lower part of layer 9.

3. Stellate neuron (SN). These are small neurons that constitute the bigger part of the neuron population in layer 9 (marked 8 in Fig. 35). The axons of these cells originate from the dendrites. This cell receives ascending axons from LP neurons. Following the original hypothesis of Székely and Lázár [1976], this type of neuron is taken to be the only inhibitory element in the FTC model.

Lara et al. considered only one "efferent" neuron, the pyramidal cell (PY), which corresponds to the large pyramidal cell of Székely and Lázár (marked 3 in Fig. 35). They are found abundantly in layer 6. These cells have an apical dendrite, which sends branches to layer 9, and dendrites arising from the base of the cell body giving it a pyramidal form. The axon originates from the main dendrite and at layer 7 it turns laterally, or medially if the neuron is close to the midline, and leaves the tectum. Therefore, this cell is regarded as an efferent element of the tectum.

Ingle [1973b, 1975] studied behavioral and physiological correlates involved in prey-catching facilitation in frogs. He reported two important results: first, if a
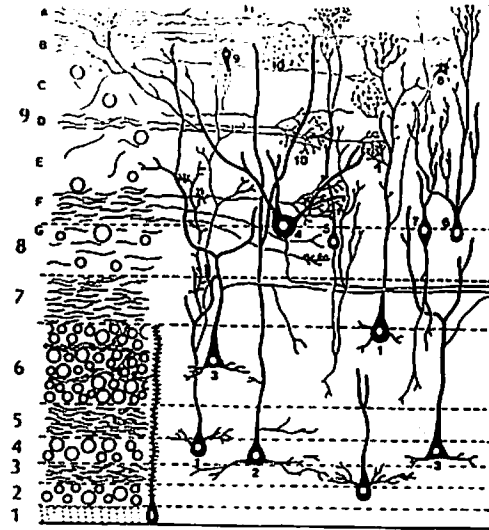
Figure 35: Synaptology of the Frog Optic Tectum.
Numbers on the left indicate the different tectal layers, while the letters indicate the sublayers of the most superficial layer 9. Tectal neurons are classified according to their shape, and labeled with numbers. (1) Large Pear-shaped cell with dendritic appendages and ascending axon. (2) Large Pear-shaped cell with dendritic collaterals. (3) Large Pyramidal neuron with axon projecting outside the tectum. (4) Large tectal Ganglionic neuron with efferent axon. (5-6) Small Pear-shaped cells with descending and ascending axons respectively. (7) Bipolar neuron. (8) Stellate neuron. (9) Amacrine cell. (10) Axon terminals from retinal ganglion cells. (11) Assumed evidence of Diencephalic fibres [from Székely & Lázár, 1976].

"dummy" prey-like stimulus subtending a visual angle of 5 deg was presented for 0.3 seconds through a 5 deg excursion, then removed and then restored for 0.3 seconds after a delay of 3.2 seconds, the probability that this second presentation would elicit a snapping response increase from 12% to 86%. Second, he observed that this facilitation effect was restricted to a small area around the part of the visual field previously stimulated. Facilitation was absent when the stimulus re-presentation was more than 30 deg distant from the area of the first presentation. These results suggest that the facilitation effect involves predominance of vertical over lateral processing of visual information.

Ingle [1975], trying to establish behavioral and physiological correlates, observed tectal neurons whose firing response accounted well for such a facilitation effect (see Fig. 36). He used as stimulus a 2 x 2 deg black square, fixed to a white background, which was moved through the visual field for 0.5 seconds. Two different types of "physiological" cells were distinguished :

1. Neurons giving a first burst of activity when the stimulus was presented, then a period of silence followed by a second burst of activity after the stimulus was removed, i.e., these cells presented rebound excitation (Fig. 36b).

2. Cells presenting a slow steady discharge for 3 to 6 seconds with a delay of 1 or 2 seconds after the stimulus was removed from the visual field (Fig. 36a).

Ingle [1973b] also observed that these cells were found more easily in animals with thalamic/pretectal lesions than in normal ones. The analysis of these results indicates that a cell of the second type might play an important role during facilitation of prey-catching behavior, normally being controlled by the thalamic-pretectal region through an inhibitory effect.

In summary, an important point indicated by anatomical studies of the frog optic tectum is that the organisation of its elements shows mainly a vertical (columnar) orientation, that is, some tectal cells have limited lateral dendritic
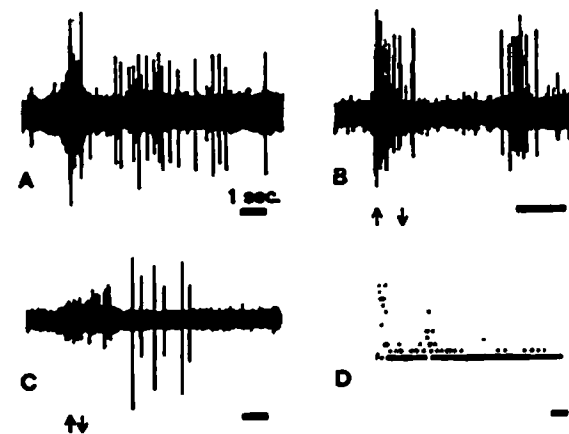
Figure 36: Physiological Response of Ingle's Attention Units.
A) Shows a brief burst of activity of a ganglion cell type R2 followed by a delayed response of a tectal cell. B) Shows the behavior of a tectal cell reponding to the stimulus presentation and again with a delay. C) Shows the behavior of a tectal cell that presents a delayed response after the stimulus has been retired from the visual field. D) Shows the postimulus histogram of a tectal cell presenting a delayed peak at 3 to 4 seconds [from Ingle, 1975].

and axonal arborizations. Similarly, behavioral and neurophysiological evidence on prey-catching facilitation suggests that the tectum processes visual information locally, since a second subthreshold stimulus presented at a distance bigger that 30 deg from the place where the first stimulus was presented did not yield prey-catching activity.

The FTC Model

In this section we describe the FTC model of Lara *et al.* [1982] which addresses facilitation at a single locus of the optic tectum. Additionally, assuming a topographical map from pretectum to tectum, we include the description of a thalamic/pretectal neuron (TP) posed to be equivalent to Ewert's TH3 [Ewert, 1971]. The TP neuron is postulated to exert an inhibitory effect upon excitatory FTC elements of its corresponding projection (see also Chapter 3). Thus, the FTC model (see the synaptology of the FTC model in Fig. 37) is comprised of one glomerulus (GL), one large pear-shaped (LP) cell, one small pear-shaped (SP) cell, one stellate neuron (SN) and one pyramidal (PY) cell in the tectum, and one thalamic/pretectal (TP) neuron.

Diencephalic and retinal inputs arrive at the superficial layer 9 of the optic tectum. Thalamic axon terminals can be seen in the most superficial sublayers, though they may ramify into deeper layers [Székely & Lásár, 1976]. In the FTC model, following Ewert's original hypothesis, the thalamic/pretectal neuron (TP) is proposed to exert an inhibitory effect upon cells responsible for maintaining the FTC internal activity (LP and SP) and also on its efferent (PY) element [Lara & Arbib, 1982], as can be seen in Fig. 37. In this way TP controls the FTC response to different configurational stimuli (see also Chapter 3). Due to the lack

FACILITATION TECTAL COLUMN
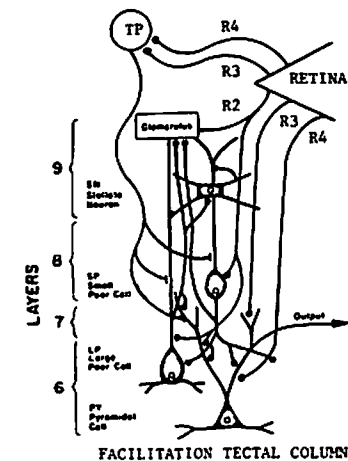
Figure 37: Facilitation Tectal Column (FTC) Model.
A single FTC is comprised by one thalamic pretectal (TP) neuron, one *glomerulus*, one large (LP) and one small (SP) pear-shaped cell, one stellate neuron (SN), and one pyramidal (PY) cell, the only tectal efferent element. The retina sends fibres in a retinotopical fashion to both optic tectum (class R2,R3 and R4), and pretectum (class R3 and R4). Whereas, the TP neuron, also projecting retinotopicaly to the optic tectum, inhibits LP, SP and PY cells of the tectal column corresponding to its retinotopic projection.

of anatomical data on the pretectal architecture, the TP cell is considered, and here we hypothesize, to be driven only by afferents from retinal ganglion cells of class R3 and R4 [Grüsser & Grüsser-Cornehls, 1976; Ewert, 1976, 1980]. Retinal axon terminals from classes R1 and R2 are seen in a deeper sublayer of layer 9, and from classes R3 and R4 in an even deeper one. Lara *et al.* only considered the effects of axon terminals from ganglion cells R2. Here we also consider the effects of ganglion cells of type R3 and R4, arguing for a direct projection to the PY cell that modulates the overt response of the tectum (see Fig. 37).

Layer 9 contains two sublayers of neurons, but the FTC model only incorporates stellate neurons (SN) and ignores amacrine cells (AC) (see Fig. 37). Following the original hypothesis of Székely and Lázár [1976], Lara and coworkers postulated that the SN is an inhibitory "internal" neuron whose function is to control the FTC internal activity, especially after the visual stimulus is removed, through negative feedback loops with LP and SP cells.

Another component in the FTC model at layer 9 is the glomerulus (GL) (see Fig. 37), an element that is considered to behave as a functional unit. GL receives axon terminals from ganglion cells class R2, and activates LP and SP cells. LP and SP cells send their axons back to the glomerulus forming positive feedback loops that tend to recruit the FTC activity when a prey-like stimulus is presented.

Fig. 37 also shows that the LP cell, located in layer 6, is activated by the glomerulus and by axon terminals from ganglion cells R2 and from the SP cell. This cell activates both positive and negative feedback loops by sending recurrent axons to GL and some axonal branches to SN respectively. Thus, it activates a competition between glomerular excitation and SN inhibition. The SP cell, located in layer 8, is also activated by GL and axon terminals from R2 ganglion cells, and it is inhibited by SN. The SP cell forms positive feedback loops with

GL, both directly and by exciting the LP cell, recruiting in this way the FTC internal activity.

The last element considered in the FTC model (see Fig. 37) is the PY cell. This cell is the only efferent element and is excited by axon terminals from ganglion cells of class R2, R3 and R4, and by both SP and LP cells. Thus, the PY cell integrates the level of activity within the FTC. This activity level is the outcome of cooperation/competition between positive, through GL, and negative, through SN, feedback loops along with retinal input and pretectal inhibition as well.

Beside the hypotheses about the tectal architecture, the FTC model includes hypothetical anatomical and physiological correlates which need confrontation with new empirical studies. It is postulated that the attention units found by Ingle [1975] correspond to the pear-shaped cells of Székely and Lázár [1976]. The LP cell corresponds to Ingle's unit that presents two burst of excitation with a period of silence in between (see Fig. 35b), and the SP cell corresponds to the unit that presents a delayed response (see Fig. 35a). It is also postulated (this is fully explained in Chapter 3) that PY and TP neurons correspond, respectively, to the tectal T5(2) and the pretectal TH3 neurons defined by Ewert [1970, 1976, 1980]. These postulates set forth specific physiological responses that need to be followed by some (LP, SP, PY and TH3) FTC elements. This, as seen during the stability and parameter sensitivity analyses below, raises a series of constraints that have to be considered during the analysis of different patterns of connectivities in the search of the one that best reproduces the empirical data.

In summary, anatomical, behavioral and physiological evidence [Székely and Lázár, 1976; Ingle, 1973b, 1976] led Lara *et al.* [1982] to suggest that the optic tectum processes visual information in a vertical fashion, by means of functional units ("Facilitation Tectal Columns") comprised of several "internal" neurons,
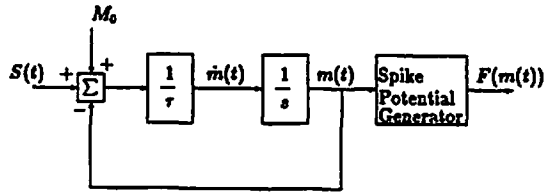
Figure 38: Block Diagram of the Dynamics of a Single Neuron.

See text for explanation.

some of them receiving direct retinal input, and one "efferent" cell that integrates the state of activity within the FTC and receives direct retinal input as well (see Fig. 37). These units explain the facilitation effect ("short-term memory") in terms of recurrent excitation and inhibition rather than in terms of short-term synaptic facilitation as, for example, that demonstrated by Kandel and collaborators [1978] in *Aplysia*. For more discussion of the FTC model refer to Lara *et al* [1982] or to Lara [1982].

Stability and Parameter Sensitivity Analyses

Each functional element in the FTC model is represented by two quantities: its membrane potential, and its firing rate (see Fig. 38). The membrane potential $m(t)$ varies linearly according to the weighted sum of its inputs $(S(t))$, and decays exponentially, according to the membrane constant (τ), to the resting level

potential M_0.

$$\tau \dot{m}(t) = -m(t) + S(t) + M_0 \qquad (4.1)$$

with

$$S(t) = E(t) - I(t)$$

where

M_0 is the resting level potential with zero input,

τ is the membrane time constant,

$E(t)$ is the weighted sum of excitatory inputs, and

$I(t)$ is the weighted sum of inhibitory inputs.

The cell's firing rate is related to its membrane potential through a transfer function $F(m(t); \Theta)$, where Θ is a suitable constant threshold. Function F may take one of the forms shown in Fig. 39. The output of the cell may be zero if the membrane potential is below threshold or constant otherwise (Fig. 39A), as is the case with the LP and SP cells.

$$f(m(t); \Theta) = \begin{cases} 1 & if\ m(t) \geq \Theta \\ 0 & otherwise \end{cases} \qquad (4.2)$$

In the second case (Fig. 39B), which corresponds to SN and GL, the output is also zero for subthreshold values of the membrane potential, but is now proportional to the input for values above threshold. GL is a special case; its threshold is zero so it behaves as a slow-potential non-spiking element.

$$h(m(t); \Theta) = \begin{cases} k_1 \cdot m(t) & if\ m(t) \geq \Theta \\ 0 & otherwise \end{cases} \qquad (4.3)$$

where

k_1 is constant.
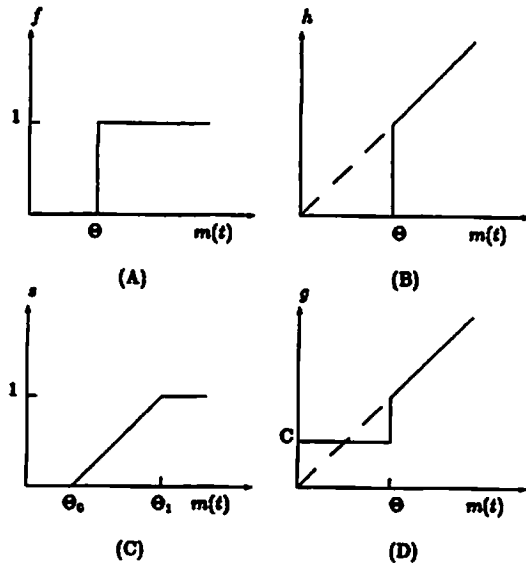
Figure 39: Transfer Functions for Action Potential generators.
A) ON-OFF threshold function. B) Linear-threshold function. C) Saturation-threshold function. D) Linear-threshold function with tonic (spontaneous) activity C.

A third case (Fig. 39C) corresponds to that of PY cell, the output once again is zero for subthreshold values, and is proportional to the difference between the input and the threshold $(m(t) - \Theta_0)$ for membrane potentials above the threshold (Θ_0), saturating when such potential grows beyond a specific value (Θ_1).

$$s\,(m(t); \Theta_0, \Theta_1) = \begin{cases} \Theta_1 - \Theta_0 & \text{if } m(t) \geq \Theta_1 \\ m(t) - \Theta_0 & \text{if } \Theta_0 \leq m(t) < \Theta_1 \\ 0 & \text{if } m(t) < \Theta_0 \end{cases} \qquad (4.4)$$

The final case (Fig. 39D) to be considered in our models is that of the TP neurons. Their output is constant (tonic activity) for subthreshold values and proportional to the input for membrane potentials above threshold.

$$g\,(m(t); \Theta) = \begin{cases} k_2 \cdot m(t) & \text{if } m(t) \geq \Theta \\ C & \text{otherwise} \end{cases} \qquad (4.5)$$

where

C represents a tonic activity, and k_2 is constant.

The deviation from linearity introduced by the threshold functions is not too large. Therefore, the state-space (internal) representation of the FTC model fits the definition of "Piecewise Linear" systems [Shinners, 1978]. The characteristics of this type of system permits the approximation of the non-linear system by the combination of several linear systems. The entire state-space may be divided into several subregions, so that within a given region the system is considered to be linear. [1] In each subregion the non-linear system

$$\dot{x}(t) = \bar{f}(x(t), r(t)) \qquad (4.6)$$

where

boldface lower case letters represent column vectors,

---

[1] Linearization principles are frequently used to analyze the stability of neural networks [Amari, 1977; An der Heiden, 1980; Scott, 1977].

$\bar{f}$ is a non-linear function of

x(t) the state vector and

r(t) the input vector,

can be approximated by a linear system of the form

$$\dot{x}(t) = f(x(t), r(t)) = A\ x(t) + B\ r(t) \qquad (4.7)$$

where

boldface upper case letters represent matrices,

f is a linear time-invariant function, that is,

A and B are constant matrices.

Within a subregion, the time solution of this equation gives the trajectories (state-transition sequence) of the system transient responses, starting at the point where the system enters such subregion.

When the matrix A is non-singular ($|A| \neq 0$) and the input vector r(t) is fixed, such linear system has a unique "equilibrium" state, i.e., $\dot{x}(t) = 0$, which may be located inside or outside the subregion corresponding to that linear operation. An "equilibrium" state is classified as an "actual" point when it lies inside the subregion where the system's transient solutions obey the linear approximation system this point is associated with; but is classified as a "virtual" point when falling outside such a region [Ogata, 1970]. The significance of this classification relies on the fact that a "virtual" point can never be reached by its own trajectories, that is, a non-linear system never converges to a "virtual" point but can converge to an "actual" point.

The location and nature of each equilibrium state depends on the linear system and the external input. The global response of the non-linear system is given by a composite trajectory obtained by, starting from a point in the state-space corresponding to the initial state, joining local trajectories at the boundaries

between linear operating regions. That is, locally, within a specific subregion, the state-transition sequence followed by the system is given by the time-solution of the corresponding linear approximation; once this trajectory reaches the frontier with a neighboring region, that point represents the initial state for the linear approximation associated with the subregion just entered; and so on, until the system either converges to or diverges from an actual point, or oscillates around some equilibrium state, or on the frontier of two or more neighboring regions.

By linearising the non-linear system in each region, we reduce our "stability" and "parameter sensitivity" analyses to an analysis of linear systems of the form given in equation (4.7). To analyse their stability we use the theory of eigenvalues [Ogata, 1970; Gibson, 1963; Raven, 1968; Shinners, 1978] which says that a linear system, $\dot{x}(t) = A\ x(t) + B\ r(t)$, of order n is asymptotically stable (i.e., $x(t) \rightarrow x_{eq}$, the equilibrium state, as $t \rightarrow \infty$ for each state x(0)) if and only if all eigenvalues (λ_i, $i = 1, 2, ..., n$) of A have negative real parts (i.e., $R_v\lambda_i < 0$ for each eigenvalue λ_i of A).

Example : A Second Order System

With a sixth order system, it is very hard to visualize the results of the stability and parameter sensitivity analyses. To motivate these analyses we start by showing an example of a second order system so we can show phase-plane portraits of the behavior of the state variables (membrane potentials). Here, we must point out that in our analysis we study two issues: "stability" of the neural network, we ask whether a departure from equilibrium tends to disappear, grow without limit or oscillate around some equilibrium state; and "parameter sensitivity", we ask whether or not a neural circuit model behaves according to its specifications under small changes on its parameters. In the case of the FTC

model, we analyse its stability and study different behaviors in the network as well as the conditions under which such behaviors are displayed, especially those cases where facilitation of PY response is explained.

Let us take, as an example of a system of second order, the negative feedback loop formed by LP and SN cells, and conduct stability and sensitivity analyses. Fig. 40A shows the relationships between LP and SN, while Fig. 40B displays the corresponding block diagram which includes all of the model parameters (synaptic weights, threshold functions and membrane constants). The LP is activated by an external input s and by its own axon, then it excites SN which in turn sends back axon terminals that inhibit LP activity. The mathematical representation of this neural net is

$$\tau_{lp} \dot{lp}(t) = -lp(t) + s + w_{lp\text{-}lp} f(lp) - w_{sn\text{-}lp} h(sn)$$

$$\tau_{sn} \dot{sn}(t) = -k_{sn} \cdot sn(t) + w_{lp\text{-}sn} f(lp)$$

where

s is external input and

k_{sn} is used to give SN a longer decay constant and,

f and h are given by equations (4.2) and (4.3) respectively.

Because of the non-linearities associated with functions f and h, the two-dimensional state-space can be divided into 2^2 regions (a factor of 2 for each of the cells); (I) where both cells are inactive, (II) LP active and SN inactive, (III) both cells active, and (IV) LP inactive and SN active (see Fig. 41). The boundaries between adjacent regions depend on the choice of thresholds Θ_{lp} and Θ_{sn}. In each region the non-linearities may be replaced by a linear piece of the f and h functions, so the trajectories within a region are governed by a system of two linear time-invariant differential equations.
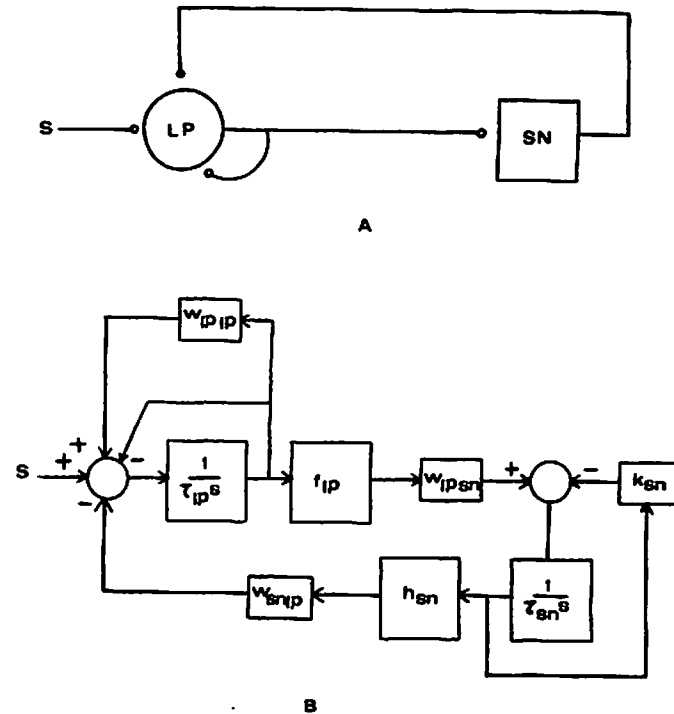
Figure 40: Feedback loop between LP and SN.
A) Neural net circuit, where s means external input, o excitation, and ● inhibition. B) Corresponding Block Diagram with all of the model parameters (weight factors, threshold functions and membrane constants).
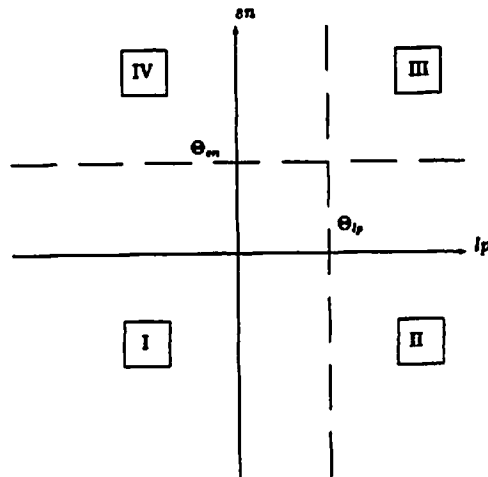
Figure 41: Phase-plane divided into four regions.
Boundaries between adjacent regions depend on the thresholds Θ_{lp} and Θ_{sn}.

In region I the system can be approximated by

$$\dot{x} = \begin{bmatrix} \frac{-1}{\tau_{lp}} & 0 \\ 0 & \frac{-k_{sn}}{\tau_{sn}} \end{bmatrix} \begin{bmatrix} lp \\ sn \end{bmatrix} + \begin{bmatrix} \frac{s}{\tau_{lp}} \\ 0 \end{bmatrix}$$

the equilibrium point is unique ($|A| \neq 0$), and it is located at

$$x_{e1} = (lp_{e1}, \ sn_{e1}) = (s, \ 0)$$

which is obtained by solving $\dot{x} = Ax_{e1} + \alpha = 0$.

Now, we want to analyze the stability of the neural circuit by asking whether a departure from equilibrium tends to disappear, grow without limit, or produce oscillations around the equilibrium state. We know that if A is diagonal or triangular then its eigenvalues are equal to the elements of the main diagonal. Thus, in this case, the eigenvalues of A are

$$\lambda_1 = \frac{-1}{\tau_{lp}}, \ \text{and} \ \lambda_2 = \frac{-k_{sn}}{\tau_{sn}}$$

so that all eigenvalues are negative real, since membrane time constants are always positive. Thus this linear system is *stable*. We defer questions of "actual" *vs.* "virtual" for later.

At this point it can be observed that, because of the characteristics of f and h, no matter what the values of functions F (threshold functions) here the eigenvalues are the main diagonal elements, and so matrix A is stable for all four regions. Furthermore, because eigenvalues are negative real, all singular points behave as stable nodes.

In region II the system is

$$\dot{x} = \begin{bmatrix} \frac{-1}{\tau_{lp}} & 0 \\ 0 & \frac{-k_{sn}}{\tau_{sn}} \end{bmatrix} \begin{bmatrix} lp \\ sn \end{bmatrix} + \begin{bmatrix} \frac{s+w_{lp\cdot ls}}{\tau_{lp}} \\ \frac{w_{ls\cdot ss}}{\tau_{sn}} \end{bmatrix}$$

with equilibrium point

$$z_{c2} = \left(|s + w_{lp\text{-}lp}| \ , \ \frac{w_{lp\text{-}sn}}{k_{sn}} \right)$$

In region III the system is

$$\dot{x} = \begin{bmatrix} \frac{-1}{\tau_{lp}} & \frac{-w_{sn\text{-}lp}}{\tau_{lp}} \\ 0 & \frac{-1}{\tau_{sn}} \end{bmatrix} \begin{bmatrix} lp \\ sn \end{bmatrix} + \begin{bmatrix} \frac{s + w_{lp\text{-}lp}}{\tau_{lp}} \\ \frac{w_{lp\text{-}sn}}{\tau_{sn}} \end{bmatrix}$$

with equilibrium state

$$x_{c3} = \left(|s + w_{lp\text{-}lp} - \frac{1}{k_{sn}} w_{sn\text{-}lp} w_{lp\text{-}sn}| \ , \ \frac{1}{k_{sn}} w_{lp\text{-}sn} \right)$$

In region IV the system can be approximated by

$$\dot{x} = \begin{bmatrix} \frac{-1}{\tau_{lp}} & \frac{-w_{sn\text{-}lp}}{\tau_{lp}} \\ 0 & \frac{-1}{\tau_{sn}} \end{bmatrix} \begin{bmatrix} lp \\ sn \end{bmatrix} + \begin{bmatrix} \frac{s}{\tau_{lp}} \\ 0 \end{bmatrix}$$

with equilibrium point

$$x_{c4} = (s \ , \ 0)$$

The next step is, based on the nature of the equilibrium states, to analyse the overt behavior of the system for different parametric conditions. We first note that singular state x_{c4} corresponding to region IV could never be an "actual" point because it always falls inside a region where SN is inactive. To show how by choosing different parametric combinations the network may display different qualitative behaviors, we have selected five different cases based on the nature of the equilibrium states. Table 2 shows the parametric combination selected for each case and the corresponding nature of the equilibrium points; whereas, Figs. 42, 43 and 47 show the phase-plane portraits, for all considered cases, with state variables *lp* and *sn* on the axes. Each graph contains trajectories for initial

Table 2: Different Parametric Combinations for the LP-SN network.

	Input			Effect from-to						Equilibrium States							
				LP-LP		LP-SN		SN-LP		reg I		reg II		reg III		reg IV	
CASE	z	w	s	w	s	w	s	w	s	v	a	v	a	v	a	v	a
A	x				x		x		x		x	x		x			x	
B		x			x		x		x		x	x		x			x	
C			x	*	*	x		x		x			x	x			x	
D			x	*	*			x	x	x		x			x	x	
E			x	*	*			x		x	x		x			x	

z- zero; w-weak; s-strong; v-virtual; a-actual; and *-doesn't matter.

conditions P, Q, R and S starting, respectively, at every one of the four regions. In all graphs, we provide a description of the equilibrium states nature ("actual" or "virtual") and broken lines to define the boundaries between adjacent regions, which depend on Θ_{lp} and Θ_{sn} values. Additionally, $\Diamond$, $\triangle$ and $\square$ show the location of the equilibrium states corresponding to the regions I, II and III respectively. As seen above, x_{c1} and x_{c4} are equal, thus, $\Diamond$ also shows the location of the equilibrium state of region IV.

CASE A.- Zero input ($s = 0$), strong effect from LP to itself and to SN ($w_{lp\text{-}lp} > \Theta_{lp}$ and $\frac{1}{k_{sn}}w_{lp\text{-}sn} > \Theta_{sn}$), and strong inhibition from SN to LP ($(w_{lp\text{-}lp} - \frac{1}{k_{sn}}w_{sn\text{-}lp}w_{lp\text{-}sn}) < \Theta_{lp}$).[2] Fig. 42A presents the phase-plane portrait for this case. Equilibrium state x_{c1} is an "actual" point while the rest (x_{c2}, x_{c3} and x_{c4}) are "virtual" points. If the initial state is given by point P within region I then the trajectory of the system transient response converges quickly to the "actual" equilibrium point x_{c1}. That is, if the trajectory starts at a point where LP and SN membrane potentials have subthreshold values then, because in this

[2]The choice of algebraic form for these conditions comes from the components of the equilibrium points which are affected by the choice of synaptic weights, threshold values and input *s*.

region there is no activity in the network and input s is zero, they decay exponentially to the resting level, that is, to the origin of the phase-plane portrait.

When the trajectory initiates at point Q, $lp > \Theta_{lp}$ and $sn > \Theta_{sn}$, excitation from LP keeps its own potential above threshold and, at the same time, drives SN potential above threshold; that is, the system tends to converge to singular point x_{c2}. The system, then, enters region III, where both cells' axon potentials become active, and within this region the trajectory obeys a new set of two linear differential equations. At this point, LP and SN membrane potentials are above threshold, which starts a competition between excitation (LP to SN & LP to LP) and inhibition (SN to LP) in the circuit. Inhibition upon LP is stronger than self-excitation so the trajectory tends to converge to singular point x_{c3}, where SN potential remains above threshold while LP goes into subthreshold values, but again the linear operation controling the system dynamics is switched when the trajectory reaches the frontier between regions III and IV. In region IV the only activity left in the network is the inhibitory effect from SN; thus both cells' membrane potentials keep on decaying until the system reaches the boundary between regions IV and I. From here, due to the fact that input s is zero and both cells' axon potentials are inactive, the system converges to the "actual" equilibrium point x_{c1}, where membrane potentials are at their resting level.

The trajectory starting at point R converges to the "actual" point x_{c1} visiting several regions in the following sequence $III \rightarrow IV \rightarrow I$. LP and SN begin with potentials above threshold which triggers a competition between positive (LP-LP) and negative (LP-SN-LP) feedback loops. Since the negative is stronger than the positive, LP potential goes below threshold and the trajectory tends to converge to x_{c3}, entering region IV. Within region IV, because at this point

Figure 42: Phase-plane portraits of the LP-SN network (Cases A and B).
In both figures, P, Q, R and S represent initial states for different trajectories, and $\Diamond$, $\triangle$ and $\square$ show the location of the equilibrium points corresponding to the four regions I, II, III and IV. The broken lines define the boundaries between adjacent regions, which are defined by a circle with a roman number inside. Such boundaries depend on the choice of Θ_{lp} (horizontal broken line) and Θ_{sn} (vertical broken line). Equilibrium point x_{c1} is an "actual" state and x_{c2}, x_{c3} and x_{c4} are "virtual" points. A) No external input, and B) weak external input (see text for explanation).
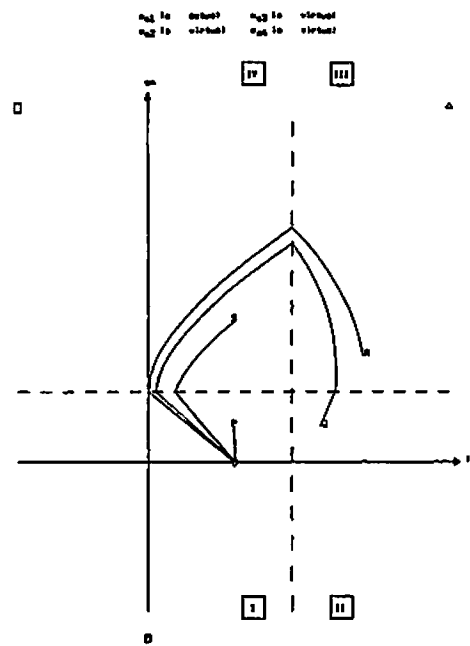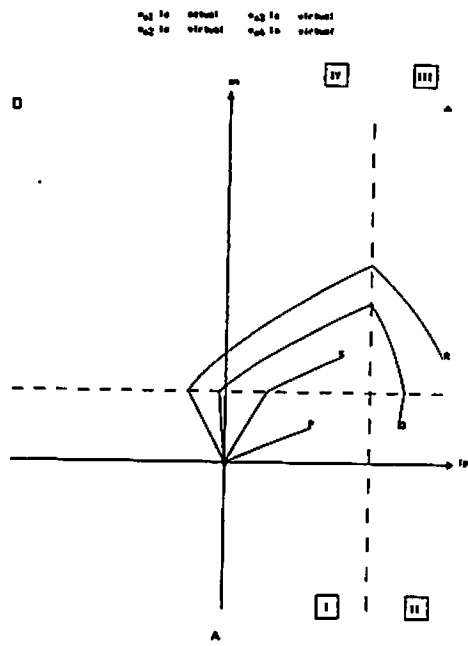
there is only inhibition left in the network, both cells' membrane potentials decay towards their resting levels in a manner similar to the one described previously when the initial state was given by Q and the system reached region IV.

When the initial state is given by S, $lp < \Theta_{lp}$ and $sn > \Theta_{sn}$, there is no excitation but only inhibition in the net, so both cells' membrane potentials decay tending to converge to x_{s4}. The transient responses of the non-linear system follow trajectories parallel to those described above for the situations where the initial state was given by R or by Q and the system entered region IV. In this situation SN is the only active element in the net. Therefore, LP is hyperpolarised while SN potential is above threshold. Once SN becomes inactive, both cell's membrane potentials converge to their resting levels according to their decay constants.

CASE B.- Weak input ($s < \Theta_{lp}$), strong effect from LP to itself and to SN ($w_{lp\cdot lp} > \Theta_{lp}$ and $\frac{1}{k_{sn}}w_{lp\cdot sn} > \Theta_{sn}$), and strong inhibitory effect from SN to LP ($(s + w_{lp\cdot lp} - \frac{1}{k_{sn}}w_{sn\cdot lp}w_{lp\cdot sn}) < \Theta_{lp}$). The phase-plane portrait for this case can be observed in Fig. 42B. We note that equilibrium state x_{s1} fits the classification of an "actual" point, while singular points x_{s2}, x_{s3} and x_{s4} are "virtual" points. Therefore, the trajectories followed by the system transient responses starting at states P, Q, R and S are similar to those explained in Case A, the only variation being the location of the equilibrium points. In this case, input s, though different from zero, is not strong enough to take LP potential above threshold so the system converges to a state where SN membrane potential is at the resting level and that of LP is at a level proportional to the amount of external input s.

CASE C.- Strong input ($s > \Theta_{lp}$), weak excitatory effect from LP to SN ($\frac{1}{k_{sn}}w_{lp\cdot sn} < \Theta_{sn}$), and weak inhibition from SN to LP ($(s + w_{lp\cdot lp} - \frac{1}{k_{sn}}w_{sn\cdot lp}w_{lp\cdot sn}) > \Theta_{lp}$). The trajectories in the phase-plane, for this case, are shown in Fig. 43C.

Here, equilibrium state x_{s2} is an "actual" point and singular states x_{s1}, x_{s3} and x_{s4} are "virtual" points. The trajectory starting at state P in region I tends to converge to the equilibrium state x_{s1}, but the linear operation of the system switches when the trajectory reaches the frontier with region II, from which the system directly converges to x_{s2}, the "actual" equilibrium point. That is, if the initial state is given by a point where LP and SN membrane potentials have subthreshold values then input s drives LP potential above threshold, taking the system into region II. Within this region, LP self-excitation raises its own potential to the level corresponding to the combined effect of external input s and LP firing rate. At the same time, because the LP effect upon SN is not strong enough to raise SN potential above threshold, SN membrane potential grows to the value that corresponds to the level of excitation provided by LP.

When the system starts at point Q, where $lp > \Theta_{lp}$ and $sn < \Theta_{sn}$, then the trajectory, as just described, converges to the "actual" equilibrium point x_{s2}, where LP membrane potential is proportional to the sum of external input s plus LP recurrent excitation, and SN level of activity is proportional to the excitation it receives from LP axons.

If the initial state is given by R, both cells having potentials above threshold, then LP potential tends to converge to a point corresponding to the combined effect of excitation (s-LP & LP-LP) and inhibition (SN-LP) it receives; whereas SN potential, because its source of excitation (LP) is not strong enough to maintain it above threshold, decays towards a level that is proportional to its input. When the trajectory reaches the frontier between regions II and III, the system response converges to the "actual" point x_{s2} in the same way as described above for the case when the initial state is given by Q.

If the initial state is given by S, $lp < \Theta_{lp}$ and $sn > \Theta_{sn}$, then SN potential level

Figure 43: Phase-plane portraits of the LP-SN network (Cases C and D).

See legend of Fig. 42 for an explanation of the graphs. C) Equilibrium point z_{c2} is an "actual" state and z_{c1}, z_{c3} and z_{c4} are "virtual" points. D) Equilibrium point z_{c3} is an "actual" state and z_{c1}, z_{c2} and z_{c4} are "virtual" points.
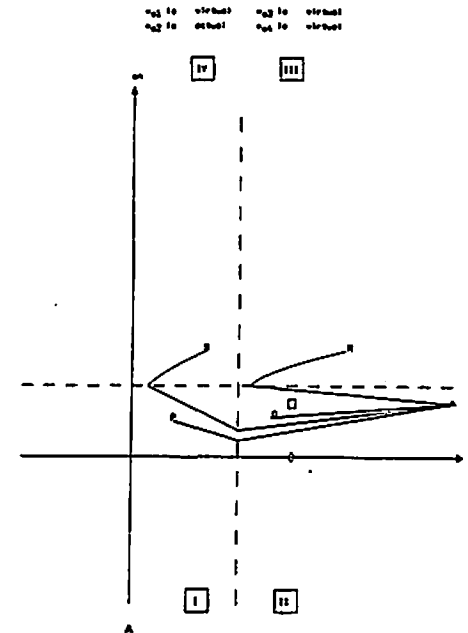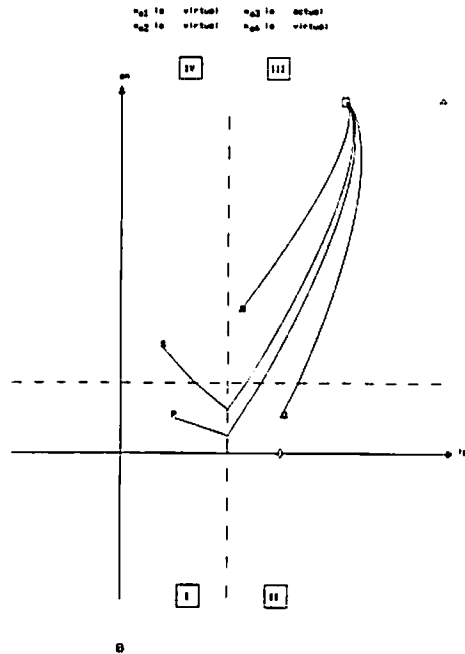
decays in the absence of excitation and LP membrane potential varies according to the combined effect of SN inhibition and input s excitation; that is, the trajectory of the system transient response tends to converge to singular point x_{e4}. After the trajectory reaches the boundary between regions IV and I, the system converges to the "actual" equilibrium point x_{e2} following a trajectory similar to the one described for the situation where the initial state is given by point P.

CASE D.- Strong input ($s > \Theta_{lp}$), strong excitatory effect from LP upon SN ($\frac{1}{k_{sn}}w_{lp-sn} > \Theta_{sn}$), and weak inhibition from SN to LP (($s+w_{lp-lp}-\frac{1}{k_{sn}}w_{sn-lp}w_{lp-sn}) > \Theta_{lp}$). In this case, equilibrium state x_{e3} is the "actual" point, while the rest (x_{e1}, x_{e2} and x_{e4}) are "virtual" points (see Fig. 43D). Whenever the initial state is given by a point R where both cells respond ($lp > \Theta_{lp}$ and $sn > \Theta_{sn}$), the inhibitory effect from SN to LP is not strong enough to overcome the excitation received by LP from its own recurrent axons and from input s. Therefore, SN membrane potential goes to a level proportional to the excitation it receives from LP axons, and LP potential gets to a level proportional to the combined effect of self-excitation, input s and the inhibition it receives from SN. In other words, the trajectory starting at point R converges quickly to the "actual" equilibrium state x_{e3}.

If point S ($lp < \Theta_{lp}$ and $sn > \Theta_{sn}$) is the initial state then SN potential decays in the absence of LP axon potentials, while LP membrane potential varies according to the activity of its afferents (s and SN). The system trajectory, then, enters into region I, that is, SN potential goes below threshold where input s is the only activity left in the net. Here the system trajectory obeys the linear differential equations associated with region I, thus, it tends to converge to the "virtual" point x_{e1}. This means that input s drives LP potential above threshold taking the system into region II, where LP axon potentials become active. The

operation of the system switches again and a new set of linear differential equations takes control of the system dynamics. Here, because LP axon potentials are active, SN potential starts increasing until it gets above threshold; whereas LP activity tends to grow to a level proportional to the sum of s plus self-excitation. This causes the non-linear system to enter region III. In this region, as seen above, SN and LP membrane potential quickly converge to a level proportional to their inputs; in other words, the trajectories followed by the system transient responses converge to the "actual" point x_{e3}.

If the initial state is given by Q, $lp > \Theta_{lp}$ and $sn < \Theta_{sn}$, then the system tends to converge to a state x_{e2} where LP potential is proportional to input s plus its own self-excitation, and SN potential is proportional to the excitation coming from LP. Before reaching such a point the trajectory gets into region III where a different linear operation controls the system dynamics. As seen above, once in region III, SN axon potential becomes active and starts a competition between excitation and inhibition within the net. In this case excitation is stronger than inhibition keeping LP and SN membrane potentials above threshold, and the system converges to the equilibrium state x_{e3}, where both cells' membrane potentials reach levels that are proportional to their inputs.

When point P ($lp < \Theta_{lp}$ and $sn < \Theta_{sn}$) is the initial state the only activity in the network is given by input s, which makes LP membrane potential grow above threshold. That is the trajectory enters into regio III. It is clear that this situation is similar to the one, just described, that has Q as initial state. That is, the system converges to the "actual" point x_{e3} visiting several regions in the following sequence: $I \to II \to III \to x_{e3}$.

CASE E.- Strong input ($s > \Theta_{lp}$), strong excitatory effect from LP over SN ($\frac{1}{t_{sn}} w_{lp-sn} > \Theta_{sn}$), and strong inhibition from SN to LP (($s + w_{lp-lp} -$

$\frac{1}{t_{sn}} w_{sn-lp} w_{lp-sn}) < \Theta_{lp}$). The last case to be analyzed is when all four singular states x_{e1}, x_{e2}, x_{e3} and x_{e4} are "virtual" points. This parametric combination presents the most interesting case (see Fig. 47). All four equilibrium points are stable, but none of them can be reached by any trajectory. Thus, the system, under these circumstances, would present an "oscillation". What has to be shown is whether or not this oscillation can be represented as converging towards a closed path in the phase-plane portrait. There are different types of closed paths, such as a "center" or a "limit cycle" for example. A "center" is a closed path that always occurs as a part of a family of closed curves, so that there are other closed curves in the neighborhood of a given one. The trajectory followed by the system depends on the initial state it starts from; whereas a "limit cycle" is defined as an isolated closed path in the phase-plane portrait that represents a steady-state oscillation to which all trajectories nearby, starting inside or outside this closed path, may converge or diverge. That is, it divides the phase-plane into an inside and an outside. Additionally, because limit cycles are isolated from each other, there cannot be another limit cycle in the neighborhood of a given one. It should also be noted that in a limit cycle the amplitude of oscillation is independent of the initial state [Ogata, 1970; Gibson, 1963; Shinners, 1978; Raven, 1968].

First, we want to know whether the oscillation presented by the neural net model corresponds to a "limit cycle", and then we analyse the model's qualitative behavior in terms of neural activity.

To prove the existence of a limit cycle, Bendixson's second theorem will be considered [Gibson, 1963]. Assume that two finite closed curves C_1 and C_2 can be established in the phase-plane portrait, with C_2 enclosing C_1 (see Fig. 44). The region contained between C_1 and C_2 is called D. Assume further that region D does not contain any equilibrium point. The second theorem of Bendixson asserts
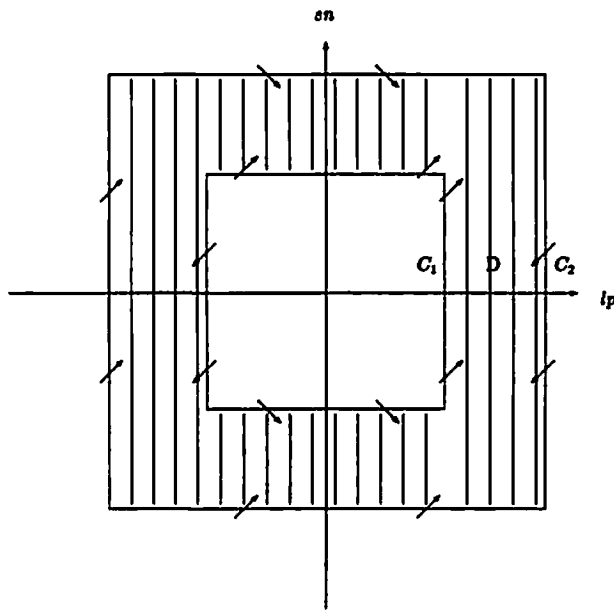
Figure 44: Graphical illustration for Bendixson's second theorem

that if the solution trajectory enters and remains inside region D as $t \to \infty$, then the trajectory is either a limit cycle itself or approaches a limit cycle, that is, there is assurance that D does contain a "limit cycle".

Thus our problem is reduced to proving whether or not such curves C_1 and C_2 and region D can be defined for our example. Let us start by analysing how trajectories behave around the equilibrium points. We have that for regions I and II matrix **A** is diagonal

$$ \mathbf{A} = \begin{bmatrix} \frac{-1}{\tau_{lp}} & 0 \\ 0 & \frac{-k_{nn}}{\tau_{nn}} \end{bmatrix} $$

so both eigenvalues are negative real. There are two possible cases, they may have either equal or different magnitude. If they have different values, when they are far from the equilibrium state, solution trajectories tend to converge to the equilibrium point parallel to the "principal direction" that corresponds to the larger eigenvalue, also referred to as the "faster eigenvector", and reach it parallel to the "principal direction" corresponding to the smaller eigenvalue, also referred to as the "slower eigenvector". Fig. 45A shows the phase-plane portrait for the condition of $\lambda_2 > \lambda_1$. The slope of the "principal directions" is calculated from the "modal" matrix **T** of **A**, which is formed by the "eigenvectors" of **A**, that is,

$$ \mathbf{T} = \begin{bmatrix} \mathbf{v}_1 & \mathbf{v}_2 \end{bmatrix} = \begin{bmatrix} T_{11} & T_{12} \\ T_{21} & T_{22} \end{bmatrix} $$

where $\mathbf{v}_1$ and $\mathbf{v}_2$ are the eigenvectors of **A**. It can be demonstrated [see Gibson, 1963] that the slopes of the eigenvectors are uniquely defined by

$$ m_1 \triangleq \frac{T_{21}}{T_{11}}, \quad \text{and} \quad m_2 \triangleq \frac{T_{22}}{T_{12}} $$

In this case, the modal matrix is the identity matrix, thus the slope of the "principal direction" associated with λ_1 is 0, and with λ_2 is ∞.
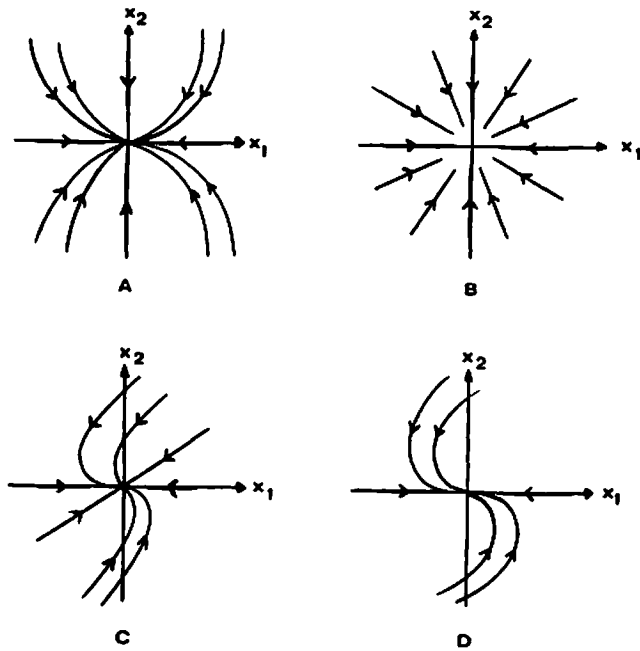
Figure 45: Typical phase-plane portraits for second order systems. Phase-plane portraits for the equilibrium points corresponding to regions I and II: A) for the condition of different real negative eigenvalues ($\lambda_2 > \lambda_1$); and B) for the case of equal negative real eigenvalues. For regions III and IV: C) for the condition of distinct negative real eigenvalues, $m_2 > 0$ and $\lambda_2 > \lambda_1$; and D) for the situation of equal negative real eigenvalues.

In case both eigenvalues are equal, the trajectories in the phase-plane portrait are straight lines that cross each other only at the equilibrium point, as can be seen in Fig. 45B.

We know that for regions III and IV matrix A is triangular

$$A = \begin{bmatrix} \frac{-A}{n_p} & \frac{-w_{mis}}{n_p} \\ 0 & \frac{-k_m}{r_{os}} \end{bmatrix}$$

Again, we have two possible cases for the eigenvalues; they may have equal or different negative real magnitude. If the eigenvalues are distinct then [see Espinosa, 1978] the eigenvectors are given by any non-zero column of the matrix

$$adj(A - \lambda I_n)\,|_{\lambda=\lambda_i}$$

so the eigenvectors of A are

$$v_1 = \begin{bmatrix} \frac{-w_{mis}}{n_p} \\ 0 \end{bmatrix} \quad \text{and} \quad v_2 = \begin{bmatrix} \frac{-w_{mis}}{n_p} \\ \frac{-k_m}{r_{os}} + \frac{1}{n_p} \end{bmatrix}$$

thus, the slope of the eigenvector associated with λ_1 is

$$m_1 \triangleq \frac{T_{21}}{T_{11}} = 0$$

and the slope of the eigenvector associated with λ_2 is

$$m_2 \triangleq \frac{T_{22}}{T_{12}} = \frac{\frac{-n_s}{r_{os}}k_m + 1}{-w_{m-p}}$$

Without loss of generality, let us assume that $\frac{n_s}{r_{os}}k_m > 1$ so m_2 is positive. Under these circumstances, Fig. 45C shows the phase-plane portrait corresponding to the condition $\lambda_2 > \lambda_1$. The trajectories approach the equilibrium state asymptotically to the slowest eigenvector.

When the eigenvalues are equal, then the modal matrix T is

$$T = \begin{bmatrix} \frac{-\omega_{th/k}}{r l_p} & 0 \\ 0 & -1 \end{bmatrix}$$

where v_1 was obtained from $(A - \lambda_1 L_n)v_1 = 0$, and v_2 (not an eigenvector) was obtained from $(A - \lambda_1 L_n)v_2 = v_1$. In this case the trajectories approach the equilibrium state asymptotically to the eigenvector v_1 whose slope is 0. This can be observed in Fig. 45D.

Now, based on the characteristics of the eigenvectors defined above, we proceed to define the closed paths C_1 and C_2 as well as region D for our second order system example.

Thus C_1 can be defined as a tiny square around the point whose coordinates are the threshold values Θ_{lp} and Θ_m. In Fig. 46 this point falls where the broken lines cross each other. Any trajectory starting inside the part of regions I, II or IV enclosed by C_1 would cross C_1 outwardly or, eventually, would reach the boundary between regions II and III from where, because of the way trajectories approach x_3, the trajectory would cross C_1 outwardly getting into region D. For simplicity just one trajectory is shown in Fig. 46.

Now, a closed curve C_2 that is crossed inwardly by all trajectories must be established. The choice of C_2 can be observed in Fig. 46. It starts with a straight line perpendicular to the lp axis which goes from point $([s + \omega_{lp-lp}], 0)$ to the location of x_{i3}. Then, it continues right to left along a straight line parallel to the eigenvector v_1 of the matrix A associated with x_{i3} until it reaches the frontier between regions III and IV, that is, until the point $(\Theta_{lp}, \frac{\omega_{lp-lp}}{k_n})$. The next segment of C_2 falls inside region IV, and it is a straight line that runs tangential to the trajectory that passes through the point $(\Theta_{lp}, \frac{\omega_{lp-lp}}{k_n})$ until it reaches the line perpendicular to sn axis that passes through Θ_m. Then, it continues along a
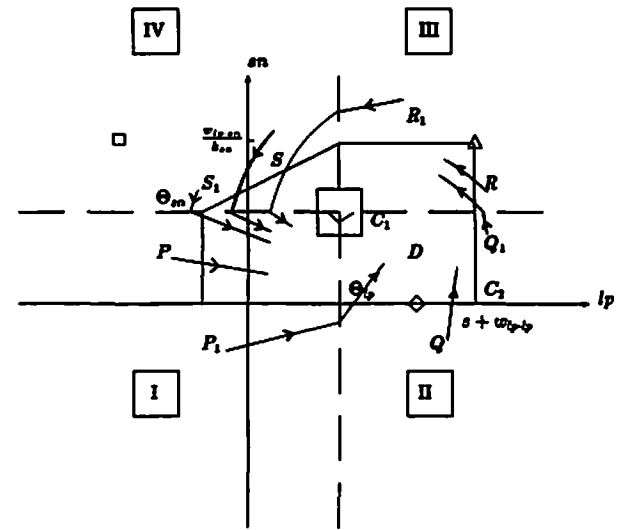
Figure 46: Definition of the curves of Bendixson's Theorem. $\Diamond$, $\triangle$ and $\square$ show the location of the equilibrium points. Application of Bendixson's second theorem to check if, under the parametric combination assumed in CASE E, the system presents a limit cycle (see text for explanation). See legend of Fig. 42 for an explanation of the graph.

straight line parallel to the sn axis until it reaches the lp axis. Finally, it continues left to right along the eigenvector v_1 of the matrix A associated with z_{s4} until the point $([s + w_{lp.lp}], 0)$, forming in this way a closed curve. Because of the way they approach equilibrium points, all trajectories with initial states falling outside the region enclosed by C_2 eventually enter, and remain in, region D crossing C_2 inwardly. In each of the regions I, II, III and IV there are always two possible cases: trajectories going directly into region D through C_2, starting at points P, Q, R and S in Fig. 46, and trajectories that get first into adjacent regions and then cross C_2 inwardly entering region D, starting at points P_1, Q_1, R_1 and S_1 in Fig. 46.

To complete Bendixson's second theorem we must note that region D contains no equilibrium points, thus, the existence of a stable "limit cycle" has been established. However, this does not prove that there is only one such limit cycle. This uniqueness is suggested (but not proved) by the following simulations.

Now, we want to analyse the qualitative behavior presented by the neural net model under these circumstances. Fig. 47 shows the phase-plane portrait for different initial states, P, Q, R and S. If the initial state is given by P, $lp < \Theta_{lp}$ and $sn < \Theta_{sn}$, then the system tends to converge to equilibrium state z_{s1}. Here, input s is the only active element in the network and its excitatory effect upon LP makes this cell's membrane potential go above threshold, moving the system into region II. The system now tends to converge to "virtual" point z_{s2}. LP response starts exciting SN until its potential gets above threshold and, at the same time, LP potential tends to grow to a level corresponding to the combined effect of input s and LP self-excitation. Thus, the system enters region III, where SN axon potentials become active and initiate a competition between excitation, from s and LP, and inhibition, from SN, in the net. In this case inhibition is
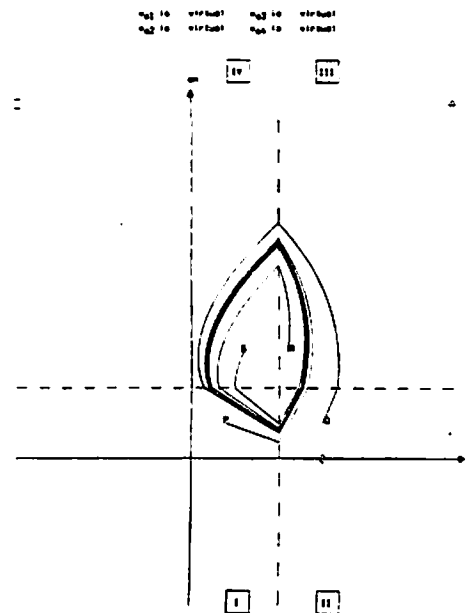
Figure 47: Phase-plane portraits of the LP-SN network (Case E). Again, in this figure $\Diamond$, $\triangle$ and $\square$ show the location of the equilibrium points. In this case all equilibrium points are "virtual" points. This figure shows a phase-plane portrait of the limit cycle presented by the LP-SN neural net model. See legend of Fig. 42 for an explanation of the graph.

stronger than excitation, which takes LP potential to a subthreshold value so the system trajectory enters region IV. In this region the inhibition from SN to LP is still stronger than the excitation LP receives from input s, thus, LP potential remains below threshold. In the absence of LP response, SN potential decays towards its resting level. That is, the trajectory tends to converge to equilibrium point x_{ri}, but it reaches the frontier between regions IV and I. The linear system associated with region I takes control of the system dynamics once again. So, the system tends to converge to equilibrium point x_{ii} following a trajectory parallel to the one described when the initial state was given by P. Input s is the only active element in the net and its excitatory effect upon LP makes this cell's membrane potential grow above threshold taking the system, once more, into region I. Fig. 47 shows that from state P the system trajectory coverges to the closed path, which is shown by a thicker line. That is, in steady state, the network presents a cycle of four stages: first, a period of time where only LP response is active; second, a period with both cells LP and SN responding; third, a period where only SN responds; and fourth, a period where both LP and SN become inactive.

If the initial state is given by Q, $lp > \Theta_{lp}$ and $sn < \Theta_{sn}$, then the system converges to the closed path ("limit cycle") following a trajectory parallel to that described above for the situation where P was the initial state and the system entered region II (see Fig. 47). Here, the system presents the cycle starting with a period where only LP responds, and so on, until it converges to the proper amplitud and frequency of the steady oscillation.

Trajectories starting at states located inside the closed path also converge to it. The trajectory beginning at a state R within region III, $lp > \Theta_{lp}$ and $sn > \Theta_{sn}$, converges to the "limit cycle", as can be seen in Fig. 47. At point R both SN and LP are active so the competition between excitation and inhibition in the

net drives LP potential below threshold moving the system into region IV. Then the linear system approximating the non-linear system switches when the trajectory reaches the frontier between regions III and IV. In this case, as seen above, inhibition is stronger than excitation which keeps LP membrane potential below threshold and takes SN potential to a subthreshold value. Thus, the trajectory moves the systme from region IV to region I. At this point the only activity in the network is the external input s whose effect upon LP drives this cell's membrane potential above threshold. This causes the system to reach the frontier between regions I and II, and it keeps on going from one region to the next until it converges to the "limit cycle".

When the initial state is given by S, $lp < \Theta_{lp}$ and $sn > \Theta_{sn}$, the system converges to the closed path following a trajectory parallel to the one described above for the situation where R was considered as the initial state and the trajectory entered region IV (see Fig. 47). The system starts the oscillation with the period of time where SN is the only active element in the network, followed by the time where both cells are inactive, then by the period where only LP responds and finally the period with both cells becoming active.

Thus, the "limit cycle" shown by the system transient response is *stable* because any trajectory starting at an initial state that falls inside or outside the closed path always converges to it. The amplitude of the oscillation is a function of the location of the equilibrium points, which depends on the choice of the external input s and the model parameters, such as, synaptic weight factors and threshold values. Additionally, the time the system spends within each subregion in the closed path depends on the membrane time constants.

This example shows how methodologies from Non-linear Systems Theory can be used to analyse the stability and the sensitivity of neural net models to differ-

ent parametric combinations. In this analysis we only dealt with models whose mathematical representation is given by a set of first order differential equations with small non-linearities (threshold functions). In next section we apply the same analysis to the model of a single Facilitation Tectal Column.

FTC Qualitative Analysis

The interconnections among elements of the FTC model are shown in the block diagram displayed in Fig. 48 (see also Fig. 37). The extrinsic inputs to elements in the FTC come from ganglion cells of type R2 (to GL, LP, SP and PY), R3 and R4 (both to PY and TP). In our computer simulations we consider two different situations with respect to the retinal input, it is either zero, no visual stimulus in the FTC receptive field, or constant for a period of time, a visual stimulus is presented for a finite period of time.

The glomerulus is the first element in the model to be activated by an input and it excites LP and SP cells. These cells, in turn, send recurrent axons to GL forming positive feedback loops. LP is also the source of excitation to the only inhibitory element in the model (SN), which controls the FTC level of activity by inhibiting LP and SP cells, thus keeping in this way the positive feedback loops from becoming unstable. The efferent element (PY) integrates the internal activity of the FTC model and the retinal response level, by receiving excitation from both pear-shaped (LP and SP) cells and from ganglion cells R2, R3 and R4. Finally, the FTC response to different configurational stimuli is also controlled by the TP neuron, through an inhibitory effect upon LP, SP and PY cells, when large ("predator-like") objects are presented in the animal's visual field (see Chapter 3). The corresponding mathematical representation of the model is:
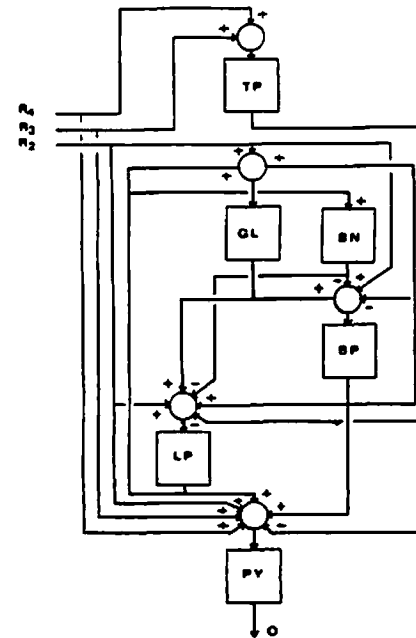
Figure 48: Block Diagram of FTC element's interconnections.
O means synapse, ↓ − means inhibition, and ↓ + means excitation. This diagram shows the connectivity pattern of the pretectal (TP) neuron, glomerulus (GL), large pear (LP) cell, small pear (SP) cell, stellate neuron (SN) and pyramidal cell (PY). O means output, and R2, R3 and R4 represent the retinal input.

for membrane potentials:

$$\tau_{gl}\dot{gl}(t) = -k_{gl} \cdot gl(t) + w_{r2\text{-}gl}R2 + w_{sp\text{-}gl}f(sp) + w_{lp\text{-}gl}f(lp) \qquad (4.8)$$

$$\tau_{lp}\dot{lp}(t) = -lp(t) + w_{r2\text{-}lp}R2 + w_{gl\text{-}lp}h(gl) + w_{sp\text{-}lp}f(sp) - $$
$$w_{lp\text{-}lp}g(tp) - w_{sn\text{-}lp}h(sn) \qquad (4.9)$$

$$\tau_{sp}\dot{sp}(t) = -sp(t) + w_{r2\text{-}sp}R2 + w_{gl\text{-}sp}h(gl) - w_{lp\text{-}sp}g(tp) - $$
$$w_{sn\text{-}sp}h(sn) \qquad (4.10)$$

$$\tau_{sn}\dot{sn}(t) = -k_{sn} \cdot sn(t) + w_{lp\text{-}sn}f(lp) \qquad (4.11)$$

$$\tau_{tp}\dot{tp}(t) = -tp(t) + w_{r3\text{-}tp}R3 + w_{r4\text{-}tp}R4 \qquad (4.12)$$

$$\tau_{py}\dot{py}(t) = -py(t) + w_{r2\text{-}py}R2 + w_{r3\text{-}py}R3 + w_{r4\text{-}py}R4 + $$
$$w_{lp\text{-}py}f(lp) + w_{sp\text{-}py}f(sp) - w_{tp\text{-}py}g(tp) \qquad (4.13)$$

and for axon potentials:

$$h(gl) = \begin{cases} k1_{gl} \cdot gl(t) & if \; gl(t) \geq 0 \\ 0 & otherwise \end{cases} \qquad (4.14)$$

$$f(lp) = \begin{cases} 1 & if \; lp(t) \geq \Theta_{lp} \\ 0 & otherwise \end{cases} \qquad (4.15)$$

$$f(sp) = \begin{cases} 1 & if \; sp(t) \geq \Theta_{sp} \\ 0 & otherwise \end{cases} \qquad (4.16)$$

$$h(sn) = \begin{cases} k1_{sn} \cdot sn(t) & if \; sn(t) \geq \Theta_{sn} \\ 0 & otherwise \end{cases} \qquad (4.17)$$

$$g(tp) = \begin{cases} k1_{tp} \cdot tp(t) & if \; tp(t) \geq \Theta_{tp} \\ C_{tp} & otherwise \end{cases} \qquad (4.18)$$

$$s(py) = \begin{cases} \Theta_{py1} - \Theta_{py0} & if \; py(t) \geq \Theta_{py1} \\ py(t) - \Theta_{py0} & if \; \Theta_{py0} \leq py(t) < \Theta_{py1} \\ 0 & if \; py(t) < \Theta_{py0} \end{cases} \qquad (4.19)$$

where

$k1_{gl}$, $k1_{sn}$ and $k1_{tp}$ are constants, and

k_{gl} and k_{sn} are used to give GL and SN longer decay constants.

Our analysis is conducted keeping in mind the anatomical and physiological correlates embedded in the FTC model. From Ingle's experiments we may conclude that, within a reasonable period of time after the visual stimulus is removed the FTC elements return to their resting level potentials. In the model we assume null activity as the resting level. So, during this first part of our analysis the retinal input is considered zero ($R_i = 0$, $i = 2, 3, 4$), and we analyse those cases when the system enters one of the subregions in the state-space that are reachable during the process of prey-catching facilitation. Moreover, the system would return to the equilibrium state of the region where all FTC elements are inactive (resting level) if that state is stable and fits the classification of an "actual" state, whereas the equilibrium points corresponding to all the other regions in the state-space, while being stable, are "virtual" points. Thus, at this stage we look for the parametric combinations that allow the FTC elements to display the proper physiological behavior during the process of PY response facilitation. We pay especial attention to the trajectories followed by the system transient responses in their convergence to the "actual" equilibrium state.

The FTC's six-dimensional state-space, membrane potentials represent state variables, can be divided into 96 different subregions (a factor of 3 for PY and of 2 for each other cell), whose boundaries depend on the choice of the threshold values. Analysing the FTC architecture we find that the number of subregions in

the state-space that need to be analysed can be reduced. It is clear from Fig. 48, and from the FTC mathematical representation (equations 4.8 & 4.13), that the PY cell integrates the internal column activity with information coming from the retina and from the pretectum, but it does not affect the dynamics within the column in any way. That is, there are no projections from PY axons to any other element in the FTC. Therefore, the "stability" analysis can be reduced to the analysis of two subsystems connected in cascade: one given by the PY cell, and the other by the rest of the FTC elements (GL, LP, SP, SN & TP). Thus, instead of having to analyse 96 different subregions, we need only to study the PY cell by itself on one side and 32 regions in a reduced state-space corresponding to the second subsystem on the other side.

In the model, PY cell input is represented by axon terminals coming from the retina (R2, R3 & R4), the optic tectum (LP & SP) and the pretectum (TP) whose values are either zero or constant, when those elements are inactive or active respectively. Amari [1977, 1982] and An der Heiden [1980] have shown that for a single neuron, represented by equations (4.1) and (4.4) and whose input s is constant, the neuron response $m(s)$ converges to a unique level, corresponding to the equilibrium state of the differential equation (4.1) that models the neuron's membrane potential. Furthermore, this neuron's membrane potential eventually converges to the equilibrium state no matter what the initial state it starts from. Amari calls a neuron that behaves in this fashion "monostable".

The FTC model includes the hypothesis that PY response corresponds to the probability of getting a prey-catching behavior from the animal. Thus, any visual stimulus that drives the system into a region where PY becomes active would represent a potential prey.

Ingle [1975] also showed that the "attention" units are more easily found in

animals with pretectal lesion than in normal ones. Pretectal cell TP is also postulated to respond when "predator-like" objects are present in the animal's visual field (see Chapter 3). Therefore, when studying facilitation in the response to a prey-like stimulus, we can analyze the FTC model behavior when TP membrane potentials have subthreshold values. This reduces the number of regions to be studied from 32 subregions to 16.

During prey-catching facilitation, when a visual stimulus appears in the FTC receptive field, GL is the first element to be activated. In addition, one of the postulates embedded in the FTC model of Lara et al [1982] is that facilitation in tectal activity after removing the visual stimulus from the column receptive field is traced to the accumulation of excitation in GL and SP potentials (see also Arbib [1982]). This means that GL is also the last element to be deactivated. Thus, the number of regions to be studied during our "stability" and "parameter sensitivity" analyses can be reduced to 9. That is, the regions that need to be analyzed are those where GL is active plus the one where all FTC elements, including GL, are at their resting level (inactive).

The stability of the FTC model is conducted by analyzing the set of first order linear differential equations that approximates the non-linear system inside the region where all FTC elements have membrane potentials above threshold. At this point, we want to analyze the neural net stability by asking whether a departure from equilibrium tends to disappear, grows without limit or presents an oscillation. In this subregion the FTC mathematical representation is given

by

$$\tau_{gl}\dot{gl}(t) = -k_{gl}gl(t) + w_{sp\text{-}gl} + w_{lp\text{-}gl}$$
$$\tau_{lp}\dot{lp}(t) = -k_{lp}lp(t) + w_{gl\text{-}lp}gl(t) + w_{rp\text{-}lp} - w_{tp\text{-}lp}tp(t) - w_{sn\text{-}lp}sn(t)$$
$$\tau_{sp}\dot{sp}(t) = -k_{sp}sp(t) + w_{gl\text{-}sp}gl(t) - w_{tp\text{-}sp}tp(t) - w_{sn\text{-}sp}sn(t)$$
$$\tau_{sn}\dot{sn}(t) = -k_{sn}sn(t) + w_{lp\text{-}sn}$$
$$\tau_{tp}\dot{tp}(t) = -k_{tp}tp(t)$$

so, matrix A is

$$A = \begin{bmatrix} \frac{-k_{gl}}{\tau_{gl}} & 0 & 0 & 0 & 0 \\ \frac{w_{gl\text{-}lp}}{\tau_{lp}} & \frac{-k_{lp}}{\tau_{lp}} & 0 & \frac{-w_{sn\text{-}lp}}{\tau_{lp}} & \frac{-w_{tp\text{-}lp}}{\tau_{lp}} \\ \frac{w_{gl\text{-}sp}}{\tau_{sp}} & 0 & \frac{-k_{sp}}{\tau_{sp}} & \frac{-w_{sn\text{-}sp}}{\tau_{sp}} & \frac{-w_{tp\text{-}sp}}{\tau_{sp}} \\ 0 & 0 & 0 & \frac{-k_{sn}}{\tau_{sn}} & 0 \\ 0 & 0 & 0 & 0 & \frac{-k_{tp}}{\tau_{tp}} \end{bmatrix}$$

This linear system has a unique equilibrium state ($|A| \neq 0$). It is located at

$$z_{eq} = \begin{bmatrix} gl_{eq} \\ lp_{eq} \\ sp_{eq} \\ sn_{eq} \\ tp_{eq} \end{bmatrix} = \begin{bmatrix} \frac{w_{sp\text{-}gl} + w_{lp\text{-}gl}}{k_{gl}} \\ \frac{w_{gl\text{-}lp}(w_{sp\text{-}gl} + w_{lp\text{-}gl})}{k_{gl}k_{lp}} + \frac{w_{rp\text{-}lp}}{k_{lp}} - \frac{w_{sn\text{-}lp}w_{lp\text{-}sn}}{k_{sn}k_{lp}} \\ \frac{w_{gl\text{-}sp}(w_{sp\text{-}gl} + w_{lp\text{-}gl})}{k_{gl}k_{sp}} - \frac{w_{sn\text{-}sp}w_{lp\text{-}sn}}{k_{sn}k_{sp}} \\ \frac{w_{lp\text{-}sn}}{k_{sn}} \\ 0 \end{bmatrix}$$

and its eigenvalues, obtained by solving the characteristic equation $|\lambda I - A| = 0$, are

$$\lambda_1 = -\frac{k_{gl}}{\tau_{gl}}, \quad \lambda_2 = -\frac{k_{lp}}{\tau_{lp}}, \quad \lambda_3 = -\frac{k_{sp}}{\tau_{sp}}, \quad \lambda_4 = -\frac{k_{sn}}{\tau_{sn}}, \quad \lambda_5 = -\frac{k_{tp}}{\tau_{tp}}$$

Since the membrane time constants are always positive, the eigenvalues are negative real and matrix A is *stable*. It is clear that the matrices A for all the other regions in the state-space would have *at most* the same non-zero elements. Thus, it is observed at this point that no matter what the values of the F's

(threshold functions) here the eigenvalues are the main diagonal elements, and so matrices A are *stable*. That is, all equilibrium states associated with the linear operations that approximate the non-linear system inside any of the reachable subregions are locally *stable*.

Before analyzing such regions, let us consider Fig. 49, which shows a trajectory the system may follow in order to produce facilitation of the PY cell's response. Note that we are not deducing Fig. 49 from our model. Rather Fig. 49 summarizes how the model is to behave if it is to capture important properties of facilitation. We will then analyse the FTC mathematically to find constraints on its parameters which will let it behave as required by Fig. 49. This behavior was abstracted from Ingle's empirical results [Ingle, 1973b, 1975] and from theoretical results reported by Lara et al [1982]. The right hand side of this figure displays the state of each FTC element within the region shown at the left, 1 means the element is active and 0 inactive. Here, it is assumed that the system is at its resting level, within region 0, when the visual stimulus is presented for the first time. The stimulus presentation activates GL moving the system into region 1. Then, the retinal input and GL activity cooperate in driving LP membrane potential above a threshold value, taking the system inside region 5, and in producing a depolarizing effect on the SP cell. At this moment, LP presents its first burst of activity, which increases GL potential through recurrent axon terminals and, at the same time, activates the SN neuron moving the system into region 6. The stimulus is removed before the SP cell responds, avoiding in this way that a PY cell response be elicited. Then, SN inhibitory effect, in the absence of retinal input, makes LP become inactive moving the system into region 2. At this point, SN and GL sources of excitation are off, thus their potentials start to decay towards their resting level. SN is the first to become inactive taking
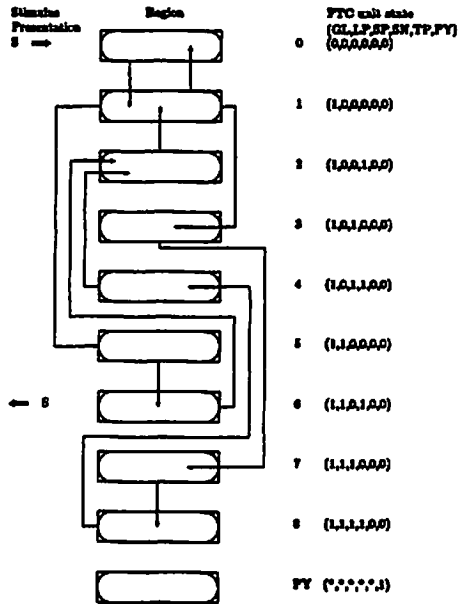
Figure 49: Prey-catching facilitation state sequence
Trajectory (state sequence) followed by the FTC neural network model during the process of prey-catching facilitation (see text for explanation).

the system, once again, inside region 1. Here, the remaining activity in GL, after SN becomes inactive, drives SP potential above threshold presenting the SP characteristic delayed response. The SP response increases GL activity through recurrent axons, and both elements activate the LP cell which presents its second burst of activity, moving the system into region 7. At this point, GL activity is increased by recurrent axons from both pear-shaped cells, while LP response activates the SN neuron taking the system inside region 8. Here, competition between recurrent excitation and inhibition within the FTC model becomes crucial. Inhibition, through SN, has to be stronger than excitation, through GL, so that membrane potentials of both pear-shaped cells are taken below threshold moving the system into region 4 and then into region 2. Once again, with LP and SP being inactive, GL and SN potentials decay towards their resting levels. The SN potential is the first to go below threshold taking the system inside region 1. Here, the GL remaining activity increases LP and SP potentials, but is not strong enough to elicit a response from either of these cells. Thus, GL keeps certain degree of neural activity within the FTC, which will produce a facilitation of PY cell's response if a second stimulus of subthreshold duration is presented after a short delay of few seconds. If a second stimulus is not presented then the system converges to the equilibrium point z_{eo} where all FTC elements are at their resting level.

Now, based on the nature and location of the equilibrium states corresponding to the 9 subregions to be reviewed, we want to analyse the different qualitative behaviors displayed by the FTC model under different parametric combinations. We will start by analysing region 0 where all the FTC elements are at their resting

level. The state-variable representation is

$$\tau_{gl}\dot{gl}(t) = -k_{gl}gl(t)$$
$$\tau_{lp}\dot{lp}(t) = -k_{lp}lp(t) - w_{tp\text{-}lp}C_{tp}$$
$$\tau_{sp}\dot{sp}(t) = -k_{sp}sp(t) - w_{tp\text{-}sp}C_{tp}$$
$$\tau_{sn}\dot{sn}(t) = -k_{sn}sn(t)$$
$$\tau_{tp}\dot{tp}(t) = -k_{tp}tp(t)$$

The equilibrium point, obtained by solving $\dot{x}(t) = A\,x_{eq} + \alpha = 0$, is

$$x_{e0} = \begin{bmatrix} 0 \\ \frac{-w_{tp\text{-}lp}C_{tp}}{k_{lp}} \\ \frac{-w_{tp\text{-}sp}C_{tp}}{k_{sp}} \\ 0 \\ 0 \end{bmatrix}$$

In order to match results from Ingle's experiments we want this singular state to be an "actual" point, which occurs if

$$\Theta_{lp} > \frac{-w_{tp\text{-}lp}C_{tp}}{k_{lp}} \qquad (A)$$

and

$$\Theta_{sp} > \frac{-w_{tp\text{-}sp}C_{tp}}{k_{sp}} \qquad (B)$$

are true. That is, the tonic effect of TP neurons upon LP and SP cells must not take these cells' membrane potentials above threshold. Because in the FTC model it is hypothesized that TP effect on tectal elements is of an inhibitory nature, conditions (A) and (B) are true, and so equilibrium state x_{e0} is an "actual" point. When presenting a prey-like object for the first time, the system goes from region 0 to region 1 where only GL becomes active. This is accomplished if GL membrane potential reaches the threshold (Θ_{gl}) value faster than all the other elements receiving direct retinal input (LP, SP, TP & PY). The FTC model

considers GL as a slow-potential non-spiking element with zero threshold. Thus, as soon as the visual stimulus is presented GL becomes active, whereas it takes longer for the other cells' potential to reach the threshold.

The next region to be analyzed is region 1. Inside this region the FTC state-variable representation becomes

$$\tau_{gl}\dot{gl}(t) = -k_{gl}gl(t)$$
$$\tau_{lp}\dot{lp}(t) = -k_{lp}lp(t) + w_{gl\text{-}lp}gl(t) - w_{tp\text{-}lp}C_{tp}$$
$$\tau_{sp}\dot{sp}(t) = -k_{sp}sp(t) + w_{gl\text{-}sp}gl(t) - w_{tp\text{-}sp}C_{tp}$$
$$\tau_{sn}\dot{sn}(t) = -k_{sn}sn(t)$$
$$\tau_{tp}\dot{tp}(t) = -k_{tp}tp(t)$$

and the equilibrium point is

$$x_{e1} = \begin{bmatrix} 0 \\ \frac{-w_{tp\text{-}lp}C_{tp}}{k_{lp}} \\ \frac{-w_{tp\text{-}sp}C_{tp}}{k_{sp}} \\ 0 \\ 0 \end{bmatrix}$$

x_{e1} coincides with x_{e0}, thus if conditions (A) and (B) are true, then x_{e1} falls outside of region 1, and is, therefore, a "virtual" point. During the process of PY response facilitation this is a critical region (see above). It is reached under three different circumstances: first, if a stimulus is presented when the system is at the resting level; second, right after LP's first burst of activity and SN membrane potential goes below threshold; and third, when the system is returning to its resting state.

When region 1 is reached from rest, the other FTC elements that can be activated are LP or SP. The SN neuron cannot be activated because its only source of excitation (LP) is off. In the FTC model, the LP and SP cells are proposed to be equivalent to the "attention" units reported by Ingle [1973b,

1975]; LP being correlated to the one presenting two bursts of activity with an intermediate period of silence, and SP being equivalent to the one presenting a delayed response (see Fig. 36). This means LP has to be activated before SP does, which may be accomplished by choosing a slower time constant

$$\tau_{lp} < \tau_{rp} \qquad (C)$$

or a bigger threshold value

$$\Theta_{lp} < \Theta_{sp} \qquad (D)$$

for SP than for LP, or a combination of both conditions.

From the description of Fig. 49, it is clear that the trajectory followed by the system after being in region 1, during the second and third situations, depends on GL residual activity. If region 1 is reached during the second situation, then GL residual activity must be strong enough to take SP membrane potential above threshold to produce the SP hypothesised characteristic delayed response; whereas, during the third situation the remaining GL activity must not elicit a response from either of the pear-shaped cells to allow the system to converge to the equilibrium state z_{o} where all FTC elements are at their resting level.

In these two situations the value of GL residual activity depends on three factors. In the second situation it depends on: first, the combined effect coming from retinal ganglion cell R2 and LP cell; second, the elapsed time from the moment the visual stimulus is removed to the moment SN becomes inactive; and third, how fast GL activity decays. In the third situation it depends on: first, the combined excitatory effect coming from LP and SP cells; second, the elapsed time from the moment LP response is overcome by SN inhibition to the moment SN becomes inactive; and third, how fast GL activity decays.

Thus, in order to get the FTC model to present the proper sequence of events a combination of these three factors should be assumed. First, let us assume that

the the level of activity reached by GL during the second situation is stronger than the one it reaches during the third situation. This is accomplished if

$$[w_{r2\text{-}gl} + w_{lp\text{-}gl}] > [w_{lp\text{-}gl} + w_{sp\text{-}gl}] \qquad (E)$$

is true. The other two factor that need to be considered are the choices of SN and GL time decay constants (k_{sn} and k_{gl}). If GL potential decays slowly and SN potential decays fast ($k_{sn} > k_{gl}$) then the system may present more than one alternation of LP, SP and SN periods of activity (see Fig. 53 in the next section). On the other hand, if we assume the opposite case, GL potential decays fast and SN potential decays slowly ($k_{sn} > k_{gl}$), then the system would not present SP characteristic delayed response and GL may not be the last element to be deactivated (see Fig. 52 in the next section). The calculation of the optimal values for k_{sn} and k_{gl} requires a quantitative analysis of the FTC temporal response (see Discussion). Here, it will be assumed that both constants are equal, that is, it will be assumed that

$$\frac{\tau_{sn}}{k_{sn}} = \frac{\tau_{gl}}{k_{gl}} \qquad (F)$$

is true. To preserve our assumption that GL is the last FTC element to be deactivated we have to make sure that the residual activity of GL when the system enters region 2, where only GL and SN are active, is greater than that of SN. This is accomplished if

$$w_{lp\text{-}gl} > w_{lp\text{-}sn} \qquad (G)$$

The next region to be studied is where GL and SN are the only active elements

in the column. Inside this region 2 the FTC mathematical representation is

$$\begin{aligned}
\tau_{gl}\dot{gl}(t) &= -k_{gl}gl(t) \\
\tau_{lp}\dot{lp}(t) &= -k_{lp}lp(t) + w_{gl\text{-}lp}gl(t) - w_{lp\text{-}lp}C_{lp} - w_{sn\text{-}lp}sn(t) \\
\tau_{sp}\dot{sp}(t) &= -k_{sp}sp(t) + w_{gl\text{-}sp}gl(t) - w_{lp\text{-}sp}C_{lp} - w_{sn\text{-}sp}sn(t) \\
\tau_{sn}\dot{sn}(t) &= -k_{sn}sn(t) \\
\tau_{lp}\dot{tp}(t) &= -k_{lp}tp(t)
\end{aligned}$$

and the equilibrium point is

$$x_{c2} = \begin{bmatrix} 0 \\ \frac{-w_{lp\text{-}lp}C_{lp}}{k_{lp}} \\ \frac{-w_{lp\text{-}sp}C_{lp}}{k_{sp}} \\ 0 \\ 0 \end{bmatrix}$$

State x_{c2} coincides with x_{c0}, thus, because $sn_{c2} = 0$, x_{c2} fits the definition of a "virtual" point. During prey-catching facilitation this region must be reached every time SN becomes active, that is, the inhibitory effect from SN to LP and to SP must be strong enough to overcome the excitation impinging upon these cells so their membrane potentials go to subthreshold values. Otherwise the system might converge to a state where all FTC elements (GL, LP, SP & SN) are active (see Fig. 57 in the next section). Additionally, in the absence of its only source of excitation (LP), the potential of SN decays towards its resting level taking the system inside region 1 (see Fig. 49).

The next case is region 3 where GL and SP are the only FTC active elements. Here, the FTC mathematical representation is

$$\begin{aligned}
\tau_{gl}\dot{gl}(t) &= -k_{gl}gl(t) + w_{sp\text{-}gl} \\
\tau_{lp}\dot{lp}(t) &= -k_{lp}lp(t) + w_{gl\text{-}lp}gl(t) + w_{sp\text{-}lp} - w_{lp\text{-}lp}C_{lp} \\
\tau_{sp}\dot{sp}(t) &= -k_{sp}sp(t) + w_{gl\text{-}sp}gl(t) - w_{lp\text{-}sp}C_{lp} \\
\tau_{sn}\dot{sn}(t) &= -k_{sn}sn(t) \\
\tau_{lp}\dot{tp}(t) &= -k_{lp}tp(t)
\end{aligned}$$

and the equilibrium point is

$$x_{c3} = \begin{bmatrix} \frac{w_{sp\text{-}gl}}{k_{gl}} \\ \frac{w_{gl\text{-}lp}w_{sp\text{-}gl}}{k_{gl}k_{lp}} + \frac{w_{sp\text{-}lp} - w_{lp\text{-}lp}C_{lp}}{k_{lp}} \\ \frac{w_{gl\text{-}sp}w_{sp\text{-}gl}}{k_{gl}k_{sp}} - \frac{w_{lp\text{-}sp}C_{lp}}{k_{sp}} \\ 0 \\ 0 \end{bmatrix}$$

Because it was assumed that GL acts as a functional unit with zero threshold, we have that, $\frac{w_{sp\text{-}gl}}{k_{gl}} > \Theta_{gl} = 0$, holds. So, one way x_{c3} can be a "virtual" point is if

$$\left[\frac{w_{gl\text{-}sp}w_{sp\text{-}gl}}{k_{sp}k_{gl}} - \frac{w_{lp\text{-}sp}C_{lp}}{k_{sp}} \right] < \Theta_{sp} \qquad (H)$$

is true. In other words, x_{c3} is a "virtual" point if the recurrent activity caused by SP axon terminals upon GL is not strong enough to keep SP membrane potential above threshold. Another way of getting x_{c3} to be a "virtual" point is if

$$\left[\frac{w_{gl\text{-}lp}w_{sp\text{-}gl}}{k_{lp}k_{gl}} + \frac{w_{sp\text{-}lp} - w_{lp\text{-}lp}C_{lp}}{k_{lp}} \right] > \Theta_{lp} \qquad (I)$$

holds. This means that the excitation, direct and through GL, from SP to LP must take LP membrane potential above threshold. Fig. 49 shows that during the process of prey-catching facilitation the system trajectory goes from region 3 to region 7 where LP cell becomes active. It is clear that condition (I) must be true if a second LP burst of activity is ever to occur.

If condition (H) is false the system presents more than one alternation of LP, SP and SN periods of activity (see Fig. 53 in the next section). If both (H) and (I) are false the equilibrium state x_{c3} would be an "actual" point, which means that the neural net activity might converge to it and not return to the resting level state x_{c0} (see Fig. 54 in the next section).

The next region to be studied is where GL, SP and SN are active while the rest of the FTC elements are inactive. Within region 4 the FTC state-variable representation is

$$\tau_{gl}\dot{gl}(t) = -k_{gl}gl(t) + w_{op-gl}$$
$$\tau_{lp}\dot{lp}(t) = -k_{lp}lp(t) + w_{gl-lp}gl(t) + w_{op-lp} - w_{lp-lp}C_{lp} - w_{sn-lp}sn(t)$$
$$\tau_{sp}\dot{sp}(t) = -k_{sp}sp(t) + w_{gl-sp}gl(t) - w_{lp-sp}C_{lp} - w_{sn-sp}sn(t)$$
$$\tau_{sn}\dot{sn}(t) = -k_{sn}sn(t)$$
$$\tau_{tp}\dot{tp}(t) = -k_{tp}tp(t)$$

so that the equilibrium point is

$$x_{e4} = \begin{bmatrix} \frac{w_{op-gl}}{k_{gl}} \\ \frac{w_{gl-lp}w_{op-gl}}{k_{gl}k_{lp}} + \frac{w_{op-lp} - w_{lp-lp}C_{lp}}{k_{lp}} \\ \frac{w_{gl-sp}w_{op-gl}}{k_{gl}k_{sp}} - \frac{w_{lp-sp}C_{lp}}{k_{sp}} \\ 0 \\ 0 \end{bmatrix}$$

In this case, the element of x_{e4} corresponding to SN is located in a region where SN is inactive, therefore x_{e4} falls outside region 4 fitting in this way the classification of a "virtual" point. This region is reached during prey-catching facilitation after the first stimulus has been removed and the system transient response is on its way to disappear. This means that SN inhibitory effect upon SP must counteract the recurrent excitation SP might cause on itself and on the LP cell if we want the system to present the proper qualitative behavior. Such behavior shows (see Fig.49) that from region 4 the system must go into region 2.

The next case is region 5 where only GL and LP are active. The FTC mathematical representation becomes

$$\tau_{gl}\dot{gl}(t) = -k_{gl}gl(t) + w_{op-gl}$$
$$\tau_{lp}\dot{lp}(t) = -k_{lp}lp(t) + w_{gl-lp}gl(t) - w_{lp-lp}C_{lp}$$
$$\tau_{sp}\dot{sp}(t) = -k_{sp}sp(t) + w_{gl-sp}gl(t) - w_{lp-sp}C_{lp}$$
$$\tau_{sn}\dot{sn}(t) = -k_{sn}sn(t) + w_{lp-sn}$$
$$\tau_{tp}\dot{tp}(t) = -k_{tp}tp(t)$$

and the equilibrium point is

$$x_{e5} = \begin{bmatrix} \frac{w_{op-gl}}{k_{gl}} \\ \frac{w_{gl-lp}w_{op-gl}}{k_{gl}k_{lp}} - \frac{w_{lp-lp}C_{lp}}{k_{lp}} \\ \frac{w_{gl-sp}w_{op-gl}}{k_{gl}k_{sp}} - \frac{w_{lp-sp}C_{lp}}{k_{sp}} \\ \frac{w_{lp-sn}}{k_{sn}} \\ 0 \end{bmatrix}$$

Again, by our assumption of GL being modelled as a functional unit with zero threshold, $\frac{w_{op-gl}}{k_{gl}} > \Theta_{gl}$, holds. Additionally, from the FTC architecture, it is clear that the only source of excitation for SN comes from LP. Thus if we want SN to ever fire then

$$\frac{w_{lp-sn}}{k_{sn}} > \Theta_{sn} \qquad (J)$$

must be true. Otherwise the system would converge to a state where GL, LP, SP and SN are active, which is explained below when we analise region 8 (see Fig 55 in the next section). Condition (J) is enough to make equilibrium state x_{e5} a "virtual" point.

In prey-catching facilitation, region 5 is reached during the first presentation of the visual stimulus. Fig. 49 shows that the system goes from here to region 6 where, besides GL and LP, SN becomes active. So, in order to produce the proper qualitative behavior conditions (C) and (D) or a combination of both must hold. These conditions must not only be true but one must also consider that after LP becomes active, and before SP responds, SN membrane potential has to go above threshold. This requires SN time constant (τ_{sn}) to be fast and SN threshold (Θ_{sn})

to be low. Inside region 6, the FTC model representation becomes

$$
\begin{aligned}
\tau_{gl}\dot{gl}(t) &= -k_{gl}gl(t) + w_{lp\text{-}gl} \\
\tau_{lp}\dot{lp}(t) &= -k_{lp}lp(t) + w_{gl\text{-}lp}gl(t) - w_{lp\text{-}lp}C_{lp} - w_{sn\text{-}lp}sn(t) \\
\tau_{sp}\dot{sp}(t) &= -k_{sp}sp(t) + w_{gl\text{-}sp}gl(t) - w_{lp\text{-}sp}C_{lp} - w_{sn\text{-}sp}sn(t) \\
\tau_{sn}\dot{sn}(t) &= -k_{sn}sn(t) + w_{lp\text{-}sn} \\
\tau_{tp}\dot{tp}(t) &= -k_{tp}tp(t)
\end{aligned}
$$

and the equilibrium point is

$$
z_{e6} = \begin{bmatrix}
\frac{w_{lp\text{-}gl}}{k_{gl}} \\
\frac{w_{gl\text{-}lp}w_{lp\text{-}gl}}{k_{gl}k_{lp}} - \frac{w_{sn\text{-}lp}w_{lp\text{-}sn}}{k_{sn}k_{lp}} - \frac{w_{lp\text{-}lp}C_{lp}}{k_{lp}} \\
\frac{w_{gl\text{-}sp}w_{lp\text{-}gl}}{k_{gl}k_{sp}} - \frac{w_{sn\text{-}sp}w_{lp\text{-}sn}}{k_{sn}k_{sp}} - \frac{w_{lp\text{-}sp}C_{lp}}{k_{sp}} \\
\frac{w_{lp\text{-}sn}}{k_{sn}} \\
0
\end{bmatrix}
$$

We have that $\frac{w_{lp\text{-}gl}}{k_{gl}} > \Theta_{gl}$ and $\frac{w_{lp\text{-}sn}}{k_{sn}} > \Theta_{sn}$, as described earlier, are true. Thus, z_{e6} can be a "virtual" point if condition

$$
\left[\frac{w_{gl\text{-}lp}w_{lp\text{-}gl}}{k_{gl}k_{lp}} - \frac{w_{sn\text{-}lp}w_{lp\text{-}sn}}{k_{sn}k_{lp}} - \frac{w_{lp\text{-}lp}C_{lp}}{k_{lp}}\right] < \Theta_{lp} \qquad (K)
$$

or

$$
\left[\frac{w_{gl\text{-}sp}w_{lp\text{-}gl}}{k_{gl}k_{sp}} - \frac{w_{sn\text{-}sp}w_{lp\text{-}sn}}{k_{sn}k_{sp}} - \frac{w_{lp\text{-}sp}C_{lp}}{k_{sp}}\right] > \Theta_{sp} \qquad (L)
$$

or both are true. That is, the competition between positive, through GL, and negative, through SN, feedback loops triggered by LP must have two different effects on FTC overall activity: first, inhibition upon the LP cell must be stronger than its recurrent excitation; second, GL residual activity after removing the visual stimulus must be strong enough to take SP potential above threshold. Condition (L) cannot be true because that would mean that SN inhibitory effect is not able to control SP firing response. As seen above, this is a very important

condition in order for the system to elicit the SP characteristic delayed response (see Figs. 55 and 57 in the next section). In case both conditions (K) and (L) are false then z_{e6} becomes an "actual" point, and FTC activity might converge to it (see Fig. 56 in the next section). The system would present a different qualitative behavior, it would not return to the resting level state z_{e0}.

Region 6 is a critical region for the system. Here is where the first visual stimulus must be retired, otherwise the SP cell might become active setting up the conditions that would take the system into a region where a PY response is produced. That is, whenever LP and SP are active and a prey-like object is in the FTC receptive field a PY response is obtained, which, as mentioned earlier, represents the probability of getting the animal to exhibit a prey-catching behavior (see Fig. 51 in the next section).

The next region to be analyzed is region 7 where GL, LP and SP are active while the rest of the FTC elements are inactive. In this region the FTC mathematical model is

$$
\begin{aligned}
\tau_{gl}\dot{gl}(t) &= -k_{gl}gl(t) + w_{sp\text{-}gl} + w_{lp\text{-}gl} \\
\tau_{lp}\dot{lp}(t) &= -k_{lp}lp(t) + w_{gl\text{-}lp}gl(t) + w_{sp\text{-}lp} - w_{lp\text{-}lp}C_{lp} \\
\tau_{sp}\dot{sp}(t) &= -k_{sp}sp(t) + w_{gl\text{-}sp}gl(t) - w_{lp\text{-}sp}C_{lp} \\
\tau_{sn}\dot{sn}(t) &= -k_{sn}sn(t) + w_{lp\text{-}sn} \\
\tau_{tp}\dot{tp}(t) &= -k_{tp}tp(t)
\end{aligned}
$$

and the equilibrium point is

$$
z_{e7} = \begin{bmatrix}
\frac{w_{lp\text{-}gl} + w_{sp\text{-}gl}}{k_{gl}} \\
\frac{w_{gl\text{-}lp}(w_{lp\text{-}gl} + w_{sp\text{-}gl})}{k_{gl}k_{lp}} + \frac{w_{sp\text{-}lp} - w_{lp\text{-}lp}C_{lp}}{k_{lp}} \\
\frac{w_{gl\text{-}sp}(w_{lp\text{-}gl} + w_{sp\text{-}gl})}{k_{gl}k_{sp}} - \frac{w_{lp\text{-}sp}C_{lp}}{k_{sp}} \\
\frac{w_{lp\text{-}sn}}{k_{sn}} \\
0
\end{bmatrix}
$$

Because of the functional role posed to GL, $\frac{w_{lp\text{-}gl} + w_{sp\text{-}gl}}{k_{gl}} > \Theta_{gl}$ is true. It

164

was also shown earlier (condition J) that $\frac{w_{l-m}}{k_{sn}} > \Theta_{sn}$ must be true in order for the system to perform correctly. That is, in this case condition (J) is one way z_{e7} becomes a "virtual" point. The system would also perform incorrectly if condition (J) is false and recurrent excitation (LP-GL & SP-GL) keeps LP and SP membrane potential above threshold. In that case equilibrium state z_{e7} would be an "actual" point to which the system might converge (see Fig. 55 in the next section).

In prey-catching facilitation, inside region 7 there is only excitation in the network, but with no retinal input, thus the only region that might be reached from here is region 8 where SN becomes active, in addition to GL, LP and SP. Inside region 8 the FTC mathematical model is

$$\tau_{gl}\dot{gl}(t) = -k_{gl}gl(t) + w_{sp-gl} + w_{lp-gl}$$
$$\tau_{lp}\dot{lp}(t) = -k_{lp}lp(t) + w_{gl-lp}gl(t) + w_{sp-lp} - w_{lp-lp}C_{lp} - w_{sn-lp}sn(t)$$
$$\tau_{sp}\dot{sp}(t) = -k_{sp}sp(t) + w_{gl-sp}gl(t) - w_{lp-sp}C_{lp} - w_{sn-sp}sn(t)$$
$$\tau_{sn}\dot{sn}(t) = -k_{sn}sn(t) + w_{lp-sn}$$
$$\tau_{tp}\dot{tp}(t) = -k_{tp}tp(t)$$

and the equilibrium point is

$$z_{e8} = \begin{bmatrix} \frac{w_{sp-gl} + w_{lp-gl}}{k_{gl}} \\ \frac{w_{gl-lp}(w_{sp-gl} + w_{lp-gl})}{k_{gl}k_{lp}} + \frac{w_{sp-lp} - w_{lp-lp}C_{lp}}{k_{lp}} - \frac{w_{sn-lp}w_{lp-sn}}{k_{sn}k_{lp}} \\ \frac{w_{gl-sp}(w_{sp-gl} + w_{lp-gl})}{k_{gl}k_{sp}} - \frac{w_{sn-sp}w_{lp-sn}}{k_{sn}k_{sp}} - \frac{w_{lp-sp}C_{lp}}{k_{sp}} \\ \frac{w_{lp-sn}}{k_{sn}} \\ 0 \end{bmatrix}$$

From previous cases, we know that $\frac{w_{sp-gl} + w_{lp-gl}}{k_{gl}} > \Theta_{gl}$ and $\frac{w_{lp-sn}}{k_{sn}} > \Theta_{sn}$ are true (assuming that the visual stimulus has been removed from the FTC receptive field). Therefore, z_{e8} is a "virtual point" only if condition

$$\left[\frac{w_{gl-lp}(w_{sp-gl} + w_{lp-gl})}{k_{gl}k_{lp}} + \frac{w_{sp-lp} - w_{lp-lp}C_{lp}}{k_{lp}} - \frac{w_{sn-lp}w_{lp-sn}}{k_{sn}k_{lp}} \right] < \Theta_{lp} \quad (M)$$

165

or

$$\left[\frac{w_{gl-sp}(w_{sp-gl} + w_{lp-gl})}{k_{gl}k_{sp}} - \frac{w_{sn-sp}w_{lp-sn}}{k_{sn}k_{sp}} - \frac{w_{lp-sp}C_{lp}}{k_{sp}} \right] < \Theta_{sp} \quad (N)$$

or both are true. This means that recurrent inhibition, through SN, must be strong enough to overcome recurrent excitation, through GL and LP, initiating in this way the system's return to equilibrium state z_{e0} (resting level potential) after the proper physiological behavior of LP and SP has been displayed. At this point it is required that the inhibitory effect from SN to LP and SP be strong enough to stop them from firing until GL decreases to a level incapable of taking either LP or SP membrane potential above threshold (see Fig. 50 in the next section). It is clear that the role played by SN is quite important for the system to display the proper qualitative behavior.

If both conditions (M) and (N) are false z_{e8} would become an "actual" point and FTC activity might converge to it (see Fig. 57 in the next section). If only condition (N) is false then the system would present alternating periods of activity between LP and SN neurons (see Fig. 58 in the next section). Finally, if only condition (M) is false the system would go from region 8 to region 6 where equilibrium state z_{e6} would become an "actual" point so the system might converge to it (see Fig. 56 in the next section). In either case the system would not return to the resting level state z_{e0} presenting a qualitatively different behavior.

Computer Simulations

Our stability and parameter sensitivity analyses generated a set of conditions (A to N) that have to be met in order for the FTC model to yield the proper physiological behavior during the process of prey-catching facilitation. Additionally, our analysis predicted certain behaviors for the FCT elements under specific

parametric combinations. In this section we present the results of computer simulations that test such predictions. These results are shown through graphs displaying the membrane potential temporal behavior of every FTC element. During each computer experiment, we check whether the conditions are true (T) or false (F). Therefore, each figure includes at the top the description of the state of all conditions, going left to right from condition (A) to condition (N). The spikes in these graphs are a graphical convention to show when the membrane potential of a cell (LP, SP or PY) reaches the threshold. The simulations were run during 5 sec of real time to reproduce the behavioral and physiological observations. For facility the conditions are summarised in here:

$$\Theta_{lp} > \frac{- w_{lp\text{-}lp}C_{lp}}{k_{lp}} \qquad (A)$$

$$\Theta_{sp} > \frac{- w_{lp\text{-}sp}C_{lp}}{k_{sp}} \qquad (B)$$

$$\tau_{lp} < \tau_{sp} \qquad (C)$$

$$\Theta_{lp} < \Theta_{sp} \qquad (D)$$

$$|w_{r2\text{-}pl} + w_{lp\text{-}pl}| > |w_{sp\text{-}pl} + w_{sp\text{-}pl}| \qquad (E)$$

$$k_{sn} = k_{pl} \qquad (F)$$

$$w_{lp\text{-}pl} > w_{lp\text{-}sn} \qquad (G)$$

$$\left[\frac{w_{pl\text{-}sp}w_{sp\text{-}pl}}{k_{sp}k_{pl}} - \frac{w_{lp\text{-}sp}C_{lp}}{k_{sp}} \right] < \Theta_{sp} \qquad (H)$$

$$\left[\frac{w_{pl\text{-}lp}w_{sp\text{-}pl}}{k_{lp}k_{pl}} + \frac{w_{sp\text{-}lp} - w_{lp\text{-}lp}C_{lp}}{k_{lp}} \right] > \Theta_{lp} \qquad (I)$$

$$\frac{w_{lp\text{-}sn}}{k_{sn}} > \Theta_{sn} \qquad (J)$$

Table 3: Threshold Functions.

$LP = f\,(lp\,;\,1.0)$
$SP = f\,(sp\,;\,1.7)$
$SN = h\,(sn\,;\,0.2)$
$TP = g\,(tp\,;\,3.7)$
$PY = s\,(py\,;\,1.91, 5.0)$

Table 4: Membrane Constants.

$\tau_{pl} = 0.5$	$k_{pl} = 0.5$
$\tau_{lp} = 0.3$	
$\tau_{sp} = 0.9$	
$\tau_{sn} = 0.5$	$k_{sn} = 0.5$
$\tau_{tp} = 0.02$	
$\tau_{py} = 0.4$	

$$\left[\frac{w_{pl\text{-}lp}w_{lp\text{-}pl}}{k_{pl}k_{lp}} - \frac{w_{sn\text{-}lp}w_{lp\text{-}sn}}{k_{sn}k_{lp}} - \frac{w_{lp\text{-}lp}C_{lp}}{k_{lp}} \right] < \Theta_{lp} \qquad (K)$$

$$\left[\frac{w_{pl\text{-}sp}w_{sp\text{-}pl}}{k_{pl}k_{sp}} - \frac{w_{sn\text{-}sp}w_{sp\text{-}sn}}{k_{sn}k_{sp}} - \frac{w_{lp\text{-}sp}C_{lp}}{k_{sp}} \right] > \Theta_{sp} \qquad (L)$$

$$\left[\frac{w_{pl\text{-}lp}(w_{sp\text{-}pl} + w_{lp\text{-}pl})}{k_{pl}k_{lp}} + \frac{w_{sp\text{-}lp} - w_{lp\text{-}lp}C_{lp}}{k_{lp}} - \frac{w_{sn\text{-}lp}w_{lp\text{-}sn}}{k_{sn}k_{lp}} \right] < \Theta_{lp} \qquad (M)$$

$$\left[\frac{w_{pl\text{-}sp}(w_{sp\text{-}pl} + w_{lp\text{-}pl})}{k_{pl}k_{sp}} - \frac{w_{sn\text{-}sp}w_{sp\text{-}sn}}{k_{sn}k_{sp}} - \frac{w_{lp\text{-}sp}C_{lp}}{k_{sp}} \right] < \Theta_{sp} \qquad (N)$$

The analysis showed that the FTC model displays the behavior that produces PY response facilitation, during the second presentation of a subthreshold prey-like object, when all but condition (L) are true. Tables 3, 4 and 5 show the set of parameters chosen during the computer simulation to produce such behavior.

Table 5: Weighting Factors.

$w_{r2\text{-}gl} = 1.5$	$w_{sn\text{-}sp} = 10.0$
$w_{lp\text{-}gl} = 2.0$	$w_{lp\text{-}sn} = 1.0$
$w_{sp\text{-}gl} = 0.2$	$w_{r3\text{-}lp} = 0.3$
$w_{r2\text{-}lp} = 1.5$	$w_{r4\text{-}lp} = 5.0$
$w_{gl\text{-}lp} = 1.0$	$w_{r2\text{-}py} = 1.5$
$w_{sp\text{-}lp} = 1.6$	$w_{r3\text{-}py} = 0.3$
$w_{sn\text{-}lp} = 8.0$	$w_{r4\text{-}py} = 4.0$
$w_{r3\text{-}sp} = 2.7$	$w_{lp\text{-}py} = 2.0$
$w_{gl\text{-}sp} = 3.5$	$w_{sp\text{-}py} = 2.0$

Fig. 50 shows the temporal behavior of the FTC neurons during the process
of prey-catching facilitation. In this simulation, a square of 2×2 deg moving
with a velocity of 8 deg/sec was applied for 0.3 sec then, after a 3.2 sec delay, the
same stimulus was re-presented for another period of 0.3 sec. When the stimulus is
presented for the first time, GL produces a long EPSP which in combination with
retinal input excites the LP and SP cells. LP is the first in getting activated, and
then it sends recurrent excitation to GL and at the same time makes SN respond.
SN in turn produces a long hyperpolarisation on LP and SP, while GL keeps its
state of excitation until SN potential goes below threshold. Once SN inhibitory
effect disappears, the GL residual activity makes SP to become active. When SP
and GL are active, they make LP respond presenting a second burst of activity.
At this point, LP activates SN, once again producing a stronger SN response than
before. This response takes LP and SP potentials below threshold and lasts long
enough to eliminate the possibility of GL eliciting new bursts of activity in either
of the pear-shaped (LP or SP) cells. Although the residual activity left in GL
produces a level of excitability inside the column, mainly through the SP cell,
that elicits a PY response during the re-presentation of the stimulus after a few

seconds delay (3.2 sec).

The duration of the stimulus presentation may also produce a PY cell re-
sponse. As seen above, if the stimulus is not retired when the system reaches
region 6 where GL, LP and SN are active, then SP may get activated and a PY
response can be elicited. Fig. 51 shows computer simulations for three different
periods of stimulation. In Fig. 51A a square of 2×2 deg with a velocity of 8
deg/sec was applied for 0.3 sec, in Fig. 51B the same stimulus was presented
for a period of 0.4 sec and Fig. 51C corresponds to the presentation of the same
stimulus for 0.5 sec. When the stimulus presentation lasts 0.3 or 0.4 sec no PY
response is elicited, though the FTC elements display the proper physiological
behavior for prey-catching behavior; whereas if the stimulus is applied for 0.5 sec
then a PY response is produced. That is, as in empirical observations, a critical
presentation length below which no PY cell response is elicited can be established.

From now on, during the computer simulations a square stimulus of 2×2 deg
moving with a velocity of 8 deg/sec is presented for a subthreshold duration
period of time (0.3 sec). Table 6 shows the experiments to be conducted, and the
parameters changes considered during each one of them.

Fig. 52 shows the computer simulation results corresponding to experiment 1
in Table 6, that is, the case of a slower SN decay constant. The system activity
increases until the first burst of LP activity is presented. This activates SN
inhibitory effect, which keeps LP and SP membrane potentials below threshold
long enough so the GL residual activity, after SN becomes inactive, is not strong
enough to elicit an SP response. The physiological behavior exhibited by the
FTC model in this case differs qualitatively from the proper one. The delayed
response of the SP cell is never presented. Additionally, it is clear that a PY cell
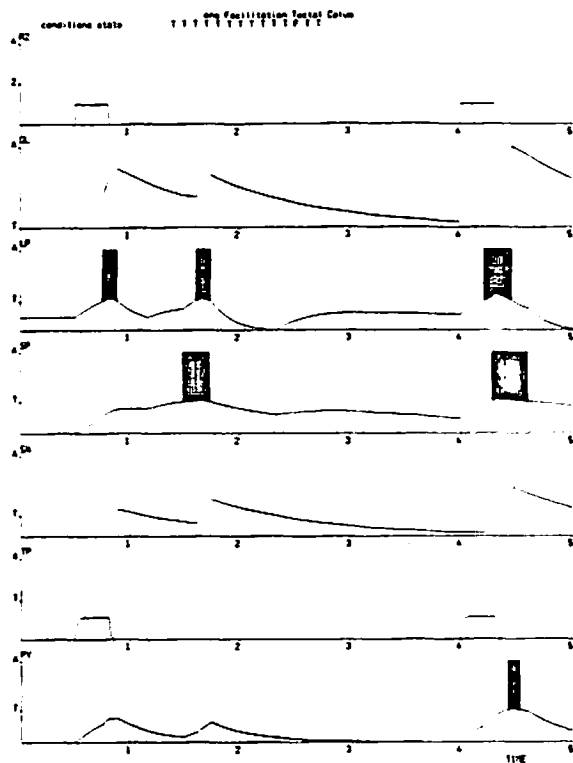
Figure 50: Computer Simulation of PY response facilitation
When all conditions but (L) are true, the FTC model displays PY response facilitation. That is, during the first presentation of a prey-like object (square of 2×2 deg with a velocity of 8 deg/sec) for a period of 0.3 sec there is no PY response, but during the second presentation of the same stimulus, after an intervening delay of 3.2 sec, the residual activity left after the first stimulation allows the network to elicit a PY response.

Figure 51: Simulation for longer duration of stimulus presentation
If the stimulus is not removed before SP cell responds then the FTC model enters a region where a PY cell response is elicited. A) A square of 2×2 deg with a velocity of 8 deg/sec is presented during 0.3 sec. This is a subthreshold duration so there is no PY response. B) Same stimulus is applied for a period of 0.4 sec. This is also a subthreshold duration so PY response is not elicited. C) Same stimulus is presented by 0.5 sec. Here the duration of the stimulus presentation is long enough to yield a PY response.
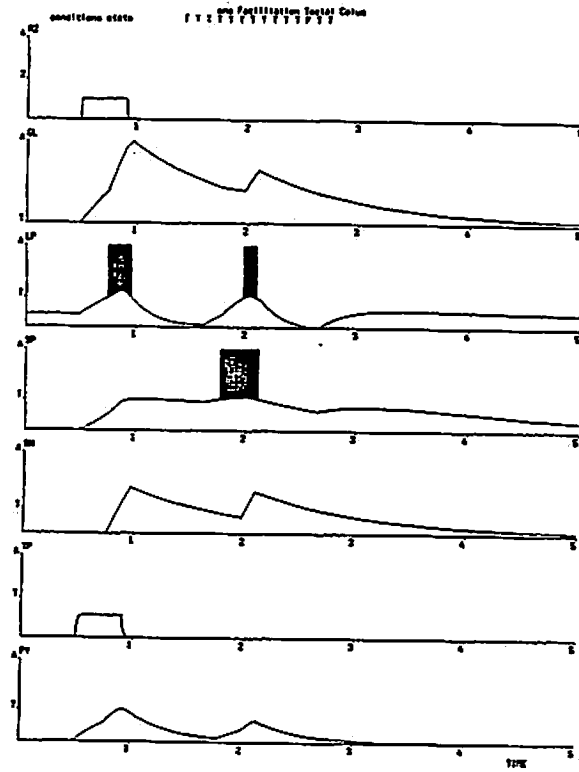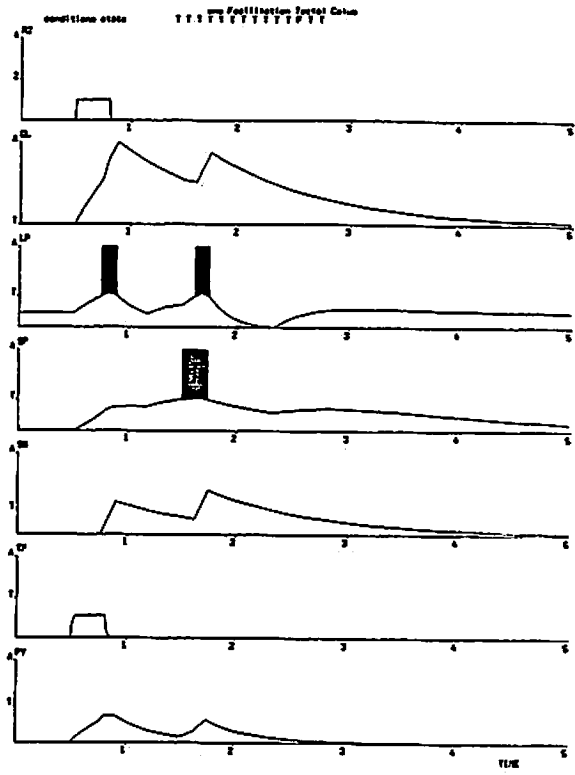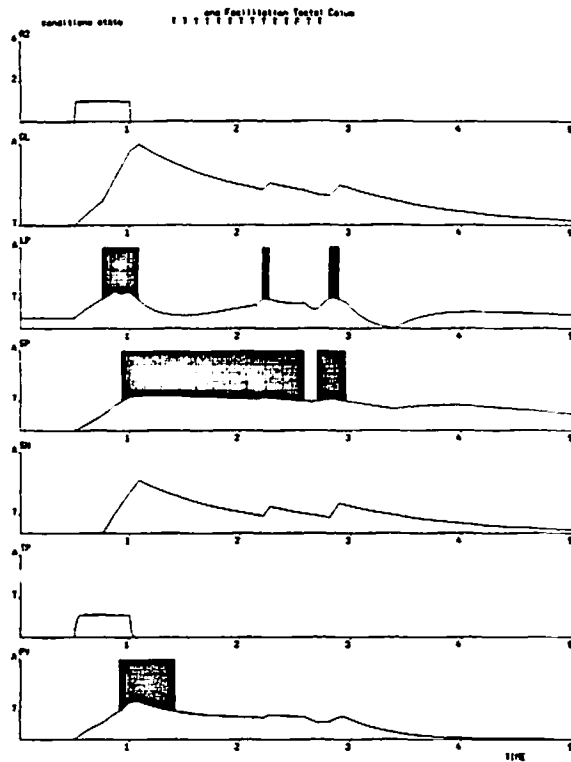
Table 6: Parameter Changes for Computer Experiments.

	Parameters Changed							
Exp	$w_{op\text{-}gl}$	$w_{gl\text{-}lp}$	$w_{sp\text{-}lp}$	$w_{sn\text{-}lp}$	$w_{sn\text{-}sp}$	$w_{lp\text{-}sn}$	k_{gl}	k_{sn}
1								1.5
2							0.1	
3								0.1
4	0.77							
5	0.5	0.8	0.2					
6						0.09		
7				1.0				
8				2.0	5.0			
9					5.0			

response facilitation during the re-presentation of a stimulus with subthreshold duration would not be produced.

The next computer simulation corresponds to Experiments 2, 3 and 4 in Table 6. Fig. 53 shows that if after the second LP burst of activity the recurrent excitation within the FTC (LP-GL, SP-GL & SP-LP-GL) produces a GL residual potential, after the pear-shaped cells and SN become inactive, strong enough to produce new SP responses then the network presents more than one alternation of LP, SP and SN periods of activity. This may occur if GL potential decays slowly, if SN potential decays fast, or if SP recurrent excitatory effect upon GL is very strong. In the first two cases, in addition to (L), condition (F) becomes false; whereas in the third case, condition (H) is the one that becomes false. Fig. 53A corresponds to the case when GL potential decays slowly. It shows that when SN potential goes below threshold, after being activated for the first time, the GL residual activity is very strong so that its excitatory effect over the SP cell cannot be counteracted by SN inhibition. The LP cell presents alternating short bursts of activity, during which GL potential is increased towards its saturation level.
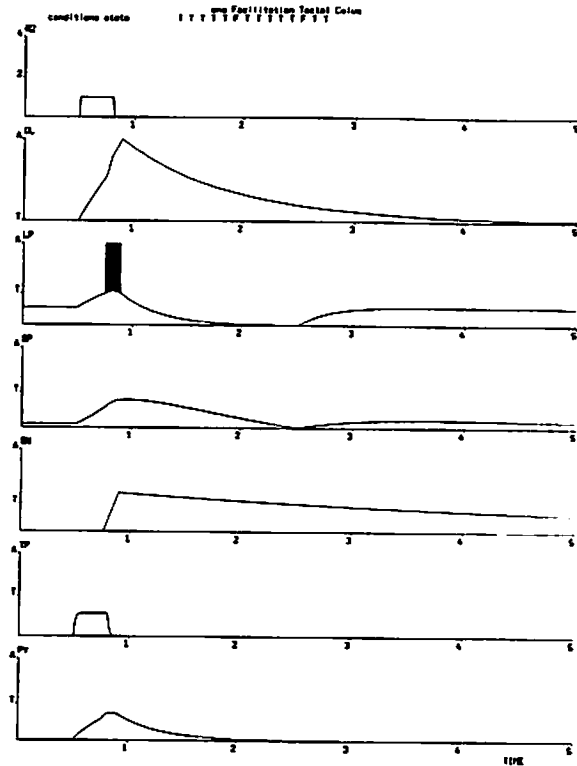
Figure 52: Simulation of a slow SN time decay constant
When SN membrane potential decays slowly, the GL residual activity after SN becomes inactive is not strong enough to elicit a response from either of the pear-shaped cells (LP or SP).

Additionally, a gradual increase on PY cell membrane potential is observed until, because of the combined effect of SP continuous and LP oscillatory responses, it reaches threshold. This means that the animal might present a prey-catching behavior even in the absence of visual stimulation. In the case when SN potential decays faster in the absence of LP activity (see Fig. 53B), the FTC model presents a similar behavior. But, in this case the periods of activity presented by the LP cell are longer, which produces a stronger effect upon the PY cell. After a short period of time, the PY cell presents a sustained response, increasing in this way the probability of the animal presenting a prey-catching behavior with no visual stimulation. Finally, Fig. 53C shows how by increasing SP recurrent excitatory effect upon GL the network presents more than one alternation of SP, LP and SN periods of activity. It is clear that under these conditions a second presentation of the same stimulus would suffice to yield a PY response even for longer intervening delays. But, the pattern of activity presented by the FTC elements would be qualitatively different from the proper physiological behavior.

If in addition to the previous situation (conditions (H) and (L) being false) the excitation, direct and through GL, that SP causes upon LP only produces LP subthreshold potentials (condition (I) is also false) then the FTC activity converges to a state (x_{s3}) where GL and SP remain active. This corresponds to the experiment 5 in Table 6, and it can be seen in Fig. 54. It is interesting to note that under these circumstances the FTC model would present facilitation of PY response during a second presentation of the same stimulus regardless of the length of the intermediate delay. This occurs because one of the hypotheses embedded in the model is that facilitation is due to the residual activity left in GL and SP. But, again, the FTC elements would not display the proper physiological

Figure 53: Computer simulation of an oscillatory behavior
When the combined effect of LP and SP upon GL produces a residual GL poten-
tial, after the pear-shaped cells and SN become inactive, strong enough to drive
SP membrane potential above threshold, the system presents more than one al-
ternation of LP, SP and SN periods of activity. A) Slow GL time decay constant.
B) fast SN time decay constant; and C) strong SP recurrent excitatory effect.
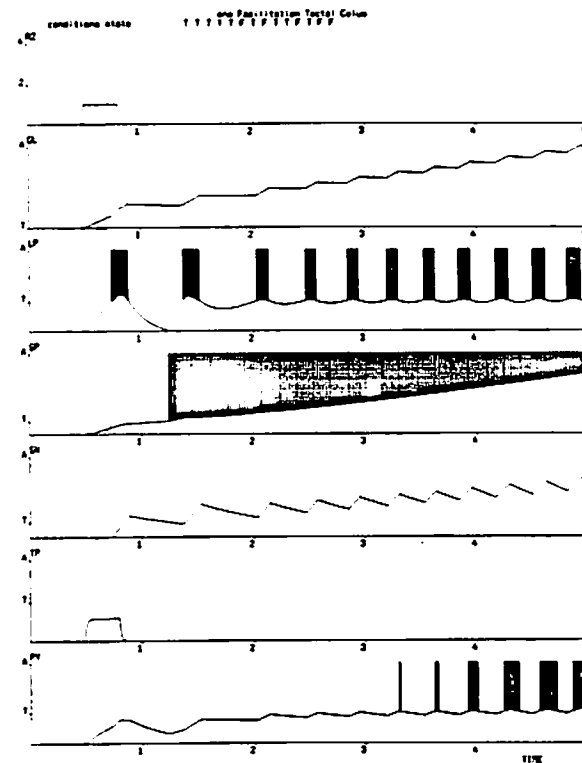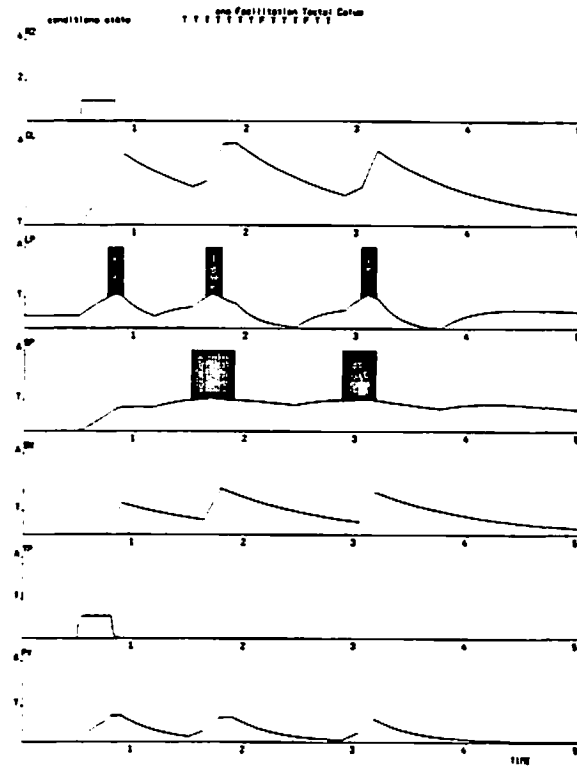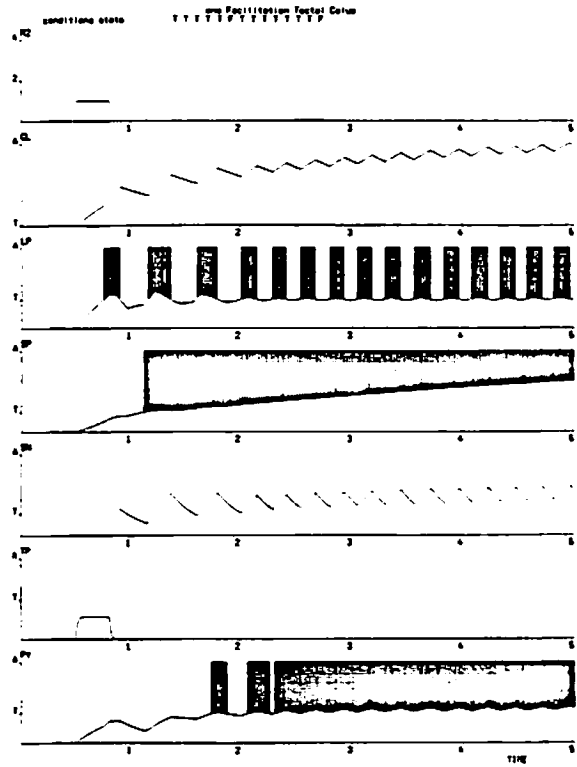
behavior.

The next case to be tested is when the excitatory effect from LP upon SN does not take SN membrane potential above threshold, that is, the situation when the effect of the only inhibitory element in the FTC model is eliminated (experiment 6 in Table 6). This causes conditions (J), (K), (M) and (N) to be false, and at the same time condition (L) becomes true. Under these circumstances the control exerted by SN over FTC internal activity is lost so recurrent excitation keeps LP and SP responding. Fig. 55 shows the results of the corresponding computer simulations. The FTC activity converges to as state (z_{e7}) where GL, SP and LP are active. In this case, because of the sustained response of the LP and SP cells, the degree of excitability within the FTC is so high that a strog PY response is elicited. That is, the probability of the animal displaying a prey-catching behavior is greatly increased.

Another result from our stability analysis says that when LP recurrent excitation is stronger than its recurrent inhibition, and the inhibitory effect from SN keeps SP potential below threshold (conditions (K) and (L) are false) then FTC activity converges to a state (z_{e6}) where GL, LP and SN are active (experiment 7 in Table 6). This causes condition (M) to be false too. Fig. 56 displays the results of the corresponding computer simulation. It can be observed that, in this case, SP would never respond during the re-presentation of a stimulus with a subthreshold duration because its potential is kept by SN at a level that is lower than its resting potential. This means that under this parametric combination the FTC model would not present the phenomenon of a PY cell response facilitation, unless the delay between stimulations is very short. Additionally, the qualitative behavior of FTC elements differs from the proper behavior, that is, LP shows a continuos burst of activity while SP never shows its characteristic
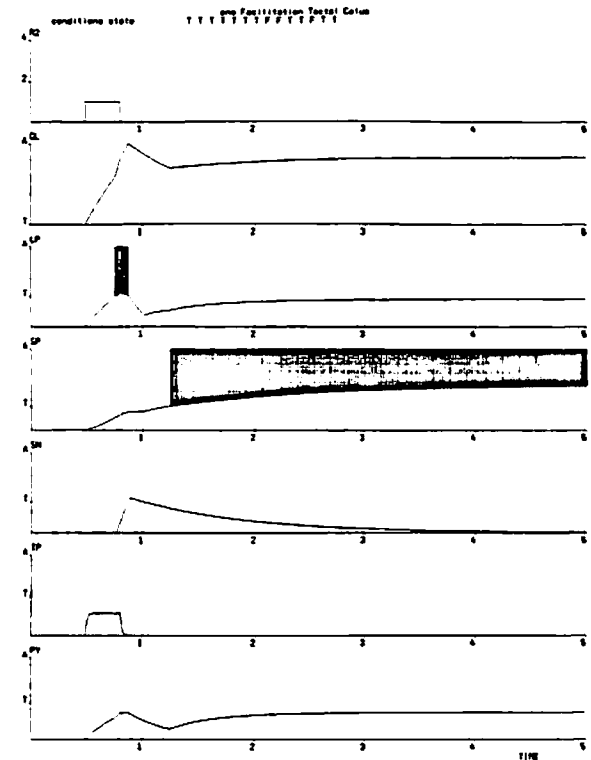
Figure 54: Computer simulation of a weak SP-GL effect on LP
When the SP effect upon LP, direct and through GL, does not produce a response in LP, and SP recurrent excitation through GL is strong enough to keep SP membrane potential above threshold, the system converges to a state where GL and SP are active.
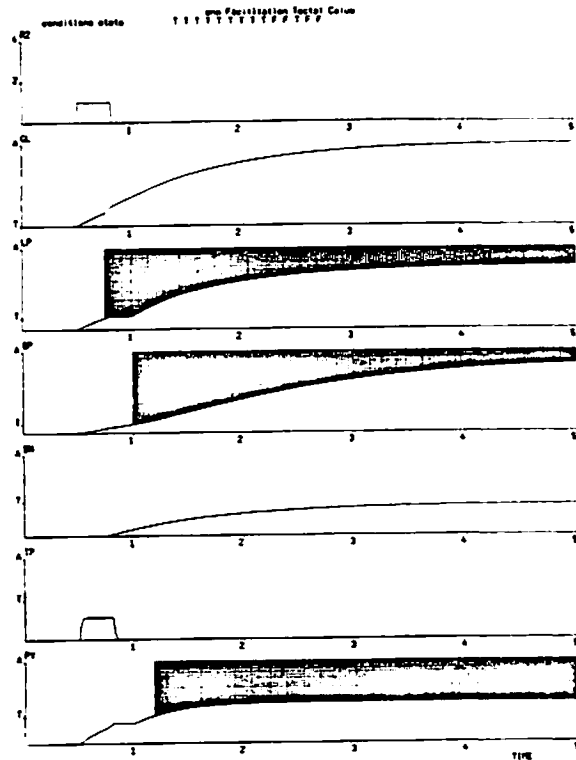
Figure 55: Computer simulation of a weak LP effect on SN
When LP effect upon SN does not elicit a response in SN, and SP recurrent excitation through GL is strong enough to keep SP and LP membrane potentials above threshold, the system converges to a state where GL, LP and SP are active.

delayed response.

The next case to be tested through a computer simulation is when FTC recurrent inhibition cannot overcome its recurrent excitation (experiment 8 in Table 6). Under this situation conditions (M) and (N) are false while (L) becomes true. In this case, FTC activity converges to a state (z_{ci}) where GL, LP, SP and SN potentials remain above threshold. The results can be observed in Fig. 57. For this parametric combination, the level of activity inside the column is very high because the recurrent inhibition cannot control the increasing recurrent excitation. Therefore, because of the continuous response of the pear-shaped cells, a strong PY response is elicited, and the probability of the animal showing a prey-catching response without visual stimulation is greatly increased.

Finally, we present the computer simulation results corresponding to experiment 9 in Table 6. If the SN inhibitory effect does not counteract GL excitatory effect on the SP cell (condition (N) is false while (L) becomes true) then FTC activity reaches a state where GL and SP potentials remain above threshold, whereas LP and SN present alternating periods of activity. The duration of LP bursts of activity is very short, so that its combined effect with SP sustained response is not enough to make the PY cell respond. The computer simulation results are shown in Fig. 58. It was hypothesized that PY response facilitation is due to the residual activity in GL and SP after the first stimulation. Therefore, a second stimulation with subthreshold duration would elicit a PY response. This would be accomplished no matter what the length of the delay between stimulations. But, again, the qualitative behavior displayed by LP and SP does not match that of Ingle's "attention" units.
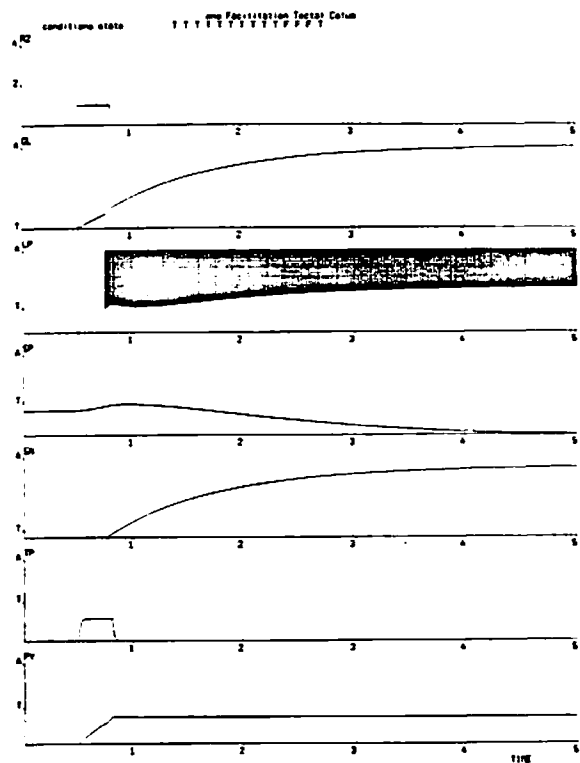
Figure 56: Computer Simulation for strong LP recurrent excitation.
When the recurrent excitation triggered by LP is stronger than the recurrent inhibition and, at the same time, the inhibitory effect from SN to SP is stronger than the excitatory effect produced by LP on SP the system converges to a state where GL, LP and SN are active.
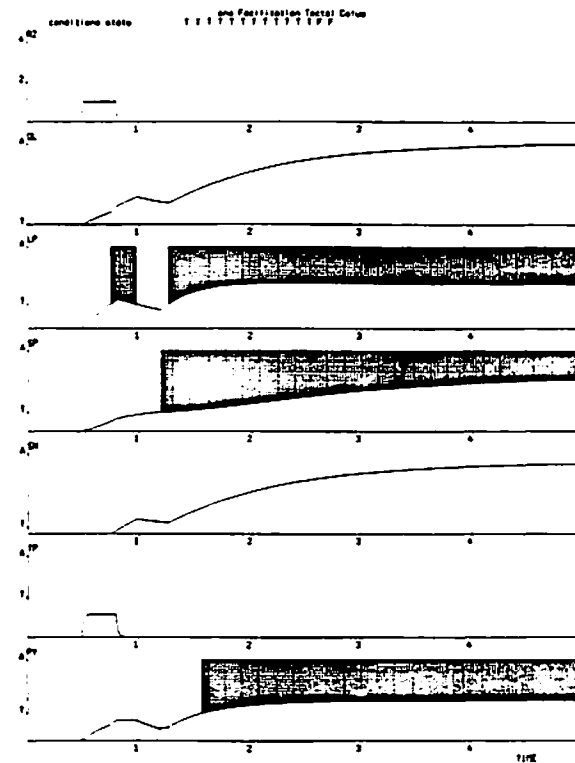
Figure 57: Computer simulation for a weak SN inhibitory effect.
If SN inhibitory effect upon LP and SP cells is not strong enough to overcome the recurrent excitation impinging upon these cells then the system converges to a state where GL, LP, SP, and SN become active.
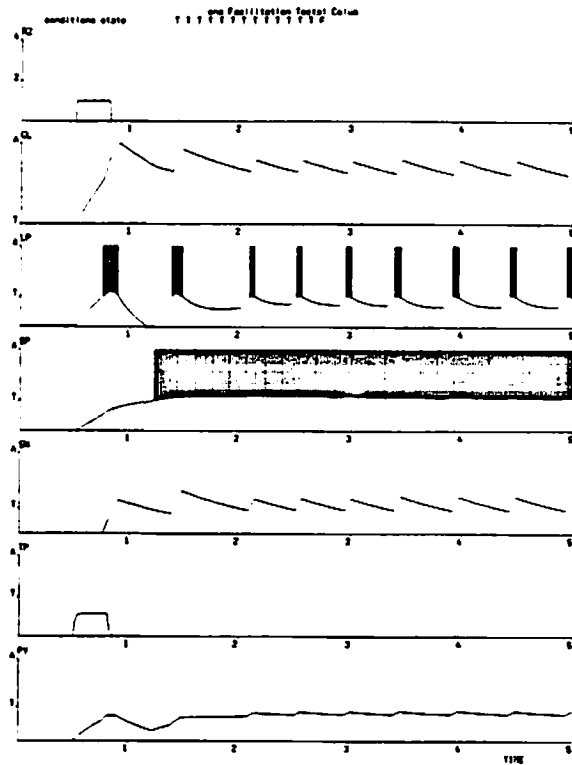
Figure 58: Computer Simulation for weak inhibition from SN to SP.
If the recurrent excitation produced by SP on LP is stronger than the inhibitory effect LP receives from SN, and the recurrent excitation produced by LP and SP upon SP overcomes the inhibition SP gets from SN then the sytem presents alternating periods of activity between LP and SN, whereas GL and SP remain active all the time.

Discussion

Stability and parameter sensitivity analyses combined with computer simulations of a single Facilitation Tectal Column (FTC) model have been conducted. The benefits of such an analysis can be grouped into two parts: first, the value of using techniques derived from the analysis of non-linear systems to develop and analyse simple neural network models; and second, a deeper understanding of the different qualitative behaviors presented by the FTC model under different parametric combinations.

In order to make our theoretical analysis of visuomotor coordination in anuran amphibia tractable and to obtain, analytically and through computer simulations, a clear understanding of the capabilities of our neural net models, we simplify the mathematical representation of a neuron as much as possible so long as the global neural model contains the intrinsic properties shown, or hypothesised, by empirical studies. Such mathematical models are composed by first order differential equations with small non-linearities (threshold functions). Thus, non-linear systems theory techniques that analyse "piecewise" linear systems are suitable to analyse our models. The analysis presented in this Chapter illustrates how the question of "actual" vs. "virtual" equilibrium state can be used to study parametric combinations under which a neural model may present different qualitative behaviors. An example of a second order system was presented to show graphically, through phase-plane portraits, the utility of this methodology. With this example we showed that a neural circuit, formed by one excitatory and one inhibitory neuron, involving recurrent excitation and inhibition may present an interesting oscillatory behavior ("limit cycle") depending on the values of the external input and model parameters, such as, synaptic weights and threshold functions. Similar results have been reported by Amari [1977].

When analysing the FTC model, it was shown that if the equilibrium state corresponding to the region where all the FTC elements are at rest is an "actual" point and the equilibrium states corresponding to the other reachable regions in the system state-space are virtual points, then there exists a set of parameters under which the FTC presents the appropriate behavior. That is, if a small prey-like object is presented in the FTC receptive field for a subthreshold duration, then the LP cell would present two bursts of activity with an intermediate period of silence, the SP cell would display its hypothesized delayed response and a facilitation of the PY cell response would be observed if the same stimulus is re-presented after a short delay. When there is no second presentation of the stimulus the FTC elements' potentials return to their reting level.

Even though this study has been limited to the analysis of the network parameter sensitivity based on the location and nature of the system equilibrium states, it has already shown the advantages of combining analytical techniques with computer simulations over the process, previously used in developing our models [Lara, Arbib & Cromarty, 1982; see also Chapter 3], of using only computer simulations in the search of a reasonable set of parameters that produced results consistent with empirical data.

Our analytical study not only generated the relationships among some of the parameters of the FTC model in order to display the phenomenon of PY response facilitation, but it also served to establish different qualitative behaviors that may be presented by the model under specific parametric combinations. Then, computer simulations were conducted, first, to find the appropriate values for those parameters not defined during the analytical part, and, second, to analyse in detail some of the qualitative behaviors that the FTC model is able to display. Thus, our analytical approach defined those computer experiments that should

stimulate new empirical studies.

Lara [1982] also conducted a parameter sensitivity analysis of the FTC model by using only computer simulations. He studied the model's behavior to different values of parameters, changing one at a time for a given range and then conducting a computer simulation for each case. It is clear that this approach requires massive computer simulations to define ranges of parametric combinations under which the model presents the appropriate behavior. The results obtained in this Chapter are in agreement with those obtained by Lara through computer simulations. The FTC model presented different types of behavior. When the excitatory effect was increased, the FTC elements presented decayed oscillations, sustained oscillations or continuous responses. In these cases, facilitation of a PY response during the re-presentation of a stimulus with subthreshold duration was enhanced; furthermore, in some cases a PY response was produced even in the absence of re-stimulation. In those cases where the inhibitory effect was increased, the FTC model displayed a decayed excitation, and facilitation of PY response was not exhibited.

In this Chapter, the methodology borrowed from the non-linear systems theory was used to study an already developed and analysed neural net model, but it should be pointed out that this methodology can actually be used during the developement and analysis of such models. The steps to be followed are:

1. Consider the data generated by empirical disciplines (i.e., anatomy, physiology and ethology) which is relevant to the phenomenon under study.

2. Based on this data, generate neural net "family-models" which might explain the empirical observations.

3. Use Non-linear Systems Theory techniques to determine the ranges of model parameters, as well as the interelationships among those parameters, under which the models exhibit the proper response (testing the hypotheses embodied in the models), and to study the qualitative behaviors that may be

presented by the models under different parametric combinations (predictions generated by the models).

4. Conduct computer simulations to tune the set of parameters under which the models display the appropriate behavior, and to study in detail the predictions about the models' qualitative behaviors generated by the analytical study.

Additionally, these methodologies can be used to extract other kind of information about the models. We could prove the impossibility of a neural network model yielding a certain behavior, by showing that in order for the model to exhibit such a behavior some parametric relationships that contradict each other had to be true. This would be a very useful tool to have when analysing alternative models that may explain specific empirical observations. It would allow us to rule out those models which could not elicit the appropriate behaviors. Also, a quantitative analysis of the temporal pattern of activity presented by individual elements inside the network model may be developed. For example, in our case, the ranges of the parameters (membrane time constants) responsible for the FTC temporal behavior, and their relationships with the rest of the parameters, could be determined analytically. This will allow us to address the question of what are the neural mechanisms that determine the FTC "ignition" time, where by "ignition" time we mean the time the subthreshold stimulus has to remain in the FTC receptive field before a PY cell response is elicited.

As a final conclusion, we think that in this Chapter we have shown how analytical approaches to the study of the brain, when applied to neural models tied to anatomical and physiological observations, could help us to get a better understanding of the processing of information carried out by the Central Nervous System. Thus, the development of analytical techniques or the application of methodologies already developed in other disciplines, such as Non-linear Systems Theory, to the study of neural net models is an urgent topic in Brain Theory.

TABLE OF CONTENTS

CHAPTER V

DEPENDENCE OF TECTAL COLUMN RESPONSE ON STIMULUS VELOCITY

Introduction

In Chapter 3 a model of the retino-tectal-pretectal interactions, i.e., an array of Facilitation Tectal Column (FTC) Units, was developed. With this model we were able to study how such interactions might underly prey-predator discrimination. The model embodies a series of hypotheses about tectal intrinsic organisation and anatomical-physiological correlations, abstracted from the Golgi studies of Székely and Lázár [1976] and electrophysiological recordings from tectal and pretectal elements obtained by Ingle [1973b, 1975], Ewert and coworkers [1971, 1976, 1980, 1984], and Grüsser and Grüsser-Cornehls [1976, 1984]. In addition, some correlations between neurophysiology and behavior were suggested during the analysis of the possible role that tectal PY cells might play in the elicitation of prey-catching orienting behavior.

Considering, as Ewert [1976] and Ingle [1973b] did, an inhibitory effect from pretectum over tectum, it was shown how the physiological behavior of a PY cell may be the outcome of the integration of information coming from retinal ganglion cells, internal tectal elements (LP and SP), and a thalamic pretectal (TP) neuron. We postulated that the TP neuron (i.e., Ewert's TH3 neuron) inhibits those tectal cells (LP and SP) that are responsible for the internal activity in the

tectum and the PY cell, giving the latter, in that way, the ability to discriminate between prey and predator. Additionally, it was studied how, by modulating the level of inhibition exerted by the TP cell upon tectal elements, the motivational state of the animal might control the response latency and the size-preference phenomenon presented by the PY cell.

Here, we want to exploit the "predictive" characteristic of brain modelling. Thus, computer experiments were conducted to address empirical data about the physiological properties of the PY cell not considered during the development of the model. We analyse the controversial issue of whether or not the preference of the PY cell's response between worm-like and square objects is invariant to the stimulus velocity. Our aim was to try to identify what neural mechanisms, if any, from those embodied in our model may explain under what conditions such a preference might be velocity dependent.

In this Chapter the behavioral and physiological findings that created this "velocity controversy" are described. Then, we discuss the changes required by our models to enable us to study this phenomenon, and continue with the presentation of the results obtained with our model during computer simulations. Finally, we discuss the implications of these results, pinpointing some gaps in our current knowledge of the anuran brain which, once investigated, will help us to clarify the real nature of this phenomenon.

Velocity Controversy

The model developed in Chapter 3 adequately reproduces the physiological behavior of Ewert's [1976, 1980] tectal cell T5(2), which has been hypothesized to be equivalent to the pyramidal (PY) cell described anatomically by Székely

and Lázár [1976]. In seeking the neural mechanisms underlying prey-predator recognition, Ewert and coworkers have conducted extensive studies both on prey-catching behavior and on physiological properties of tectal neurons. They have studied in detail the physiology of tectal cells of type T5(2) in several species: in toads [Ewert, 1976, 1980, 1983, 1984; Ewert et al, 1979], frogs [Schürg-Pfeiffer & Ewert, 1981] and salamanders [Finkenstädt & Ewert, 1983]. These authors found that this type of cell responded to different configurations of moving stimuli with an overall firing level that resembled the probability that the stimulus under investigation fitted the prey category. That is, they respond better to a rectangle moving along its longest axis (as "worm-like") than to a compact ("square") object, and present their weakest response to a rectangle moving perpendicular to the direction of motion (as an "antiworm-like") (see Chapter 3). Ewert [1976, 1983, 1984] also found that behaviorally the animal's preference was invariant to changes in the stimulus velocity, and he and his group showed that, at the physiological level, the response preference of T5(2) cells was invariant to the stimulus direction of motion [Ewert et al, 1979] and velocity [Ewert & Wietersheim, 1974; Schürg-Pfeiffer & Ewert, 1981]. Although, with respect to the velocity invariance they did not provide quantitative physiological data, Fig. 59A shows that when a rectangle subtending a visual angle of 32 × 2 deg is moved as worm-like or as an antiworm-like stimulus then, behaviorally the former is preferred to the latter regardless of the stimulus velocity.

Luthardt and Roth [1979] observed, during a behavioral study in salamandra salamandra, that the animal's preference between different configurational stimuli was velocity dependent. They found that the prey-catching response of these animals to rectangular stimulus of 32×4mm moved as worm-like and as antiworm-like was dependent on the stimulus velocity (see Fig. 59B). That is, these animals
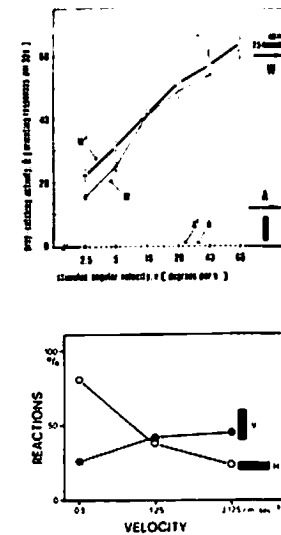
Figure 59: Dependence of worm-antiworm preference on stimulus velocity.

A) The unbroken curve represents the prey-catching orienting response of toads to a rectangle of 32 × 2 deg moved as a worm-like stimulus and the broken line corresponds to the same stimulus moved as antiworm-like [from Ewert, 1982]. B) Prey capture reactions of Salamandra Salamandra to a rectangule of 32 × 4 mm moved as worm-like (H) and as antiworm-like (V) [from Luthardt and Roth, 1979].

presented an "inversion phenomenon" which consists in that at low velocities the worm-like stimulus is preferred to the antiworm-like, but at high velocities the antiworm-like stimulus was more effective. It must be noted, however, that other authors [Himstedt, 1982; Finkenstädt & Ewert, 1983] did not observed the "inversion phenomenon" reported by Luthardt and Roht [1979]. Himstedt [1982] argues that this phenomenon perhaps depends on the animal's experience with certain prey. He bases this argument on the fact that he conducted the same experiments with animals that were fed mainly with mealworms, while in Luthardt and Roth's experiments the animals were fed mainly with crickets. This result agrees with what Ewert [1980] says about animal care in different laboratories. First, he says, "animals do not always exhibit their natural repertoire of behavior in captivity; second, gross differences in animal maintenance (including feeding) between different research groups using the same experimental animal may be an unrecognised cause of the criticism that one and the same experiment is not always reproducible in every hand".

The results obtained by Luthardt and Roth motivated their group to investigate if this was the case for other amphibians, not only at the behavioral level but also at that of the physiology of tectal cells. Roth and collaborators have reported a larger number of response types of neurons in the optic tectum based on the type of response to the stimulus geometry and velocity. They found five different types of cells in the tectum of toads [Roth & Jordan, 1982] and of salamanders [Himstedt & Roth, 1980; Roth, 1982], some of which showed changes in their stimulus preference as the stimulus velocity was varied. The stimuli used during their studies were "squares" (S) of 8×8 deg, and rectangles of 8×2 moved with the longest axis parallel (H) or perpendicular (V) to the stimulus direction of motion. That is, the latter were rectangles moved as "worm-like" or

"antiworm-like" stimuli, respectively. They have shown that a subgroup of cells, 16 out of 41, behaved as Ewert's T5(2) when the stimulus was moved with a velocity of 2 deg/sec (i.e., they preferred "worm-like" to square stimuli), but they switched their preference when the stimulus was moved at velocities higher than 6 deg/sec, while the antiworm-like stimulus was the least efficient at all velocities (this group of cells is denoted as $H \times S > V$ by these authors). This can be observed in Fig. 60. This result completely disagrees with Ewert's observations [1980, 1982] in toads where he found that T5(2) stimulus preference was invariant to the stimulus velocity.

Physiologically, a similar "inversion phenomenon" has been observed by Ewert [1980], although in his case it was not related to the stimulus velocity. He showed that when pretectal ablation occurs the animal's (and T5(2) cells') ability to discriminate among configurational visual patterns was lost, and the preference between squares and worm-like stimuli was switched. That is, in normal toads the "worm-like" stimulus was preferred to a square, whereas in lesioned animals the square was more effective than the "worm-like" stimulus, even at the same velocity of 7.6 deg/sec (see Chapter 3). In addition, he also observed that the phenomenon of habituation of prey catching behavior to a specific stimulus was greatly diminished, which suggests that the pretectum seems to be involved in some processes that represent experience (learning). Furthermore, Ewert [1980] and Ingle [1982b] have shown that tectal-pretectal interactions are modulated by the motivational state of the animal (e.g. the kind and the amount of food the animal gets before an experiment, the time the experiment lasts, etc.). Therefore, in this Chapter, based on the facts just described, we enquire whether the mechanisms responsible for the differences between the results obtained by Ewert and collaborators, and those reported by Roth and his group might be related to
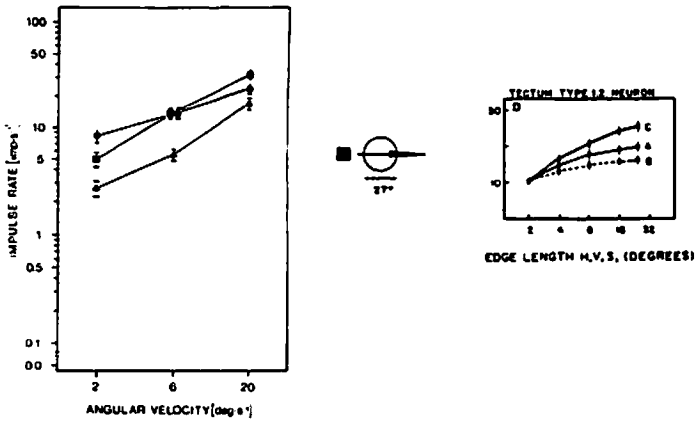
Figure 60: Inversion phenomenon of tectal cells in toad.
A) The curve with square symbols correspond to the response of tectal cells to
"squares"(S) of 8 × 8 deg, the one with circles correspond to horizontal rectan-
gles (H) of 8 × 2 deg, and the one with triangles to vertical rectangles (V) of
2 × 8 deg stimuli. In all cases, the stimulus was moved at different velocities
(2, 6 and 20 deg/sec. These curves show the type of neurons with preference in-
version between horizontal rectangles and squares ($H \times S > V$) [from An der
Heiden and Roth, 1983]. B) Response of tectal cell T5(2), after pretectal lesion,
to squares (type c), worm-like (type a) and antiworm-like (type b) stimuli moved
at 7.6 deg/sec [from Ewert, 1976].

parameters controlling the level of pretectal inhibition upon the tectum.

The Model

In order to analyse what neural mechanisms might be responsible for the "in-
version phenomenon" observed by Roth and collaborators in the response prefer-
ence of the PY cell [Himstedt & Roth, 1980; Roth & Jordan, 1982], we introduced
slight changes into the two-dimensional model of the retino-tectal-pretectal inter-
actions described in Chapter 3 (see also Appendix A). First, the modelling of
the temporal characteristics of the PY response was modified so that instead of
measuring the level of activity reached by this cell through the number of pulses,
we rather measure it by the average activity presented by these cells during visual
stimulation. The firing rate of the PY was modelled as follows:

$$s_{py}(py(t); \Theta_{py0}, \Theta_{py1}) = \begin{cases} \Theta_{py1} - \Theta_{py0} & if \; py(t) \geq \Theta_{py1} \\ py(t) - \Theta_{py0} & if \; \Theta_{py0} \leq py(t) < \Theta_{py1} \\ 0 & if \; py(t) < \Theta_{py0} \end{cases}$$

that is, it is proportional to the cell's membrane potential for values above thresh-
old and it saturates for values above a specific value Θ_{py1}. Second, due to the
lack of empirical evidence about the intrinsic organisation of the pretectum, we
have modeled the TP neuron membrane potential as if it is completely driven
by axon terminals from retinal ganglion cells type R3 and R4. In Chapter 3 it
was assumed that the maximum response of a TP cell cannot exceed the amount
of excitation produced by the sum of the effects from ganglion cells R3 and R4
corresponding to the "focal" receptive field of TP. Here, this assumption was elim-
inated, assuming instead that, because of the overlapping of receptive fields of
ganglion cells projecting to the pretectum required to match the size of TP recep-
tive field (15-30 deg), the TP cell's response should be higher to bigger compact

objects. Finally, through computer simulations we readjust some parameters so that the preference shown by PY cells at medium velocities (8 deg/sec) [Ewert, 1976, 1980] was reproduced. The new values of those variables that were changed are:

$$\Theta_{tp} = 5.4$$
$$\tau_{tp} = 0.04$$
$$C_{tp} = 1.0$$

The rest of the model parameters remained with the same values as in Chapter 3 (see Appendix A for final choices).

Results

Empirical evidence suggests that the causes for getting different results with similar biological preparations may be related to animal's experience with particular prey [Himstedt, 1982] or to different manipulations of the animals within the laboratory [Ewert, 1980]. In addition, processes of learning (e.g., habituation) [Lara & Arbib, 1985] and the animal's motivational state [Ewert, 1982; Ingle, 1982a] have been postulated to modulate the inhibitory effect exerted by the pretectum upon the tectum. Ewert [1976, 1980] has shown that after pretectal lesion, a switch in preference between square and worm-like stimuli occurs at the level of the animal's behavior and of the physiological response of the T5(2) cell.

In this section we investigate the behaviors presented by the PY cell to variations in three mechanisms that subserve the pretectal inhibition over the tectum: the TP threshold (Θ_{tp}), the membrane time constant (τ_{tp}), and the strength of its inhibitory effect upon the PY cell ($w_{tp_{PY}}$).

Results of a series of computer experiments are summarized in graphs that may be compared directly with physiological data. In these graphs, the x-axis

represents the stimulus velocity in deg/sec, while the y-axis represents the average level reached by the PY cell of a specific (ith, jth) tectal column during the presentation of a stimulus. Our current model consists of an array of 8 × 8 FTC units that covers approximately 32 × 32 deg of visual field, thus we cannot conduct simulations presenting stimulus as big as those used in Ewert's experiments (32 × 2 deg). Therfore, we used stimuli with dimensions as those used by Roth and Jordan [1982], i.e., a rectangle of 8 × 2 deg moving with its longitudinal axis parallel to the direction of motion (as a "worm-like" object), and a square of 8 × 8 deg. In each experiment, both stimuli were presented moving with velocities of 4, 8, 12 and 16 deg/sec.

TP response to different velocities

This experiment has not been reported in the literature, and needs confrontation with empirical results. Fig. 61 shows the response of the TP neuron projecting to the tectal column ($4th, 4th$). It is clear that the response preference of the TP neuron is invariant to the stimulus velocity. At all velocities, TP responds better to a square object than to an antiworm-like stimulus, and it gives the weakest response to a worm-like stimulus. This discrimination becomes more evident at higher velocities. This result is not surprising because our model considers, and here we hypothesize, that the pretectal response is the outcome of the weighted sum of the excitation coming from retinal ganglion cells type R3 and R4, the effect of the latter being much stronger than that of the former. The firing rate of ganglion cells can be represented as a power function of the velocity:

$$R = k \cdot v^{\delta}$$

such that $\delta_{r3} < \delta_{r4}$ [Ewert, 1976; Grüsser & Grüsser-Cornehls, 1976]. Additionally, ganglion cells R4 respond better to squares than to antiworm-like or

TP Maximum

Membrane Potential   column (4,4)
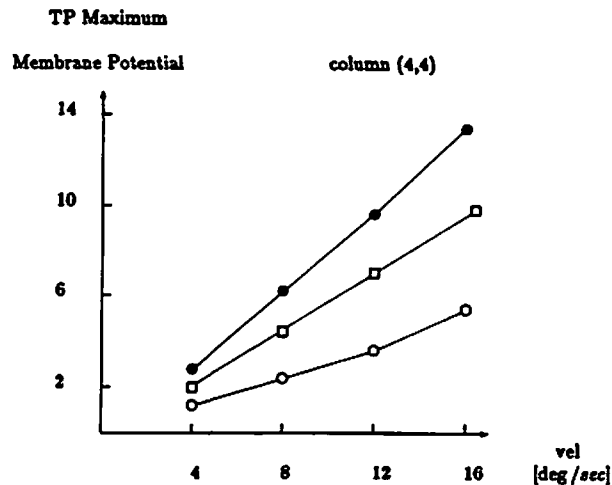
Figure 61: TP neuron's response to different stimulus velocities.
The curve with o represents TP neuron's responses to a worm-like stimulus of
8 × 2 deg, the one with • represents those to a square of 8 × 8 deg, and the one
with □ represents those to an antiworm-like stimuli of 2 × 8 deg.

worm-like stimuli (see Chapter 3). Thus, if the stimulus velocity increases then R4 response preference will remain the same and, because its effect upon the pretectum is stronger than that of R3, so is the preference of the TP cell's response. Therefore, the fact that under these circumstances TP response preference is invariant to the stimulus velocity was expected.

An inversion due to an artifact

Fig. 62 shows that for velocities above 8 deg/sec the preference of the PY cell's response remains the same, i.e., PY cell responds better to worm-like stimuli than to square objects. At lower velocities the preference is switched, but this is an artifact of the model design.

As mentioned above, in the model the TP neuron was represented mathematically by a very simple model, whose goal was (see Chapter 3) to reproduce the physiological behavior recorded by Ewert [1971] for the TH3 neuron, so that we could test the hypothesis of this cell's inhibitory influence over the tectal elements being responsible for the PY capability of prey-predator recognition. Thus, the TP threshold Θ_{tp} was calculated such that for small ("prey-like") objects the TP inhibition upon tectum had only a tonic value, while for larger ("predator-like") stimuli it was proportional to the TP membrane potential. In addition, this Θ_{tp} was calculated for the case of medium velocities (8 deg/sec). So, when the velocity of a square of 8 deg is reduced to 4 deg/sec then retinal input produces a subthreshold TP membrane potential and, at the same time, the excitation produced by retinal input upon tectal elements is stronger than that produced by a worm-like stimulus of 8 × 2 deg. The simultaneous occurrence of these events yields the change in the preference of the PY cell's response observed in Fig. 62. In order to improve the model so that this artifact can be eliminated, more em-

Average PY

Membrane Potential   column (4,4)
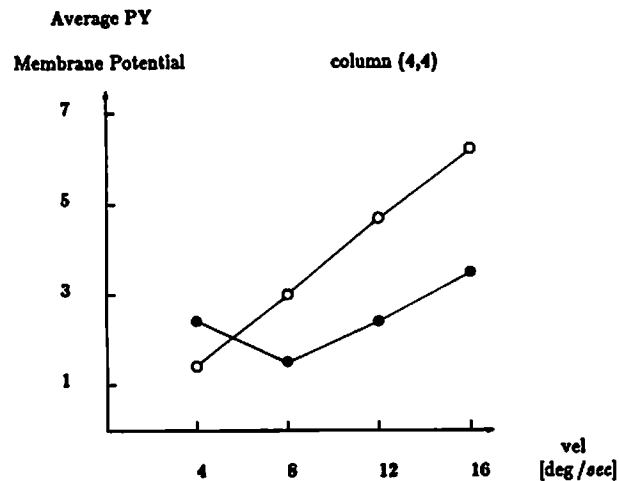
Figure 62: PY cell's response with an artifact.
The curve with o represents PY cell's responses to a worm-like stimulus of 8×2 deg
and the one with • represents those to a square of 8 × 8 deg.

pirical data about the physiological properties of the TP neuron's reponse to stimuli moved at different velocities is required; otherwise we may end up making arbitrary considerations with no experimental basis.

Variations in TP threshold value

Depending on the parameter that is changed, the inhibitory pretectal effect upon the tectum might be modulated for all velocities (global) or just for some of them (local). Here, we study the behavior of the model when such an inhibition is modulated only for high velocities. This is accomplished by lowering the value of the TP threshold Θ_{tp} in such a way that a worm-like stimulus moved at high velocities (12 and 16 deg/sec) will produce a TP membrane potential above threshold. That is, the pretectal inhibition upon tectal cells, rather than being equal to the tonic effect, becomes proportional to the TP membrane potential. Empirically, this might be interpreted as having an animal with lower motivation or one that is used to capturing slow-moving prey. Fig. 63 shows the results of reducing TP threshold, Θ_{tp}, so that a worm-like object of 8 x 2 deg moving at velocities greater than 8deg/sec (doted line) or at velocities greater than 12deg/sec (broken line) would produce TP membrane potential above threshold. It can be observed that when the Θ_{tp} value is reduced, as described above, there is a switch in the TP neuron's response preference at velocities greater that 12deg/sec, while for the case of 12deg/sec velocity, even though the PY response to the worm-like stimulus is reduced, it is still stronger than that elicited by the square object. These results resemble the physiological recordings reported by Roth and Jordan [1982] in *Bufo Bufo* for the tectal cells type $H \times S > V$ which presented the "inversion phenomenon". That is, at low (in our case at medium) velocities they prefer worm-like to square stimuli but at high velocities the square produces the

Average PY

Membrane Potential   column (4,4)
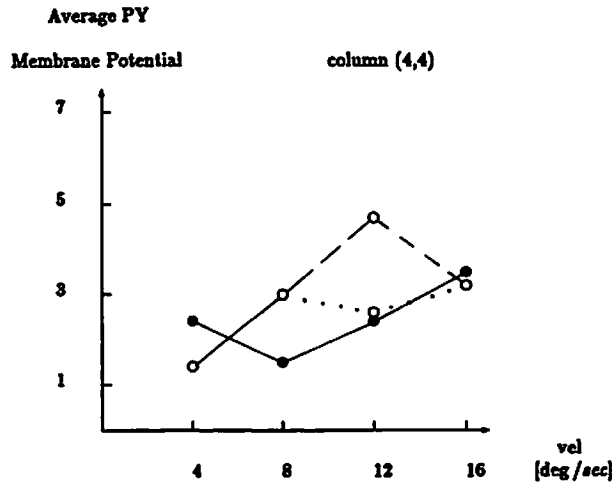
Figure 63: PY cell's response for lower TP threshold values.
o represents PY cell's responses to a worm-like stimulus of 8 × 2 deg and • represents those to a square of 8 × 8 deg. The doted line represents the case of a worm-like stimulus of 8 × 2 deg moving at velocities greater than 8 deg/sec that produces a TP membrane potential above threshold, and the broken line corresponds to the case when the same stimulus takes TP membrane potential above threshold only when it is moved at velocities greater than 12 deg/sec.

better response.

Variations in the TP membrane time constant

In this section, variations in a parameter that causes global changes (i.e., changes in the level of PY activity produced by stimuli moving with any velocity) in the behavioral pattern of the PY cell are analysed. We analyze how changes in the TP membrane time constant τ_{tp} might affect the level of PY membrane potential. In normal conditions, the model involves a very fast TP membrane constant so that the pretectal inhibition upon tectum becomes active as soon as the proper stimulus is presented, preventing in this way a build up of tectal activity that might produce a strong prey-catching orienting behavior. Thus, the variations on τ_{tp} considered in this experiment are related to the delay of pretectal inhibitory effect over the tectum. This might be interpreted empirically as producing a state of high motivation in the animal under study, that is, the inhibitory effect of TP upon tectal elements decreases as the motivational state of the animal increases. Fig. 64A shows the results for a slower TP membrane constant and ($\tau_{tp} = 0.18$), and Fig. 64B for an even slower one ($\tau_{tp} = 0.25$). In Fig. 64A can be observed that delaying the pretectal inhibitory effect upon the tectum allows the retinal ganglion to build up a strong level of excitation in the tectal lements which increases the average response of the PY cell during the period of time of stimulation. In this case the delay was not long enough to produce a switch in the preference of the PY cell's response. If we assume a longer delay (Fig. 64B) then we may obtain a switch in the PY response preference at all velocities. It is interesting to note that this resembles the empirical observations of Ewert [1976, 1980] in animals with pretectal lesions, which responded to any moving stimulus with prey-catching orienting behavior giving the strongest

Average PY

Mem. Pot.   column (4,4)

Average PY

Mem. Pot.   column (4,4)

(A)

(B)
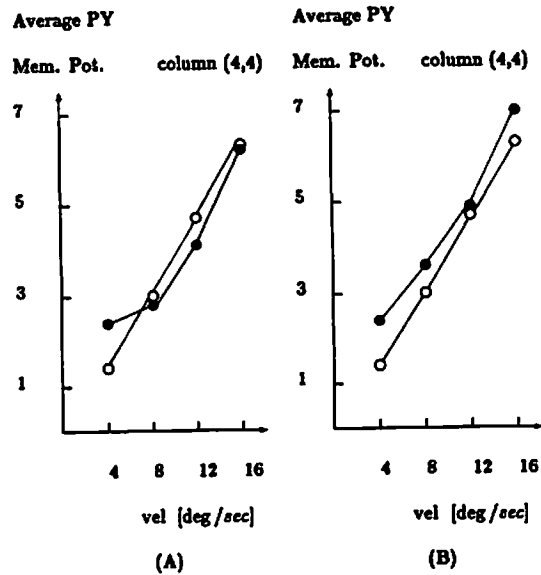
Figure 64: PY response for slow TP membrane time constants.
o represents PY cell's responses to a worm-like stimulus of 8×2 deg and ● represents those to a square of 8×8 deg. A) These curves correspond to the simulation of a slower TP membrane time constant ($\tau_{t_p} = 0.18$). B) These curves correspond to the simulation of a TP membrane time constant of $\tau_{t_p} = 0.25$.

response to square stimuli.

Variations in the TP inhibition upon PY

The last set of experiments involves variations in the strength of the inhibition exerted by the TP neuron over the PY cell, which is controlled by the weighting factor associated with the effect from TP to PY ($w_{t_p-p_y}$). If this factor is increased then the response of PY will be decreased for any type of moving stimuli, and if we keep on increasing this factor then eventually PY response to any moving stimulus would be supressed. Here, we are interested in studying if such variation might generate the "inversion phenomenon" observed by Roth and Jordan [1982]. Thus, we conducted experiments that might increase the response of PY cell to larger objects, that is, experiments that might be interpreted as increasing the motivational state of the animal in such a way that it responds better to larger objects, which under normal circumstances would be ignored (or avoided if they are big enough). This was accomplished by reducing the strength of the inhibition exerted by the TP neuron over the PY cell. Fig. 65A and Fig. 65B show the results of the computer simulations corresponding to a decrease in $w_{t_p-p_y}$ from 0.9 in "normal" conditions to 0.6 and 0.4, respectively. When the reduction in $w_{t_p-p_y}$ is moderate (to 0.6) the inversion phenomenon of Roth and Jordan [1982] is generated, as can be observed in Fig. 65A. The PY cell responds better to a worm-like than to a square object at medium velocities, while at high velocities it prefers a square object to a worm-like stimulus. Additionally, if $w_{t_p-p_y}$ is reduced further, from 0.9 to 0.4 (see Fig. 65B), then the PY cell's response becomes stronger to a square object than to a worm-like stimulus, which fits rather well the physiological data reported by Ewert [1976, 1980] when recording from tectal cells in animals with pretectal lesions, that is, PY cell responds better to larger

Average PY

Mem. Pot.   column (4,4)

vel [deg/sec]

(A)

Average PY

Mem. Pot.   column (4,4)

vel [deg/sec]

(B)
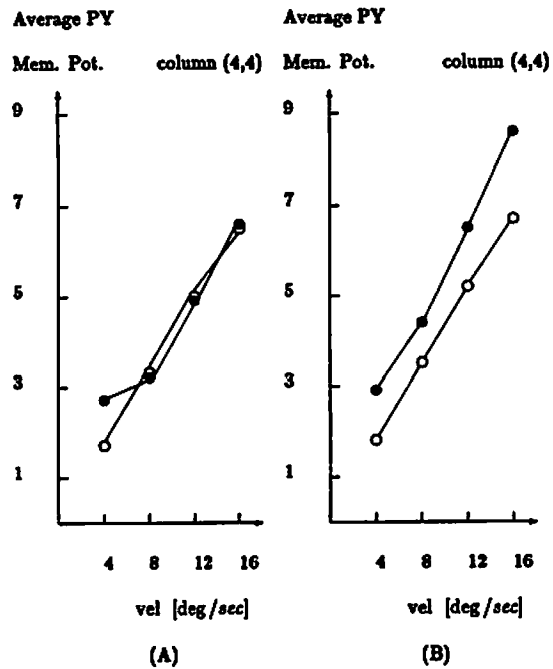
Figure 65: Tectal response for different effects from TP to PY.
A) These curves show simulation of a medium inhibitory effect from TP neuron upon the PY cell ($w_{t_pp} = 0.6$). B) These curves display the simulation of a weaker inhibitory effect from TP neuron upon the PY cell ($w_{t_pp} = 0.4$).

(square) objects that to worm-like stimulus. This set of experiments is the one that best reproduced the "inversion phenomenon" reported by Roth and Jordan in tectal cell T5(2) in toads, although a combination of variations in several parameters modulating the inhibitory effect from TP to PY might be a better option to represent the neural mechanisms subserving this phenomenon.

Discussion

In this Chapter, one of main advantages of brain modelling has been exploited. Mathematical models of neural networks not only can help us to articulate hypotheses underlying an approach to the understanding of a particular phenomenon, but they allow us to test, through computer simulations, the implications of these hypotheses.

In order for a model to be successessful in neuroscience, it has to provide information about the problem under study that can become a subject of empirical research. This philosophy has been adopted, with great success, by several laboratories [Byrne, 1980a,b, 1981, 1982; Leibovic, 1983] which have developed an interplay of theoretical and empirical approaches to the analysis of problems related to a particular biological preparation. Here, based on behavioral and physiological grounds, we have used our model of the retino-tectal-pretectal interactions to analyse whether or not the neural mechanisms underlying the hypothesised pretectal inhibitory effect over the optic tectum may account for the differences between the results obtained by Ewert's group [Ewert & Wieterheim, 1974; Schürg-Pfeiffer & Ewert, 1981; Finkenstädt & Ewert, 1983] and Roth and coworkers [Luthardt & Roth, 1979; Roth & Jordan; Himstedt & Roth, 1980; Roth, 1982] when presenting configurational stimuli at different velocities.

Our analysis showed that Roth's results can be produced when the threshold of the pretectal neuron (TP), which is exerting an inhibitory effect upon tectal elements, is decreased so that TP responds with a firing rate stronger than a tonic level to a worm-like stimulus of 8 × 2 deg moving at high velocities (above 12 deg/sec), or the strength of the inhibitory effect from TP over PY is not strong enough to counteract the excitation coming retinal ganglion cells of type R3 and R4. Based on empirical observations, the parametric changes in these simulations can be interpreted as an increase in the animal's motivation for preying. Ewert's observations, PY (his T5(2)) cell's response preference being independent to the stimulus velocity, were reproduced under opposite conditions, that is, if the TP cell response latency was shortened during the presentation of a compact (square) object, if a worm-like object of 8 × 2 deg at all velocities does not elicit a TP membrane potential above threshold, and if TP inhibition over PY counteracts the excitation coming fron retinal ganglion cells class R3 and R4. In this cases, it may be interpreted as if the animal had low motivation for attacking a prey. Our simulations also generated results that resembled Ewert's data in animals with pretectal lesions. The mechanisms responsible for this result were the TP latency of response and the strength of its inhibitory effect upon the PY cell. That is, when the response of the TP neuron is long delayed or dramatically reduced then, the PY cell responds better to a square object than to a worm-like stimulus. This suggests that a state of very low motivation, for preying, in the animal generates a similar effect as that observed when the pretectum is lesioned. Empirical evidence have suggested that pretectal inhibition over the tectum, and so the mechanisms analysed in this Chapter, may be modulated by the motivational state of the animal or by its experience with certain type of prey [Ewert, 1980; Ingle, 1982b; Himstedt, 1982], thus, the results generated in our

analysis can be tested experimentally. In such an experiment, the motivation of the animal to attack a prey must be quantitatively measured.

This analysis also pointed out some gaps in our current knowledge of the physiological and anatomical properties of the TP cell, which will be very useful to clarify the real nature of the phenomenon under study. Physiological studies of the TP response to configurational stimuli moving at different velocities need to conducted; whereas, anatomically we need studies that identify the origin of the afferent terminals impinging upon this type of pretectal cell. Our model assumes that TP activity is completely driven by retinal input, and under these conditions the preference of the TP neuron response was shown to be independent of the stimulus velocity, that is, it preferred squares to worm-like stimuli regardless of the stimulus velocity. This information about the anatomy and physiology of the pretectal cell TP will also be very usefull to improve the model so that the artifact effect, i.e., a switch in the preference of PY cell's response at velocities smaller than 8 deg/sec, presented by the model, may be eliminated. In addition, to properly address this issue, our model also requires a more refined model of the retina and of the amount of overlapping of receptive fields in the tectal columns involved in the retino-tectal mapping. It is clear that more empirical and theoretical research addressing the hypotheses tested in this Chapter is necessary and will clarify the real nature of these processes.

CHAPTER VI

CONCLUSIONS

On the Interaction of Theory and Experiment

Theoretical and Experimental studies have pursued the understanding of the brain at different levels of analysis. Over the years, both approaches have made a great deal of progress, but mainly independently from each other. With this work, it is our intention to emphasize that the interplay of empirical and theoretical analyses is necessary and will increase the pace towards the clarification of the real nature of the information processing carried out by the Central Nervous System (CNS).

Under this approach, when studying sensory-motor coordination, empirical observations have generated working hypotheses of what may be the mechanisms used by the CNS to give the animal its capabilities to interact with the external world; whereas, theoretical studies have served to create a conceptual framework where results from the laboratory can be formalized. If a neural model is tied to empirical observations (i.e., anatomy, physiology and ethology) then it can be used to predict new results which, in turn, become subject to experimental test. Such a neural model can also be used to pose new problems which will lead to further theoretical and empirical work.

Although neural systems are far more complex than any mathematical model we may come up with, such a mathematical model can help us to articulate the

hypotheses underlying our approach to a particular problem and, furthermore, it may allow us to test, through computer simulations or analytical techniques, the implications of these hypotheses.

In order to develop a model of a particular biological preparation, a general theory of brain modelling is needed. Schema Theory [Arbib, 1972, 1981a,b] provides a conceptual framework to study animal behavior in terms of interacting computations, without paying too much attention to physiological or anatomical detail at the level of neural circuits [House, 1984; Arbib & House, 1983; Lara et al, 1985]; whereas, the work presented by Hodgkin and Huxley [1952], Amari [1977], Holden [1977] and An der Heiden [1980], about mathematical models of a single neuron or a group of neurons, provides the theoretical grounds to develop neural net models, such as those in this dissertation, at different levels of detail to account for data obtained experimentally for a particular neural system.

Different laboratories have started to conduct, with great success, *hybrid* studies that involve an interplay of theoretical and empirical approaches to the analysis of problems related to a particular biological preparation. A good example of this approach is the work developed by Byrne [1980a, 1980b, 1981, 1982], who has combined empirical and theoretical approaches to direct a quantitative analysis of the correspondance of the inking behavior in *Aplysia* with the ionic conductance mechanisms in motor cells subserving such behavior. Experimentally, following Carew and Kandel's [1977a, 1977b, 1977c] work, he [Byrne, 1980a] analysed ionic conductance mechanisms in motor cells controling the inking behavior in *Aplysia*. Then, this author [Byrne, 1980b] developed a modified Hodgkin-Huxley model to quantitatively examine the correspondance between features of the inking behavior and individual ionic conductance mechanisms in motor cells subserving such behavior. This model was used to predict discharge patterns of the ink gland

motor cells under different experimental conditions which, then, were tested em-
pirically. Results from both theoretical and empirical studies were in good agree-
ment, and so this *hybrid* approach could be successfully used to determine the
extent to which each conductance mechanism contributes to the firing pattern
of the motor cells. Additionally, Byrne [1981] extended the model to analyse an
interesting form of short-term behavioral modification exhibited by the inking
behavior in *Aplysia*. For a summary of these studies refer to Byrne [1982].

Another example of a successful application of an interplay of theoretical and
empirical studies is Leibovic's [1983] analysis of the response waveforms of verte-
brate photoreceptors. Based on known and plausible data on photoreceptors, he
developed a model to account for the physical-chemical processes of light absorp-
tion, for the transduction of the stimulus to a neural signal, and for the cellular
system underlying these processes. However, many details about photoreceptors
are still unknown and had to be hypothesized during the model development.
Some of the theoretical implications of such assumptions were tested empirically,
showing that both theoretical and empirical results were consistent. Leibovic's
work revealed gaps in our knowledge of the phenomenon under study, e.g., the
need for a linking between the biochemistry of transduction to membrane bio-
physics and electrophysiology, and thus posed new questions for further research.

Some other examples can be found in the special issue on "Neural Systems
and Sensory Information Processing" of the IEEE Transactions on Systems, Man
and Cybernetics [1983].

Computational Models of Anuran Visuomotor Coordination

Our approach to the study of visuomotor coordination in frog and toad is very
similar to those described in the previous section, involving a group of theorists
and experimentalists collaborating with each other in seeking to elucidate the
neural mechanisms subserving visuomotor coordination. The theorists provide
their expertise to develop and analyse, through computer simulations and ana-
lytical techniques, neural net models trying to identify the mechanisms used by
the CNS to underly behavior. The experimentalists, on the other hand, gener-
ate the empirical data to found the models in the first place, and provide their
expertise to develop new techniques, or to apply existing ones, to conduct empir-
ical tests of the hypotheses embodied in the models and their implications. Our
models are designed to be flexible enough so that results from these new empiri-
cal studies may in turn be used to refine them. Thus, in our case, the interplay
of theoretical and empirical work is carried out by the conjoint participation of
specialists from the two fields.

In this dissertation, we have presented three different stages of a family-model
of the interactions among different structures in the anuran brain that might be
subserving visuomotor coordination. First, we developed a neural net model of
the retino-tectal-pretectal interactions that might subserve prey-predator discrim-
ination and size-preference in anuran amphibia. Second, we started to develop an
analytical treatment of our models, trying to define through stability and param-
eter sensitivity analyses a range of models that might explain the phenomenon
under study. Third, the model developed in the first part was used to address a
phenomenon not included during the neural model design, i.e., the controversial
issue of whether or not the preference of PY cell's response between "worm-like"
and "square" stimuli may be velocity dependent.

The model described is an extension of a previous model of the optic tectum [Arbib & Lara, 1982; Lara & Arbib, 1982; Lara, Arbib & Cromarty, 1982], and takes into consideration anatomical, physiological and behavioral studies in anurans, as well as earlier modelling efforts [Ewert & Von Seelen, 1974; Didday, 1970, 1976]. Our model is composed by a two-dimensional array of 8 × 8 Facilitation Tectal Columns, and it was used to study how interactions among retina, optic tectum and pretectum may give frogs and toads the ability to discriminate between prey and predator stimuli.

Our models embody hypotheses generated independently by different disciplines, such as anatomy, physiology and ethology. They also include hypothesized correlations between anatomical data, physiological results and behavioral observations, all of which need to be tested experimentally. Results from computer simulations have allowed us to reproduce empirical observations, and to suggest what neural mechanisms might be involved in some phenomena related to prey-catching orienting behavior:

1. PY cells' capability to discriminate between prey and predator is the outcome of information coming from the retina (cells type R2, R3 and R4), an inhibitory effect from pretectal cells TP and the level of internal activity within the tectum.

2. Directional invariance of the PY cell's response is the result of tectal architecture through symmetric interconnections among neighboring columns.

3. PY cell's size-preference and response latency are controlled by the motivational state of the animal through variations in the level of inhibition exerted by the pretectum upon the tectum.

4. PY cell's preference between "worm-like" and "square" stimuli might switch as the stimulus velocity varies, if pretectal inhibition over the tectal cells is delayed or reduced.

Our analysis also revealed gaps in our knowledge of anuran visuomotor coordination which will lead to further theoretical and empirical investigations. In the

model, it was necessary to make some assumptions with respect to the nature of the interconnections among tectal elements, as well as of their interactions with retinal and pretectal neurons. It is known that the effect from pretectum upon tectum is of inhibitory nature, but it is still unknown whether this inhibition is accomplished by direct inhibition of elements (GL or LP, SP and PY) responsible for the internal activity of the tectum, or by the activation of inhibitory tectal mechanisms (SN neuron). Our models assume the alternative of TP inhibiting LP, SP, and PY cells based on findings by Lara and Arbib [1982]. Through computer simulations with the FTC model, these authors determined that the model's response was more sensitive to the effect of TP fibres when they arrive at SN. As a result of this, the model's response to a new stimulus is delayed or eliminated. They also found that when TP fibres inhibit GL activity directly, then the long lasting depolarization of this element, which is very important in prey-catching facilitation, is lost. Thus, it is clear that we need studies, probably pharmacological or biochemical, in the optic tectum to identify the neurotransmiters involved in the retino-tectal and pretectal-tectal projections, as well as in the interactions among cells from different tectal layers. The results obtained during the stability and parameter sensitivity analyses of the FTC model showed what might be expected when conducting such experiments. That is, they defined different qualitative physiological behaviors that might be observed when specific changes in the interactions of tectal elements occur.

We hope that the results from computer simulations of our two-dimensional model of the retino-tectal-pretectal interactions, from the analysis of how PY cell's response might be velocity dependent, and from our analytical treatment of the FTC model will stimulate new empirical studies.

Our Models vs. Previous and Alternative Models

Our model can be considered as a way of *unlumping* the ideas of Ewert and von Seelen [1974] for the relations among retina, tectum and pretectum for prey-predator recognition. They proposed a model of prey-predator recognition in which the retina, tectum and pretectum acted as filters for specific configurations of the stimulus. The inhibitory effect of the pretectum to the tectum enabled the latter to discriminate between "worm-like" and "antiworm-like" stimuli. As such, their model set forth the basic structure of regional interactions used in our model. However, their model had a number of limitations:

1. They did not show how the architecture of the different brain regions would give rise to the properties of their postulated filters.

2. They simulated only prey-predator recognition with neither the possibility to reproduce other phenomena nor the capacity for expansion.

3. Because of the linear nature of the model, it was restricted to a given range of values.

4. Because the model was lumped both in space and time, it could not be tested against the time course of response of specific cell types with specific retinotopic coordinates.

An der Heiden and Roth [1983] have proposed a lateral inhibition model of tectum which can reproduce important properties of worm-antiworm discrimination, but does not address the issues of tectal-pretectal interactions or of intrinsic tectal geometry. They postulate that the response of tectal cells is only the outcome of the spatio-temporal summation of retinal input (ganglion cells R2 and R3) combined with inhibitory interactions among the tectal neurons. Because of the tectal architecture of their model, the response of T5(2) cells increases as the stimulus size increases, so T5(2) response to large prey objects is not reproduced. The authors mentioned that an influence, from thalamic or pretectal cells, upon

the tectum could be assumed in the presence of non-prey objects. Finally, their model could not explain the disinhibitory effect in the tectum, observed by Ewert [1976, 1980] and Ingle [1975], after pretectal lesion.

Further Research

These models are just the beginning of the development of a theoretical approach that will serve to analyze how external information is represented within different regions of the brain, and how it uses such a representation to elicit the most adequate behavior. Thus possible extensions of this work are as follows. In the development of all these phases, we must test our models against empirical data by designing experimental paradigms to confront results predicted by computer simulations or analytical studies of our models.

1. The recognition tectal unit reported in this work is only an element of a complex interaction among elements from different brain structures that give the animal the ability of representing the external world. Thus, further modelling should include the development of other functional units from the tectum (T5(1), T5(3), T2, T4, etc.), as well as from other brain regions to complete the neural machinery that represents *perceptual schemas*.

2. We need to develop also conceptual and neural models of how *motor centers* interpret neural levels of activity in primary visual centers to yield the proper motor behaviors, such as prey-predator discrimination, prey-selection, depth perception and detour behavior, so that we may have a clearer understanding of how the CNS carries out the process of visuomotor coordination.

3. Equally important is the development of neural net family-models of the Motor Programs that produce the spatio-temporal activation of muscles to produce proper motor behaviors (*motor schemas*).

4. Some of the animal's behaviors are comprised by a sequence of motor responses, where the completion of one seems to trigger the next one. For example, prey-catching behavior starts with the appearance of a prey in animal's visual field, then it orients and approaches it until the prey is located

in its binocular field within certain distance; then comes the binocular fixation of the prey and the snapping at it; the result of this is the stimulation of mechano-receptors of pharynx and snout that triggers the swallowing and, finally, the mouth wiping. Thus, the following question should be addressed:

How are *motor programs* represented by spatio-temporal patterns (some times sequentially) of neural activity in the CNS?

5. Additionally, the following questions should be considered:

What is the effect of Modulator centers over the response of elements in primary visual centers within the main visual path?

Do these modulators affect only primary visual centers or do they affect also some of the motor centers?

Is it computationally feasible to develop a model of the complete chain of visuomotor coordination?

We have shown the importance of using analytical techniques to develop and analyse neural net models. The methodology we used to analyse the FTC model is useful only for neural circuits with a small number of elements. That is, as the number of interacting elements in the network increases it would get harder to apply the question of "virtual" vs "actual" states to the design and analysis of such a models. Thus, a very important topic in Brain Theory that needs to be addressed is the development of new analytical techniques, or the adaptation of existing methodologies already developed in other disciplines, to the study of models of complex neural networks.

BIBLIOGRAPHY

Amari, S.I. (1977) A Mathematical approach to neural systems. In *Systems Neuroscience* (J. Metzler Ed.), New York: Academic Press, pp. 67-117.

Amari, S.I. (1982) Competitive and cooperative aspects in dynamics of neural excitation and self organisation. In: *Competition and Cooperation in Neural Nets* (S. Amari and M.A. Arbib, eds.), Lecture Notes in Biomathematics No. 45, Berlin: Springer-Verlag, pp. 1-28.

Amari, S. and Arbib, M.A. (1977) Competition and cooperation in neural nets. In *Systems Neuroscience* (Metzler, J., ed.), New York: Academic Press, pp. 119-165.

An der Heiden,U. (1980) Analysis of neural networks. *Lecture Notes in Biomathematics* No. 35. Berlin: Springer-Verlag.

An der Heiden, U. and Roth, G. (1983) A mathematical network model for retinotectal prey-recognition in amphibians. In: *Proceedings of Second Workshop on Visuomotor Coordination in Frog and Toad: Models and Experiments*, COINS Technical Report 83-19, University of Massachusetts, Amherst, MA 01003.

Arbib, M.A. (1972) The Metaphorical Brain: An introduction to cybernetics as artificial intelligence and brain theory. New York: Wiley-Interscience.

Arbib, M.A. (1981a) Perceptual structures and distributed motor control. In: *Handbook of Physiology-The Nervous System II. Motor Control* (ed. V.B. Brooks), Bethesda, MD: Amer. Physiological Society., pp. 1449-1480.

Arbib, M.A. (1981b) Visuomotor coordination: From neural nets to schema theory. *Cognition and Brain Theory*, 4: 23-29.

Arbib, M.A. (1982) Rana Computatrix an evolving model of visuomotor coordination in frog and toad. In *Machine Intelligence* 10 (J.E. Hayes, D. Michie and Y. H. Pao, Eds.), Chichester: Ellis Horwood, pp. 501-517.

Arbib, M. A. (1984) Levels of modelling of neural interactions underlying Visuomotor Coordination (submitted).

Arbib, M.A. and House, D. (1983) Depth and detours: Towards neural models. In: *Proceedings of second workshop on visuomotor coordination in frog and toad: Models and Experiments* (R. Lara and Arbib, M.A., Eds.). COINS-Technical report 83-19, University of Massachusetts, Amherst, MA 01003.

Arbib, M.A. and Lara, R. (1982) A neural model of the interaction of tectal columns in prey-catching behavior. *Biol. Cybernetics*, 44: 185-196.

Brodie, E.D. (1977) Hedgehogs use venom in their own defense. *Nature*, 268:627-628.

Bulirsch, R. and Stoer, J. (1966) Numerical treatment of ordinary differential equations by extrapolation methods. *Num. Mathem.* 8:1-13.

Butenandt, E. and Grüsser, O.J. (1968) The effect of stimulus area on the response of movement detecting neurons in the frog's retina. *Pflügers Archiv.*, 298: 285-293.

Byrne, J.H. (1980a) Quantitative aspects of ionic conductance mechanism contributing to firing pattern of motor cells mediating inking behavior in *Aplysia californica. J. of Neurophys.*, 43:651-668.

Byrne, J.H. (1980b) Analysis of ionic conductance mechanism in motor cells mediating inking behavior in *Aplysia californica. J. Neurophysiol.*, 43:630-650.

Byrne, J.H. (1981) Simulation of the neural activity underlying a short-term modification of inking behavior in *Aplysia. Brain Res.*, 204:200-203.

Byrne, J.H. (1982) Cellular and biophysical mechanisms contributing to regulation of reflex excitability of inking behavior in *Aplysia. Federation Proc.* 42:2147-2152.

Carew, T.J. and Kandel, E.R. (1977a) Inking in *Aplysia californica.* I. Neural circuit of an all-or-none behavioral response. *J. Neurophysiol.*, 40:692-707.

Carew, T.J. and Kandel, E.R. (1977b) Inking in *Aplysia californica.* II. Central program for inking. *J. Neurophysiol.*, 40:708-720.

Carew, T.J. and Kandel, E.R. (1977c) Inking in *Aplysia californica.* III. Two different synaptic conductance mechanisms for triggering central program for inking. *J. Neurophysiol.*, 40:721-734.

Cervantes-Péres, F., Lara, R. and Arbib, M. A. (1985) A model of neural mechanisms underlying predator-avoidance in anurans. (in elaboration).

Comer, C. and Grobstein, P. (1981a) Tactually elicited prey acquisition behavior in the frog Rana Pipiens. *J. Comp. Physiol.*, 142: 141-150.

Comer, C. and Grobstein, P. (1981b) Involvement of midbrain structures in tactually and visually elicited prey acquisition behavior in frog Rana Pipiens. *J. Comp. Physiol.*, 142: 151-160.

Comer, C. and Grobstein, P. (1981c) Organization of sensory inputs to the midbrain of the frog Rana Pipiens. *J. Comp. Physiol.*, 142: 161-168.

Dahlquist, G. and Björck, A. (1974) Numerical Methods. New Jersey: Prentice Hall.

Didday, R.L. (1970) The Simulation and Modelling of Distributed Information Processing in the Frog Visual System. Ph.D. Thesis, Stanford University.

Didday, R.L. (1976) A model of visuomotor mechanisms in the frog optic tectum. *Mathematical Biosciences.*, 30: 169-180.

Dowling, J.E. (1976) Physiology and morphology of the retina. In: *Frog Neurobiology* (Llinás, R. and Precht, W., eds.), Berlin: Springer Verlag, pp. 278-296.

Eccles, J.C. (1973) The understanding of the brain. New York: McGraw Hill.

Espinosa, I. (1978) Sistemas Lineales Multivariables. México: UNAM Press.

Ewert, J.P. (1970) Neural mechanisms of prey catching and avoidance behavior in the toad (Bufo Bufo L.). *Brain Behav. Evol.*, 3: 36-54.

Ewert, J.P. (1971) Single unit response of the toad (Bufo americanus) caudal thalamus to visual objects. *Z. Vergl. Physiol.*, 74: 81-102.

Ewert, J.P. (1976) The visual system of the toad: Behavioral and physiological studies on a pattern recognition system. In: *The Amphibian Visual System* (Fite, K., ed.), New York: Academic Press, pp. 142-202.

Ewert, J.P. (1980) Neuroethology, an introduction to the neurophysiological fundamentals of behavior. Berlin: Springer Verlag.

Ewert, J.P. (1982) Neuronal basis of configurational prey selection in the common toad. In: *Analysis of visual behavior.* (D.J. Ingle, M.A. Goodale and R.J.W. Mansfield Eds.), Cambridge: MIT Press, pp. 7-45.

Ewert, J.P. (1984) Tectal Mechanisms that underlie Prey-Catching and Avoidance Behaviors in Toads. In: *Comparative Neurology of the Optic Tectum* (Vanegas, H. ed.), Plenum Publishing Corp., pp. 247-416.

Ewert, J.P., Borchers, H.W. and Weiterschein, Von A. (1979) Directional sensitivity, invariance and variability of tectal T5 neurons in response to moving configurational stimuli in the toad Bufo Bufo (L). *J. Comp. Physiol.*, 132: 191-201.

Ewert, J.P. and Burghagen, H. (1979a) Ontogenetic aspects of visual "size constancy" phenomena in the midwife toad Alytes obstetrican (Laur.) *Brain Behav. Evol.*, 16: 99-116.

Ewert, J.P., Capranica, R.R. and Ingle, D.J., eds. (1983) *Advances in Vertebrate Neuroethology*, New York: Plenum Press.

Ewert, J.P. and Hock, F.J. (1972) Movement sensitive neurons in the toad's retina. *Exp. Brain Research*, 16: 41-59.

Ewert, J.P., Krug, H. and Schönitz, G. (1979) Activity of retinal R3 ganglion cells in the toad Bufo Bufo (L.) in response to moving configurational stimuli: Influence of the movement direction. *J. Comp. Physiol.*, 129: 211-215.

Ewert, J.P. and Rehn, B. (1969) Quantitative analyse der Reiz-Reaktionsbeziehungen bei visuellem Auslösen des Fluchtverhaltens der Wechselkröte (*Bufo viridis*, Laur.). *Behaviour*, 35:212-234.

Ewert, J.P. and Traud, R. (1979) Releasing stimuli for antipredator behavior in the common toad *Bufo-Bufo* (L.), *Behavior*, 68: 170-180.

Ewert, J.P. and Von Seelen, W. (1974) Neurobiologie und System-Theorie eines Visuellen Muster-Erkennungsmechanismus bei Krote. *Kybernetik*, 14: 167-183.

Finkelstein, D. and Grüsser, O.J. (1965) Frog retina: Detection of movement. *Science*, 150: 1050-1051.

Finkenstädt, T. and Ewert, J.P. (1983) Visual pattern discrimination through interactions of neural networks: A combined electrical brain stimulation, brain lesion, and extracellular recording study in *Salamandra Salamandra. J. Comp. Physiol.*, 153:99-110.

Fite, K.V. (1973) The visual fields of the frog and toad: A comparative study. *Behav. Biol.*, 9: 707-718.

Fite, K.V. and Scalia, F. (1976) Central visual pathways in the frog. In: *The Amphibian Visual System* (Fite, K., ed.), New York: Academic Press, pp. 87-118.

Fox, P.A. (1971) Integration of a first-order system of ordinary differential equations. In *Mathematical Software* (John Rice Ed.). New York: Academic Press, chapter 9, pp. 477-507.

Gaze, R.M. (1959) Regeneration of the optic nerve in *X. laevis. J. Physiol.* (London), 146:40.

Gaze, R.M. and Jacobson, M.(1962) The projection of the binocular field on the optic tecta of the frog. *Q.J. Exp. Physiol.*, 47:273.

Gaze, R.M. and Keating, M.J. (1968) The depth distribution of visual units in the tectum of the frog following regeneration of the optic nerve. *J. Physiol.* (London), 200:128.

Gear, C. (1971) The automatic integration of ordinary differential equations. *CACM*, 14:3, pp. 176-179 and 185-190.

Gibson, J.E. (1963) Nonlinear automatic control. New York: McGraw Hill.

Gragg, W. (1963) Repeated extrapolation to the limit in the numerical solution of ordinary differential equations. Ph. D. Thesis, UCLA.

Grobstein, P. and Comer, C., Hollyday, M. and Archer, S.M. (1978) A crossed isthmo-tectal projection in Rana Pipiens and its involment in the ipsilateral visuotectal projection. *Brain Research*, 156: 117-123.

Grobstein, P., Comer, C., and Kostyk, S.K. (1982) Frog prey capture behavior: Between sensory maps and directed motor output, In: *Proceedings of the Workshop on Visuomotor Coordination in Frog and Toad: Models and Experiments*, Technical Report 82-16 Computer and Information Science Dept., Univ. of Massachusetts, Amherst, MA-01003.

Gruberg, E.R. and Lettvin, J.V. (1980) Anatomy and physiology of the binocular system in the frog *Rana Pipiens. Brain Res.*, 192:313-325.

Gruberg, E.R. and Udin, S. (1978) Topographic projections between the nucleus isthmi and the tectum of the frog *Rana Ppiens. J. Comp. Neurol.*, 170:487-500.

Grüsser, O.J. and Grüsser-Cornehls, U. (1976) Neurophysiology of the anuran visual system. In: *Frog Neurobiology* (Llinás, R. and Precht, W., eds.), Berlin: Springer Verlag, pp. 297-385.

Grüsser, O.J. and Grüsser-Cornehls, U., Finkelstein, D., Henn, V., Patutschnic, M. and Butenandt, E. (1967) A qualitative analysis of movement detecting neurons in the frog's retina. *Pfluegers Arch. ges. Physiol.*, 293: 100-106.

Grüsser-Cornhels (1984) The neurophysiology of the Amphibian Optic Tectum. In: *Comparative Neurology of the Optic Tectum* (Vanegas, H. ed.), New York: Plenum Press, pp. 211-245.

Grüsser-Cornhels, U. and Saunders, R.McD. (1981a) Chromatic subclasses of frog retinal ganglion cells studies using black stimuli moving on a monochromatic background. *Vision Res.*, Vol.21, pp. 469-478.

Grüsser-Cornhels, U. and Saunders, R.McD. (1981b) Response of frog retinal ganglion cells to moving monochromatic spots under photopic conditions. *Vision Res.*, Vol. 21, pp. 1617-1620.

Hartline, H.K. (1940) The receptive fields of optic nerve fibers. *Amer. J. Physiol.*, 130: 690-699.

Himstedt, W. (1982) Prey selection in salamanders. In: *Analysis of visual behavior.* (D.J. Ingle, M.A. Goodale and R.J.W. Mansfield, Eds.), Cambridge: MIT Press, pp. 47-66.

Himstedt, W. and Roth, G. (1980) Neuronal responses in the tectum opticum of Salamandra to visual stimuli. *J. Comp. Physiol.*, 135: 251-257.

Hodgkin, A.L. and Huxley, A.F. (1952) A quantitative description of membrane current and its application to conduction and excitation in nerve. *J. Physiol. London*, 117:500-544.

Holdem, A (1976) Models of stochastic activity of neurones. *Lecture Notes in Biomathematics* No. 13, Berlin: Springer-Verlag.

House, D. (1984) Neural Models of Depth Perception in frogs and toads. Ph. D. thesis, University of Massachusetts at Amherst.

Hubel, D.H. and Weisel, T.V. (1963) Shape and arrangement of columns in cat's strate cortex. *J. Physiol. London*, 165:559-568.

Hull, T.E., Enright, W.H., Fellen, B.M. and Sedgwick, A.E. (1972) Comparing Numerical Methods for Ordinary Differentia equations. *SIAM J. Num. Anal.*, 9: 4: 603-637.

Ingle, D.J. (1968) Visual releasers of prey-catching behavior in frogs and toads. *Brain Behav. Evol.*, 1: 500-518.

Ingle, D.J. (1973a) Size preference for prey-catching in frogs: relationship to motivational state. *Behav. Biol.*, 9: 485-491.

Ingle, D.J. (1973c) Selective choice between double prey objects by frogs. *Brain. Behav. Evol.*, 7: 127-144.

Ingle, D. (1975) Focal attention in the frog behavioral and physiological correlates. *Science*, 180: 442-444.

Ingle, D.J. (1976a) Spatial vision in anurans. In: *The Amphibian Visual System* (Fite, K., ed.), New York: Academic Press, pp. 119-141.

Ingle, D.J. (1976b) Behavioral correlates of central visual function in Anurans. In: *Frog Neurobiology* (Llinás, R. and Precht, W., eds.), Berlin: Springer Verlag, pp. 435-451.

Ingle, D.J. (1980) Some effects of pretectum lesions on the frogs' detection of stationary objects. *Behav. Brain Res.*, 1: 139-163.

Ingle, D.J. (1981) New methods for analysis of vision in the gerbil. *Behav. Brain Res.*, 3: 151-173.

Ingle, D.J. (1982a) Motivation and prey selection by frogs and toads: A neuroethological model. In: the *Handbook of Motivation* (Teitelbaum and Satinoff, eds.).

Ingle, D.J. (1982b) Interactions between tectum and pretectum: new levels of complexity. *Proceedings of the workshop on visuomotor coordination in frog and toad: Models and Experiments* (Arbib, M.A., ed.). COINS Technical Report 82-16, University of Massachusetts, Amherst, MA-01003.

Ingle, D.J. (1982c) Organisation of visuomotor behaviors in vertebrates. In: *Analysis of Visual Behavior* (D.J. Ingle, M.A. Goodale and R.J.W. Mansfield, eds.), Cambridge: MIT Press, pp. 67-109.

Ingle, D.J. (1983) Brain mechanisms of visual localisation by frogs and toads. In: *Advances in Vertebrate Neuroethology* (J.P. Ewert, R.R. Capranica and D.J. Ingle, eds.), New York: Plenum Press, pp. 177-226.

Ingle, D.J. and Cook, J. (1977) The effect of viewing distance upon size preference of frogs for prey. *Vision Res.*, 17: 1009-1013.

Johnson, L.W. and Riess, R. (1977) Numerical Analysis. Mass.:Addison-Wesley.

Kandel, E.R. (1978) A cell biological approach to learning. Grass Lecture No. 1, Society for neuroscience. Bethesda, MD.

Lara, R. and Arbib, M.A. (1982) A neural model of interaction between pretectum and tectum in prey selection. *Cognition and Brain Theory*, 5: 149-171.

Lara, R. and Arbib, M.A. (1985) A model of the neural mechanisms responsible for pattern recognition and stimulus specific habituation in toads. (submitted).

Lara, R., Arbib, M.A. and Cromarty, A.S. (1982) The role of the tectal column in facilitation of amphibian prey-catching behavior: a neural model. *J. Neuroscience*, 2: 521-530.

Lara, R., Carmona, M. and Dasa, F. (1985) A global model of the neural mechanisms responsible for visuomotor coordination in toads. *J. of Theor. Bio.*, 110: 587-618.

Lara, R., Cervantes, F. and Arbib, M.A. (1982) Two-dimensional model of retinal-tectal-pretectal interactions for the control of prey-predator recognition and size preference in amphibia. In: *Competition and Cooperation in Neural Nets* (S. Amari and M.A. Arbib, eds.), Lecture Notes in Biomathematics No. 45, Berlin: Springer-Verlag, pp. 371-393.

Lázár, G. (1969) Efferent pathways of the optic tectum in the frog. *Acta Biol. Hung.*, 20:171-183.

Lázár, G. (1984) Structures and connections of the frog optic tectum. In: *Comparative Neurology of the Optic Tectum* (Vanegas, H. ed.), New York: Plenum Press, pp. 185-210.

Lázár, G. and Székely (1969) Distribution of the optic terminals in different optic centers of the frog. *Brain Res.*, 16:1-14.

Lázár, G., Tóth, P., Csank, G. and Kicliter, E. (1983) Morphology and location of tectal projection neurons in frogs: A study with HRP and Cobalt-filling. *J. Comp. Neurol.*, 215: 103-120.

Lee, Y. and Arbib, M.A. (1983) Computer Model of Cone Pathways in Frog's Retina. In: *Proceedings of 13th Annual Meeting of the Society for Neurosciences*, 9: 686.

Lee, Y. (1985) A neural network model of the frog retina: A discrete time-space approach. Ph. D. thesis, University of Massachusetts at Amherst (in elaboration).

Leibovic, K.N. (1983) Phototransduction in vertebrate rods: An example of the interaction of Theory and Experiment in neuroscience. *Systems, Man and Cybernetics*, 13:732-741.

Lettvin, J.Y., Maturana, H.R., McCullogh, W.S. and Pitts, W.H. (1959) What the frog's eye tells the frog's brain. *Proc. of the IRE*, pp. 1940-1951.

Lettvin, J.Y., Maturana, H.R., McCullogh, W.S. and Pitts, W.H. (1961) Two remarks on the visual system of the frog. In: *Sensory Communication* (W.A. Rosenblith, ed.), Cambridge: MIT Press, pp. 757-776.

Luthardt, G. and Roth, G. (1979) The relationship between stimulus orientation and stimulus movement pattern in the prey catching behavior of Salamandra Salamandra. *Copeia*, 3: 442-447.

Marr, D and Poggio, T. (1979) A computational theory of human stereo vision, *Proc. R. Soc. Lond.*, B 204: 301-328.

Maturana, H.R., Lettvin, J.Y., McCullogh, W.S. and Pitts, W.H. (1960) Anatomy and physiology of vision in the frog (Rana Pipiens), *J. gen. Physiol.*, 43: 129-175.

Montgomery, N., Fite, K.V. and Bengston, L. (1981) The accessory optic system of Rana Pipiens: Neuroanatomical connections and intrinsic organisation. *J. Comp. Neurol.*, 203: 595-612.

Montgomery, N., Fite, K.V. and Grigonis, A.M. (1985) The pretectal nucleus lentiformis mesencephali of Rana Pipiens. *J. Comp. Neurol.*, 234:264-275.

Mountcastle, V.B. (1978) An organising principle for cerebral function: the unit module and the distributed system. In: G.M. Edleman and V.B. Mountcastle, *The Mindful Brain*. Cambridge: MIT Press.

Ogata, K. (1970) Modern control engineering. Englewood Cliffs, N.J.: Prentice Hall.

Potter, H.D. (1969) Structural characteristics of cell and fiber populations in the optic tectum of the frog (Rana Catesbeiana). *J. Comp. Neurol.*, 136:203-232.

Potter, H.D. (1972) Terminal arborisations of retino-tectal axons in the bullfrog. *J. Comp. Neurol.*, 144: 269-284.

Reichardt, W. and Poggio, T. (1979) Visual control of flight in flies. In: *Recent Theoretical Developments in Neurobiology*, (Reichardt, Mountcastle & Poggio, eds.).

Raisma, G., W.M. and DePowel, T.P. (1965) The extrinsic afferents commisural and association fibres of the hippocampus. *Brain*, 88:963-996.

Raven, F. (1961) Automatic control engineering. New York: McGraw Hill.

Roth, G. (1976) Experimental analysis of the prey-catching behavior of *Hydromantes italicus* Dunn *(Amphibia, Plethodontidae)*. *J. Comp. Physiol.*, 109: 47-58.

Roth, G. (1982) Responses in the optic tectum of the Salamander *Hydromantes italicus* to moving prey stimuli. *Exp. Brain Res.*, 45: 386-392.

Roth, G. and Jordan, M. (1982) Response characteristics and stratification of tectal neurons in the toad Bufo Bufo (L.). *Exp. Brain Res.*, 45: 393-398.

Rubinson, K. (1968) Projections of the optic tectum of the frog. *Brain Behav. Evol.*, 1:529-561.

Scalia, F. (1976) The optic pathways of the frog nuclear organisation and connections. In: *Frog Neurobiology* (Llinás, R. and Precht, W., eds.), Berlin: Springer-Verlag, pp. 386-406.

Scalia, F. and Fite, K.V. (1974) A retinotopic analysis of the central connections of the optic nerve in the frog. *J. Comp. Neurol.*, 158:455-478.

Schneider, D. (1954) Das Gesichtsfeld und der Fixiervorgang bei einheimischen Anuren. *Z. Verg. Physiol.*, 36:147-164.

Schürg-Pfeiffer, E. and Ewert, J.P. (1981) Investigations of neurons involved in the analysis of gestalt prey features in the frog rana temporaria. *J. Comp. Physiol.*, 141: 139-152.

Scott,

Shampine, L.F. and Allen, R.C. (1973) Numerical computing: An introduction. W. B. Saunders Company.

Shampine, L.F. and Gordon, M.K. (1975) Computer solution of Ordinary Differential equations. The initial value problem. San Francisco: W. H. Freeman.

Shepherd, G.M. (1970) The olfactory bulb as a simple cortical system: experimental analysis and functional implications. In: *The Neurosciences Second Study Program* (Schmit, F., ed.). New York: The Rockefeller University Press, pp. 539-551.

Shepherd, G.M. (1979) The synaptic organisation of the brain (2nd. edition) Oxford: Oxford University Press.

Shinners, S. (1978) Modern control system theory and application. Mass.: Addison-Wesley.

Singer, W. (1977) Control of the thalamic transmition by cortifugal ascending reticular pathways in the visual system. *Physiol. Rev.*, 57:386-417.

Székely, G. and Lázár, G. (1976) Cellular and synaptic architecture of the optic tectum. In: *Frog Neurobiology* (Llinás, R. and Precht, W., eds.), Berlin: Springer-Verlag, pp. 407-434.

Ssentágothai, J. (1970) Glomerular synapses, complex synaptic arrangements, and their operational significance. In: *The Neurosciences Second Study Program* (Schmit, F., ed.). New York: The Rockefeller University Press, pp. 427-443.

Ssentágothai, J. and Arbib, M. A. (1974) Conceptual models of neural organisation. *Neurosci. Res. Program Bull.*, 12:307-510.

Trachtenberg, M.C. and Ingle, D.J. (1974) Thalamo-tectal projections in the frog. *Brain Res.*, 79: 419-430.

Werblin, F.S. and Dowling, J.E. (1969) Organisation of the retina of the mudpuppy, *Necturus maculosus*. II. Intracellular recording. *J. Neurophysiol.*, 32:339-355.

Wicsynski, W. and Northcutt, R. (1977) Afferents to the optic tectum of the leopard frog: An HRP study. *J. Comp. Neurol.*, 173:219-229.

Witpaard, J. and Ter Keurs, H. (1975) A reclassification of retinal ganglion cells in the frog, based upon tectal endings and response properties. *Vision Res.*, 15: 1333-1338.

1

APPENDIX A

MATHEMATICAL REPRESENTATION OF THE MODELS

Introduction

In this Appendix, we provide the mathematical description of all the elements in the two-dimensional model of the interactions among retina, optic tectum and pretectum. This description updates and complements the description of the one-dimensional version provided in Lara and Arbib [1982].

In these models, we have used a simple neuron model to represent the behavior of tectal and pretectal neurons, which receives n inputs $z_1, z_2, \ldots, z_n$ and produces one output Y. We use differential equations and threshold functions to model the dynamics of such a neurons' behavior. For a complete discussion of mathematical representation of the dynamics of neural behavior, the interested reader is referred to Amari [1977] and to An der Heiden [1980]. According to these equations, the state of a neuron at time t is defined by two quantities, one (shown in lower case) representing its membrane potential and the second (shown in upper case) denoting its firing rate. As seen in Chapter 4, the membrane potential varies according to the following equation:

$$r\dot{m}(t) = -m(t) + S(t) + M_0$$

that is, $m(t)$ increases in proportion to the algebraic weighted sum $S(t)$ of the excitatory and inhibitory inputs, and decays according to its membrane time constant r towards a resting potential M_0.

In the equations, the second subscript of the weighting factors represents the cell that receives afferents from the neuron represented by the first subscript. For example,

$$w_{gl \cdot sp}$$

represents the effect on a small pear (SP) shaped cell, second subscript, of the glomerulus (GL), first subscript.

The firing rate of an element at time t is determined as a function of the membrane potential $m(t)$ by the formula $F(m(t); \Theta)$, where Θ is a suitable threshold value and F may be of form

$$f(m(t); \Theta) = \begin{cases} 1 & if\ m(t) \geq \Theta \\ 0 & otherwise \end{cases}$$

or

$$h(m(t); \Theta) = \begin{cases} k_1 \cdot m(t) & if\ m(t) \geq \Theta \\ 0 & otherwise \end{cases}$$

or

$$s(m(t); \Theta_0, \Theta_1) = \begin{cases} 1 & if\ m(t) \geq \Theta_1 \\ m(t) - \Theta_0 & if\ \Theta_0 \leq m(t) < \Theta_1 \\ 0 & if\ m(t) < \Theta_0 \end{cases}$$

or

$$g(m(t); \Theta) = \begin{cases} k_2 \cdot m(t) & if\ m(t) \geq \Theta \\ C & otherwise \end{cases}$$

where k_1, k_2 are constants and C represents a tonic activity.

The final choices of the threshold functions, membrane time constants, and the weight factors are shown in Tables 7, 8 and 9, respectively. For further discussion about these values refer to Lara, Arbib and Cromarty [1982], to Lara and Arbib [1982] and to Chapter 3.

Table 7: Threshold Functions for the Two-Dimensional Model.

$LP = f\ (lp\ ;\ 1.0)$
$SP = f\ (sp\ ;\ 2.0)$
$SN = h\ (sn\ ;\ 0.2)$
$TP = g\ (tp\ ;\ 3.8)$
$PY = s\ (py\ ;\ 2.3, 5.0)$

Table 8: Membrane Constants for the Two-Dimensional Model.

$\tau_{gl} = 0.35$	$k_{gl} = 0.15$
$\tau_{lp} = 0.3$	
$\tau_{sp} = 0.9$	
$\tau_{sn} = 0.65$	$k_{sn} = 0.4$
$\tau_{tp} = 0.02$	
$\tau_{py} = 0.12$	

Table 9: Weighting Factors for the Two-Dimensional Model.

$w_{r2 \cdot gl} = 1.0$	$w_{r2 \cdot tp} = 0.3$
$w_{lp \cdot gl} = 0.8$	$w_{r4 \cdot tp} = 5.0$
$w_{sp \cdot gl} = 0.1$	$w_{r2 \cdot py} = 3.5$
$w_{r2 \cdot lp} = 1.0$	$w_{r3 \cdot py} = 0.3$
$w_{gl \cdot lp} = 1.0$	$w_{r4 \cdot py} = 7.0$
$w_{sp \cdot lp} = 0.6$	$w_{lp \cdot py} = 0.56$
$w_{sn \cdot lp} = 8.2$	$w_{sp \cdot py} = 2.0$
$w_{tp \cdot lp} = 0.1$	$w_{tp \cdot py} = 0.9$
$w_{r2 \cdot sp} = 1.0$	$w_{lp1 \cdot gl} = 1.2\ (s.c.)$
$w_{gl \cdot sp} = 0.5$	$w_{sp1 \cdot lp} = 0.8\ (s.c.)$
$w_{tp \cdot sp} = 0.1$	$w_{sn1 \cdot lp} = 8.0\ (s.c.)$
$w_{sn \cdot sp} = 20.0$	$w_{gl1 \cdot sp} = 1.0\ (s.c.)$
$w_{lp \cdot sn} = 2.1$	$w_{lp1 \cdot py} = 0.7\ (s.c.)$
note : s.c. means from the same column	

Our two-dimensional model of the interactions among retina, optic tectum and pretectum is composed of "column units" (see Chapter 3 and 4). The (ith, jth) column unit in the tectum receives, symmetrically, afferents from all of its neighbor columns and retinotopic projections from ganglion cells of types $R2$, $R3$ and $R4$, and the pretectal neuron TP. The pretectal cell TP only receives retinotopic projections from $R3$ and $R4$.

Now, we describe the equations that define the behavior of the tectal and pretectal cells considered in this model.

Glomerulus (GL)

The equation defining the behavior of the glomerulus of the (ith, jth) column of the optic tectum is given as follows:

$$\tau_{gl}\dot{gl}_{i,j}(t) = -k1 \cdot gl_{i,j}(t) + S_{gl_{i,j}}(t)$$

where

$$S_{gl_{i,j}}(t) = R2_{i,j}(t) + w_{lp1,gl}LP_{i,j}(t) + \sum_{n=-1}^{+1}\sum_{m=-1}^{+1} w_{sp,gl}SP_{i+n,j+m}(t) +$$

$$\sum_{n=-1}^{+1}\sum_{m=-1}^{+1} w_{lp,gl}LP_{i+n,j+m}(t) - w_{lp,gl}LP_{i,j}(t)$$

where $R2_{i,j}$ is the retinal input from ganglion cell type $R2$, and $S(t)$ denotes the recurrent axons from LP and SP cells of its own unit and from neighboring columns (see Chapter 3). The weight factor associated with the LP cell of the same column is larger than those of LP cells of the neighbor columns (see Table 9). This ensures a mainly vertical processing of the information, which is in accordance with experimental observations [Székely & Lázár, 1976; Ingle, 1975].

Large Pear shaped cell (LP)

The behavior of the LP cell of the (ith, jth) unit column can be described as follows:

$$\tau_{lp}\dot{lp}_{i,j}(t) = -lp_{i,j}(t) + S_{lp_{i,j}}(t)$$

where

$$S_{lp_{i,j}}(t) = E_{lp_{i,j}}(t) - I_{lp_{i,j}}(t)$$

where

$$E_{lp_{i,j}}(t) = gl_{i,j}(t) + R2_{i,j}(t) + w_{sp1,lp}SP_{i,j}(t) + \sum_{n=-1}^{+1}\sum_{m=-1}^{+1} w_{sp,lp}SP_{i+n,j+m}(t) -$$

$$w_{sp,lp}SP_{i,j}(t)$$

and

$$I_{lp_{i,j}}(t) = w_{tp,lp}TP_{i,j}(t) + w_{sn1,lp}SP_{i,j}(t) + \sum_{n=-1}^{+1}\sum_{m=-1}^{+1} w_{sn,lp}SN_{i+n,j+m}(t) -$$

$$w_{sn,lp}SN_{i,j}(t)$$

where $gl_{i,j}$ represents the afferent from the glomerulus of its own column, $R2_{i,j}$ is the retinal input from ganglion cells type $R2$, and $E(t)$ and $I(t)$ show that these cells receive afferents from SN and SP cells from its own column as well as from neighbor ones. This cell is also inhibited by the $TP_{i,j}$ cell of its corresponding projection in the pretectum. Again, to ensure a mainly vertical processing of information, the weight factor of the SP cell from its own unit is larger than those from neighbor columns.

Small Pear shaped cell (SP)

The behavior of the small pear shaped cell of the (ith, jth) column can be described as follows:

$$\tau_{sp} \dot{s} p_{i,j}(t) = -sp_{i,j}(t) + S_{sp_{i,j}}(t)$$

where

$$S_{sp_{i,j}}(t) = E_{sp_{i,j}}(t) - I_{sp_{i,j}}(t)$$

where

$$E_{sp_{i,j}}(t) = w_{gl\cdot sp} gl_{i,j}(t) + R2_{i,j}(t) + \sum_{n=-1}^{+1} \sum_{m=-1}^{+1} w_{gl\cdot sp} gl_{i+n,j+m}(t) - $$

$$w_{gl\cdot sp} gl_{i,j}(t)$$

and

$$I_{sp_{i,j}}(t) = w_{tp\cdot sp} TP_{i,j}(t) + w_{sn\cdot sp} SP_{i,j}(t)$$

where $R2_{i,j}$ is the retinal input from ganglion cells type $R2$, and $E(t)$ and $I(t)$ show that these cells receive afferents from the glomerulus of its own column and of its neighbors, with a larger weight factor associated with the glomerulus of the same column, and from the pretectal neuron $TP_{i,j}$.

Stellate Neuron (SN)

The behavior of the stellate neuron of the (ith, jth) tectal column can be defined as follows:

$$\tau_{sn} \dot{s} n_{i,j}(t) = -k2 \cdot sn_{i,j}(t) + S_{sn_{i,j}}(t)$$

where

$$S_{sn_{i,j}}(t) = \sum_{n=-1}^{+1} \sum_{m=-1}^{+1} w_{tp\cdot sn} LP_{i+n,j+m}(t) - w_{tp\cdot sn} LP_{i,j}(t)$$

where $S(t)$ shows that these neurons only receive afferents from the LP cells, from its own column and from neighboring ones.

Pyramidal Cell (PY)

The membrane potential of the (ith, jth) Pyramidal cell (PY) is defined as follows:

$$\tau_{py} \dot{p} y_{i,j}(t) = -py_{i,j}(t) + S_{py_{i,j}}(t)$$

where

$$S_{py_{i,j}}(t) = E_{py_{i,j}}(t) - I_{py_{i,j}}(t)$$

where

$$E_{py_{i,j}}(t) = w_{r2\cdot py} R2_{i,j}(t) + w_{r3\cdot py} R3_{i,j}(t) + w_{r4\cdot py} R4_{i,j}(t) +$$

$$w_{sp\cdot py} SP_{i,j}(t) + w_{lp1\cdot py} LP_{i,j}(t) +$$

$$\sum_{n=-1}^{+1} \sum_{m=-1}^{+1} w_{lp\cdot py} LP_{i+n,j+m}(t)$$

and

$$I_{py_{i,j}}(t) = w_{tp\cdot py} TP_{i,j}(t)$$

where $R2_{i,j}$, $R3_{i,j}$ and $R4_{i,j}$ are the retinal input from ganglion cells type $R2$, $R3$ and $R4$ respectively, and $TP_{i,j}$ is the inhibitory effect from one cell of the corresponding pretectal projection. Again, the weight factor of the LP cell of the same column is larger than those associated with the cells of the neighbor columns.

Pretectal cell (TP)

The behavior of the TP neuron of the (ith, jth) pretectal column (there is a retinotopic projection between tectum and pretectum) can be defined as follows:

$$\tau_{tp}\dot{tp}_{i,j}(t) = -tp_{i,j}(t) + S_{tp_{i,j}}(t) + ton$$

where

$$S_{tp_{i,j}}(t) = w_{r3-tp}R3_{i,j}(t) + w_{r4-tp}R4_{i,j}(t)$$

where ton is the tonic inhibition that these neurons exert over the tectal activity (see Chapter 3 and Chapter 5), and $R3_{i,j}$ and $R4_{i,j}$ are the input from retinal ganglion cells type $R3$ and $R4$, respectively.

TABLE OF CONTENTS

APPENDIX B

NUMERICAL METHODS

Introduction

In modelling the dynamic behavior of neural networks, we considered each element in the net to be represented by two items; a first order differential equation to represent the dynamics of the local *membrane potential*, and a threshold function to simulate the generation of *action potentials* [Amari, 1977; An Der Heiden, 1980]. Thus, the mathematical representation of a neural net model results in a system of n, number of neurons in the circuit, first order differential equations with small non-linearities (threshold functions). The number of afferents of each element depends on the network connectivity pattern.

Our current model, a two-dimensional 8×8 array of FTC's, is mathematically represented by a large system of first order differential equations cross-coupled by threshold functions. It is desired to find solutions for this system for different sets of parameters or coefficients. These solutions will be acceptable as long as the qualitative behavior of the net is not significantly degraded. During computer simulations with the model it is assumed that the initial conditions are known, which makes them fit into the classification of Initial Value Problems.

Because of the non-linearities introduced by the threshold functions, methods to determine the exact analytical solution are either very costly or unknown. Therefore, the problem is to find an approximate solution for the system of equa-

tions representing the neural net model, keeping the loss of accuracy below certain limits.

The aim of this Appendix is to consider different numerical methods for solving systems of first order differential equations, and to compare them in order to select the ones well suited to our particular application. There are many techniques that can be used to solve such a system of equations, but because our modelling effort can be considered as an Initial Value Problem, we will restrict our analysis to numerical methods that given the initial conditions can generate a function that approximates the system solution. These methods are compared according to the criteria established by Hull et. al. [1972], where the cost of a particular method applied to a specific problem is measured both by the number of function calls and the overhead cost.

In this Appendix we present the specification of numerical methods to be considered: Euler's method, Runge-Kutta formulas (second and fourth order), Adams' formulas (Adams-Bashforth, and Adams-Moulton), and extrapolation methods (Bulirsch and Stoer's, which employs rational extrapolation); next, we describe the comparison criteria used by Hull et. al. [1972], and we conclude our analysis by showing that either Runge-Kutta formulas of four order or Euler method, with an appropriate time interval Δt, are well suited to solve our mathematical models.

Description of Numerical Methods

The methods to be considered, as we mentioned above, are some of those for systems of first order differential equations, though it must be noticed that these techniques are not limited to these systems. They can also be applied to

systems expressed in differential equations of higher order, which through the use of appropriate substitutions can be converted to an equivalent system of first order differential equations.

In what follows, we assume that our differential equation is of the form

$$\dot{m}(t) = f(t, m(t))$$

where $m(t)$ is an n-dimensional vector, and that the initial value $m(t_0) = m_0$ is known. We seek the solution at the interval $[t_0, t_f]$.

Euler's Method

The simplest approximation method for the initial value problem is Euler's method. If the interval $[t_0, t_f]$ is divided into small subintervals of length Δt, this method approximates the exact values $m(t_1)$, $m(t_2)$,... to values m_1, m_2,... by approximating the derivative at point (t_i, m_i) with the difference quotient $\frac{m_{i+1} - m_i}{\Delta t}$. This gives the difference equation:

$$\frac{m_{i+1} - m_i}{\Delta t} = f(t_i, m_i)$$

or the recursion formula

$$m_{i+1} = m_i + \Delta t \cdot f(t_i, m_i)$$

with $m(t_0) = m_0$.

It is important to point out that this process may be applied iteratively to successive points (t_i, m_i) to estimate m_{i+1}. In this method it is of no importance if function f is defined by a complicated nonlinear expression. Unfortunately, as is evident, the accuracy of Euler's method depends on the step length Δt [Johnson & Reiss, 1977], which must be chosen quite small in order to get acceptable

precision. It is desired that Δt be large enough to reduce the amount of labor and yet not so large that the solution becomes too inaccurate. Dahlquist and Bjorck [1974] described a method using Euler's method in combination with Richardson's extrapolation technique, which yields a better performance and improves the order of the truncation error.

Runge-Kutta Formulas

Runge-Kutta and Euler methods are defined as one-step methods, which in general take the form:

$$m_{i+1} = m_i + \Delta t \cdot \Phi(t_i, m_i ; \Delta t)$$

where $\Delta t \cdot \Phi(t_i, m_i ; \Delta t)$ can be thought as representing an approximation to the amount by which the solution $m(t)$ increases, or decreases, as we move from t_i to t_{i+1}. Since the change in $m(t)$ between t_i and t_{i+1} is governed by the nature of the flow field in the neighborhood of point $(t_i, m(t_i))$, the idea is to sample the flow field at various points close to $(t_i, m(t_i))$ in order to get an approximation of changes to be expected in $m(t)$ for $t_i \leq t \leq t_{i+1}$. In particular, we might specify the increment function by:

$$\Phi(t_i, m_i ; \Delta t) = A_1 f(\theta_1, \gamma_1) + A_2 f(\theta_2, \gamma_2) + \cdots + A_k f(\theta_k, \gamma_k) \qquad (2.1)$$

so that $\Phi(t_i, m_i ; \Delta t)$ is a weighted average of the function slopes near point (t_i, m_i). For example, Euler's method uses just the one sample point (t_i, m_i) with $A = 1$. Runge-Kutta methods provide one logical means for choosing the weights and sample points. The second order Runge-Kutta method, probably the simplest one, uses formulas of the form given by equation (2.1) with two sample points. It uses as one sample point (t_i, m_i) and, for a sample point nearby this

point, it chooses $(t_i + \beta \cdot \Delta t, m_i + \alpha \cdot \Delta t \cdot f(t_i, m_i))$, where α and β are as yet undetermined. Given some choices for the parameters we get the formula:

$$m_{i+1} = m_i + \Delta t \cdot f(t_i + \frac{\Delta t}{2}, \; m_i + \frac{\Delta t}{2} f(t_i, m_i))$$

which is usually called the *modified Euler's Method*, or the *Euler-Cauchy* method [Shampine & Allen, 1973]. With other choices of parameters, we get the formula:

$$m_{i+1} = m_i + \frac{\Delta t}{2}[f(t_i, m_i) + f(t_{i+1}, m_i + \Delta t \cdot f(t_i, m_i))]$$

which is usually called *improved Euler's Method* or the *Heun's method*. Note that these Runge-Kutta methods require two evaluations of $f(t, m)$ at different points near (t_i, m_i). This improves the accuracy, with a truncation error of second order, over Euler's method, where the truncation error is of first order. Additionally, this method is arbitrarily extensible. Probably the fourth-order Runge-Kutta method is the most frequently used. For a given step-size, one formula, from the family of formulas of fourth order, is defined as :

$$m_{i+1} = m_i + \frac{\Delta t}{6}[K_1 + 2K_2 + 2K_3 + K_4]$$

where

$$K_1 = f(t_i, m_i)$$

$$K_2 = f(t_i + \frac{\Delta t}{2}, m_i + \frac{\Delta t}{2}K_1)$$

$$K_3 = f(t_i + \frac{\Delta t}{2}, m_i + \frac{\Delta t}{2}K_2)$$

$$K_4 = f(t_i + \Delta t, \; m_i + K_3)$$

This method has a truncation error bounded by a term of $O(\Delta t^4)$ and requires four evaluations of $f(t, m)$ per step. This shows why Runge-Kutta methods become inefficient as a higher order of accuracy is required, particularly in problems where the function evaluation is complicated [Johnson & Riess, 1977; Dahlquist & Bjorck, 1974].

Adams' Formulas (Adams-Moulton & Adams-Bashforth)

In Euler's and Runge-Kutta methods the approximate solution for $m(t)$ is obtained by evaluating $f(t, m(t))$ at points $t_1, t_2, \ldots$ in the time interval $[t_0, t_f]$. A more efficient method that produces a better solution can be made using one of the Adams' formulas. Consider the equation

$$\dot{m}(t) = f(t, m(t))$$

with $m(t_0) = m_0$. The exact solution over an interval $[t_0, t_f]$ may be expressed as

$$m(t_{i+1}) = m(t_i) + \int_{t_i}^{t_{i+1}} \dot{m}(t)dt = m(t_i) + \int_{t_i}^{t_{i+1}} f(t, m(t))dt$$

The Adams' method approximates this solution by replacing $f(t, m(t))$ with a polynomial interpolation to the derivative values f_j, and then integrating this polynomial. The Adams-Bashforth formula of order k at t_i uses a polynomial $P_{k,i}(t)$ interpolating the derivatives at the k preceding points so that

$$P_{k,i}(t_{i+1-j}) = f(t_{i+1-j}, m_{i+1-j}) \quad for \; 1 \le j \le k$$

These derivatives and m_i must be stored from the preceding step. Thus an approximate solution at t_{i+1} is obtained from

$$m_{i+1} = m_i + \int_{t_i}^{t_{i+1}} P_{k,i}dt$$

There are several ways of representing the interpolating polynomials (see Shampine and Gordon [1975]), so that this equation has several formulations. The Adams-Bashforth formula is usually written as

$$m_{i+1} = m_i + \Delta t_i \sum_{j=1}^{k} \alpha_{k,j} f(t_{i+1-j}, m_{i+1-j})$$ (2.2)

where

$$\alpha_{k,j} = \frac{1}{\Delta t_{i+1}} \int_{t_i}^{t_{i+1}} l_j(t) dt$$

and

$$l_j(t) = \prod_{\substack{h \neq j \\ h=1}}^{k} \frac{t - t_{i+1-h}}{t_{i+1-j} - t_{i+1-h}} \quad \text{with} \quad j = 1, 2, \ldots, k$$

which is the Lagrange formula for interpolation.

It seems plausible that a better approximation to $m(t_{i+1})$ could be obtained if the Adams-Bashforth value m_{i+1} of equation (2.2) is regarded as a tentative *predicted* value and incorporated into an interpolating polynomial. The Adams-Moulton formula uses a *predictor-corrector* scheme in which it uses a four point Adams-Bashforth predictor and a corrector derived from a quadrature formula for the interval $[t_i, t_{i+1}]$. This corrector is a formula of the type

$$m_{i+1} = m_i + \Delta t_{i+1} \sum_{j=1}^{k-1} \alpha^*_{i,j} f_{i+1} + \Delta t_{i+1} \alpha^*_{k,0} f(t_{i+1}, \hat{m}_{i+1})$$

where $\hat{m}_{i+1}$ is the predicted value by the Adams-Bashforth method,

$$\alpha^*_{i,j} = \frac{1}{\Delta t_{i+1}} \int_{t_i}^{t_{i+1}} l^*_j(t) dt$$

and

$$l^*_j(t) = \prod_{\substack{h \neq j \\ h=0}}^{k-1} \frac{t - t_{i+1-h}}{t_{i+1-j} - t_{i+1-h}} \quad \text{with} \quad j = 1, 2, \ldots, k$$

This predictor-corrector scheme is referred to as classical in Dahlquist and Bjorck [1974], and they represent it as

Adams-Bashforth :

$$m_{i+1} - m_i = \Delta t (f_i + \frac{1}{2} \nabla f_i + \frac{5}{12} \nabla^2 f_i + \frac{3}{8} \nabla^3 f_i + \ldots)$$

and

Adams-Moulton :

$$m_{i+1} - m_i = \Delta t (f_{i+1} - \frac{1}{2} \nabla f_{i+1} - \frac{1}{12} \nabla^2 f_{i+1} - \frac{1}{24} \nabla^3 f_{i+1} - \ldots)$$

where ∇ is the backward difference operator and $f_i = f(t_i, m_i)$.

The local truncation error is approximately of the same order as the first neglected term [Shampine and Gordon, 1975], that is, if the formula is of order $k + 1$ then the local error is of $O(H^{k+1})$ where H is the maximum step size considered in the process.

Bulirsch & Stoer Method (Extrapolation Methods)

The Bulirsch and Stoer method fits in the final category of numerical methods to be considered, the extrapolation methods. A detailed discussion of the method and a listing of the computer program is given in Fox [1971]. This method is based on a procedure called "extrapolation to zero interval size", which is a tool for improving a discrete approximation $T(\Delta t, t)$ of $m(t)$, whose truncation error can be expressed in powers of Δt. Consider,

$$T(\Delta t, t) = y_0(t) + y_1(t) \Delta t^{p_1} + y_2(t) \Delta t^{p_2} + y_3(t) \Delta t^{p_3} + \cdots$$

where $y_0(t)$ is the exact solution and the rest of the sum represents the truncation error. In extrapolation a sequence of Δt's (Δt_0, Δt_1,...) tending to zero is used to compute successive approximations $T(\Delta t_0)$, $T(\Delta t_1)$,... of $m(t)$. The first two approximations can be used to eliminate the term on Δt^{p_1}, the next one to eliminate the term on Δt^{p_2}, and so on. That is, a polynomial in powers of Δt is used to calculate the approximations, and then extrapolated to zero interval size, $\Delta t = 0$, so that $T(0, t) \triangleq m(t)$.

Bulirsch and Stoer [1966] used a rational function of Δt rather than a polynomial. In this method, rational extrapolation is applied to a modified midpoint integration rule. Let

$$\dot{m}(t) = f(t, m(t))$$

be the differential equation to be integrated with initial conditions $m(t_0) = m_0$. The modified midpoint rule at any point k is based on a *lower* value ($m_{l,k}$), and a *middle* value ($m_{m,k}$) of m at an interval $\frac{\Delta t}{2}$ ahead of $m_{l,k}$. These values are used to compute an *upper* value $m_{u,k}$ of m at an interval $\frac{\Delta t}{2}$ ahead of $m_{m,k}$, which is computed from

$$m_{u,k} = m_{l,k} + \Delta t \cdot f(t_{m,k}, m_{m,k})$$

At the next step $k + 1$, $m_{m,k}$ becomes $m_{l,k+1}$, $m_{u,k}$ becomes $m_{m,k+1}$, and the process continues until the value of $m_{m,k+l}$ is the value of $m(t)$ at t_f. A final correction sets the value of m at this point to an average

$$T(\Delta t, t) = \frac{1}{2}[m_m + (m_l + \frac{\Delta t}{2} f(t_m, m_m))]$$

To initialize the process, the algorithm uses

$$m_{l,0} = m_0$$

and

$$m_{m,0} = m_0 + \frac{\Delta t}{2} f(t_0, m_0)$$

Under suitable differentiability conditions, it can be shown [Gragg, 1963] that the asymptotic expansion $T(\Delta t))$ contains only even powers of Δt of the form:

$$T(\Delta t, t) = m(t) + A_1(t) \cdot \Delta t^2 + A_2(t) \cdot \Delta t^4 + \ldots$$

so an extrapolation to zero interval size can be applied. Fox [1971] gives a programmed implementation of a rational extrapolation of order 6, that is, at each integration step as many as six applications of the midpoint rule are computed for successively smaller Δt's and extrapolated to $\Delta t = 0$ in attempting to achieve convergence. Bulirsch and Stoer [1966] showed that this method is more accurate, easier to program and requires fewer computations than either Runge-Kutta, Adams-Moulton-Bashforth corrector-predictor formulas, and polynomial extrapolation methods.

Comparison of Methods

Hull et al. [1972] provide a rigorous conceptual basis for comparing some of the most popular numerical methods for systems of first-order differential equations. We will rely completely on their study during our analysis. These authors compare the following numerical methods: several Runge-Kutta methods, Gear's implementation of the Adams formulas, Krogh's implementation of a variable-order Adams method, and Bulirsch and Stoer (extrapolation) method.

These numerical methods were tested on a variety of initial value problems. Here, it is important to point out that the mathematical representation of our neural network models fits into a subgroup of their *Class C* problems: Moderate

systems of first-order differential equations, i.e., systems with a moderate number of equations sparsely coupled, which do not involve many arithmetic operations per component.

The authors used two different measures of cost, the *number of function evaluations* and the *overhead* (defined as the execution time less function evaluation time). These measures were chosen to indicate how well a method can carry out a relatively routine step-by-step integration procedure under a variety of accuracy requirements, rather than how well they can handle difficulties introduced by stiffness, roundoff, amount of computing memory required or getting started.

Hull and coworkers found that the relative performance of each of the tested methods is extremely consistent, not only within each problem class but also between different problem classes. Their conclusions can be summarized as follows:

1. On the basis of overhead alone, the method of Bulirsch and Stoer is the best overall, and particularly good when costs are relatively high because tolerances are relatively small.

2. On the basis of function call alone, the variable-order method based on Adams formulas (Krogh's method) is best. Gear's method is not as good mainly because it is not allowed to vary its order enough. Among the Runge-Kutta methods, the one of order 8 (RK8) is the best for small tolerances (10^{-9}), but its order is too high to be competitive with the ones of order 6 (RK6) and 4 (RK4) for bigger tolerances of 10^{-6} and 10^{-3} respectively.

3. Bulirsch and Stoer's method requires less overhead time on the whole, whereas Krogh's method requires fewer function evaluations, so this means that Bulirsch and Stoer' algorithm is best when function evaluations are not very expensive, but Krogh's is best when these evaluations are very costly.

4. Runge-Kutta methods (and Euler's method) are not competitive in general. Not only are they inefficient, especially over a wide range of tolerances, but they also have a very poor reliability. However, low order Runge-Kutta methods (e.g., fourth-order formulas) are best with fairly large tolerances of about 10^{-3}, when function evaluations are not very expensive. These authors consider a function evaluation to be expensive if it requires more than 25 arithmetic operations per component.

Based on their results, we may add that Euler's method is completely out of competition. However, there is one exceptional situation. For problems that allow large tolerances there must be an appropiate time interval (Δt) for which the cost for a Runge-Kutta method of order 4 will be higher than the cost for Euler's method with a time interval equal to $\frac{\Delta t}{2}$ or $\frac{\Delta t}{3}$ for some required accuracy. The first method requires four function evaluations at every step; whereas, even if we assume a smaller time interval, Euler's method would require fewer function evaluations.

Conclusions

The selection of the numerical methods that are well suited to our particular problem, was done based on the characteristics of our models. In order to be able to apply the criteria proposed by Hull and coworkers [1972], in Appendix A we described the system of first order differential equations that represents our neural net models following the pattern proposed by these authors. They specified a particular problem p in terms of six items arranged as follows:

$$p = (f, t_0, m_0, t_f, \epsilon, \Delta t_{max})$$

where the three first elements describe the mathematical problem. That is, the system $\dot{m}(t) = f(t, m(t))$, and the initial conditions $m(t_0) = m_0$. The fourth quantity, t_f, indicates that the integration proceeds over the interval $[t_0, t_f]$. The fifth item, ϵ, is the local error tolerance; whereas the last item, Δt_{max}, represents a measure of the "scale" of the problem, which is used to determine how fine a

mesh of points is needed for finding a reasonable solution to the problem. For further discussion about the selection of these six items to specify the problem refer to Hull et al [1972].

Mathematically, our models are represented by a system of first-order differential equations sparsely coupled through small non-linearities (threshold functions). In our simulations we chose the final value of the independent variable (time) to be $t_f = 5.0$ units of time (sec), which is the minimum value that allow us to get reliable results to direct our qualitative analysis of the neural net behavior. At the begining of a simulation we consider that all the neurons in the model are at their resting level, thus we assume null initial conditions. These models are developed to direct a qualitative analysis of different hypotheses raised to explain how neural responses within the anuran brain may be underlying the animal visuomotor coordination. Therefore, the tolerance required for the solution of such systems may be assumed to be as big as $\epsilon = 10^{-3}$. We need to monitor the behavior of these cells in the range of milliseconds to decide if their output is active or inactive, so the maximum step size may be $\Delta t_{max} = 0.1$. In addition, each element in the neural circuit is represented by a first-order differential equation that contains an operand for every afferent impinging upon this neuron. According to the connectivity pattern in the network, each cell receives afferents from at most from 20 other neurons (including the retinal ganglion and pretectal cells) involving in some cases up to two arithmetic operations per component. Therefore, the cost of function evaluations in this system may be considered as low.

It is obvious that our models belong to the problem *Class C* of Hull et al [1972]. Thus, based on their results and the, just described, characteristics of our models, it is clear that the Runge-Kutta formulas of fourth order are best suited to our particular application, although the Euler's method with an appropriate time interval Δt may be applied too. During our computer experiments we obtained the same qualitative results using the Runge-Kutta method with a time interval $\Delta t = 0.04$ or the Euler's method with $\Delta t = 0.01$. Thus, we decided to use the Euler's method because it was easier to program and maintain, and required less function evaluations.

In future stages (see Chapter 6) our models will be modified as follows:

1. It will be required to conduct quantitative analyses of the processes involved in visuomotor coordination in frogs and toads (i.e., the analysis of the temporal response of certain FTC model elements, such as the PY cells).

2. The phenomena to be addressed require an increase of the number of tectal columns, which will increase to an array of about 50 × 50.

3. The connectivity pattern among elements of different columns will be modified so that each column will receive information not only from the immediate neighboring columns but also from more distant columns.

Thus, different requirements for the computer simulations will be introduced, e.g., the tolerance will become smaller and function evaluations will get more expensive. Under those conditions Krogh's method based on Adams formulas will be best suited to our particular problem because, as determined by Hull et al [1972], with a tolerance of 10^{-3} in problems of *Class C* no matter how expensive the function evaluations are, this method is better than the Bulirsch and Stoer's method and, of course, than all of the other methods considered in our analysis.